Helsinki University of Technology Signal Processing Laboratory
Teknillinen korkeakoulu Signaalinkäsittelytekniikan laboratorio
Espoo 2007 Report 58

Performance Analysis of Multi-antenna and Multi-user Methods for 3G and Beyond

Jyri Hämäläinen

Dissertation for the degree of Doctor of Science in Technology to be presented with due permission of the Department of Electrical and Communications Engineering for public examination and debate in Auditorium S4 at Helsinki University of Technology (Espoo, Finland) on the 26th of January, 2007, at 2 p.m.

Helsinki University of Technology
Department of Electrical and Communications Engineering
Signal Processing Laboratory

Teknillinen korkeakoulu
Sähkö- ja tietoliikennetekniikan osasto
Signaalinkäsittelytekniikan laboratorio

Distribution:
Helsinki University of Technology
Signal Processing Laboratory
P.O. Box 3000
FIN-02015 HUT
Tel. +358-9-451 3211
Fax. +358-9-452 3614
E-mail: Mirja.Lemetyinen@hut.fi

© Jyri Hämäläinen

ISBN 978-951-22-8535-8 (Printed)
ISBN 978-951-22-8536-5 (Electronic)
ISSN 1458-6401

Otamedia Oy
Espoo 2007

Contents

Abstract

Performance of cellular networks has become an issue with forecasted growing public demand for medium and high data rate services. Motivated by these expectations multi-antenna techniques such as transmit diversity (TD), channel-aware scheduling and multiple-input multiple-output (MIMO) transceivers have received a lot of enthusiasm within wireless communications community.

We first focus on closed-loop (CL) TD and introduce extended mode 1 and 2 (e-mode 1 and 2) algorithms that are designed based on universal terrestrial radio access (UTRA) frequency division duplex (FDD) CL mode 1 and 2. We derive analytical performance results for e-mode 1 and 2 in terms of signal to noise ratio (SNR) gain, link capacity and bit error probability (BEP). We also consider the effect of feedback errors to the performance of closed-loop system.

In the analysis of channel-aware scheduling we focus on on-off scheduling (OOS) where user's feedback consists of only a single bit. Performance results in both downlink and uplink clearly indicate that most of the achievable gain from channel-aware scheduling can be obtained with very scarce channel state information (CSI). Results also show that the design of feedback channel is of great importance because feedback errors may seriously degrade the system performance.

The third topic of the thesis concentrates on MIMO techniques that can be implemented in UTRA FDD uplink without major revisions to the current air interface. We show that the UTRA FDD uplink coverage and capacity performance can be boosted by single-input multiple-output (SIMO) and MIMO transceivers. The information MIMO employing parallel multiplexing instead of transmit diversity shows its potential when extremely high user data rates are needed.

Tiivistelmä

Solukkoverkkojen suorituskyky on noussut tärkeään rooliin nopeiden datapalveluiden kasvuennusteiden myötä. Näiden kasvuodotusten perusteella moniantennitekniikat kuten lähetysdiversiteetti, kanavan huomioon ottava lähetyksen aikataulutus sekä useaa samanaikaista datavirtaa tukevat lähetinvastaanotinmenetelmät ovat saaneet osakseen paljon kiinnostusta langattoman tietoliikenteen tutkijayhteisössä.

Tutkimuksessa keskitytään aluksi suljettua säätöä käyttäviin lähetysdiversiteettimenetelmiin, missä yhteydessä esitellään laajennetut moodien 1 ja 2 algoritmit, jotka on aiemmin kehitetty kolmannen sukupolven WCDMA järjestelmän suljetun säädön moodien 1 ja 2 pohjalta. Laajennetuille moodien 1 ja 2 algoritmeille johdetaan analyyttisiä suorituskykytuloksia käyttäen mittarina signaali-kohinasuhteen parannusta, linkin kapasiteettia sekä bittivirheiden todennäköisyyttä. Myös säätövirheiden vaikutusta järjestelmän suorituskykyyn tarkastellaan.

Lähetyksen aikataulutuksen analyysi painottuu kytkettyyn aikataulutukseen, missä käyttäjän säätöinformaatio sisältyy yhteen bittiin. Sekä ylä- että alalinkin suorituskykytulokset osoittavat selvästi, että suurin osa mahdollisesta parannuksesta voidaan saavuttaa hyvin karkeaan kanavatilan informaatioon perustuen. Tulokset osoittavat myös, että säätökanavan suunnittelu on tärkeää, koska säätövirheet voivat vakavasti heikentää järjestelmän suorituskykyä.

Kolmannessa aihealueessa keskitytään moniantennitekniikoihin, jotka voidaan toteuttaa WCDMA järjestelmän ylälinkissä ilman perustavanlaatuisia muutoksia nykyiseen ilmarajapintaan. Tutkimuksessa osoitetaan, että ylälinkin peittoa ja kapasiteettia voidaan parantaa tutkituilla moniantennitekniikoilla olipa lähettimessä yksi tai useampia antenneja. Menetelmä, jossa informaatio jaetaan useisiin rinnakkaisiin datavirtoihin sen sijaan että käytettäisiin vain yhtä datavirtaa, osoittautuu erityisen lupaavaksi kun tarvitaan hyvin nopeita tiedonsiirtoyhteyksiä.

Preface

This thesis is based on the work that was carried out in the Nokia Networks/Strategy and Technology and Helsinki University of Technology/Signal Processing Laboratory.

I want to express my deepest gratitude to Professor Risto Wichman with who we have had many interesting journeys through various research subjects.

I wish to thank Associated Professor Mohamed-Slim Alouini and Professor Tapani Ristaniemi for refereeing this thesis.

I am grateful to my colleagues at Nokia for cooperation and discussions. I highly appreciate the open and supporting atmosphere in our team that contains many world-class experts of radio communications.

I also wish to thank Professor Visa Koivunen for partly financing my work in Signal Processing Laboratory.

I am indebted to my father, Emeritus Professor Rauno Hämäläinen for giving me basic understanding about the fundamental nature of science.

Finally, I wish to thank very deeply my wife Seija, and my children Rimma and Leevi for all the patience and understanding they have shown.

Oulu, December 18, 2006 Jyri Hämäläinen

Abbreviations

3G	3rd Generation
3GPP	3rd Generation partnership project (produces WCDMA standard)
ACK	Positive acknowledgement
ARQ	Automatic repeat request
AS	Angular spread
AWGN	Additional white Gaussian noise
BEP	Bit error probability
BF	Beam-forming
BPSK	Binary phase shift keying
BS	Base station
CCH	Control channel
CDF	Cumulative distribution function
CDMA	Code division multiple access
CL	Closed-loop
CPICH	Common pilot channel
CQI	Channel quality information
CSI	Channel state information
DCH	Data channel
DoA	Direction of arrival
DPCCH	Dedicated physical control channel
DPCH	Dedicated physical channel
DPDCH	Dedicated physical data channel
e-mode 1	Extended mode 1
e-mode 2	Extended mode 2
FBF	Fixed beam-forming
FBI	Feedback information (in UTRA FDD)
FDD	Frequency division duplex
FTP	File transfer protocol
GPS	Global positioning system
GSM	Global system for mobile communications
HARQ	Hybrid automatic repeat request
HS-DSCH	High speed downlink shared channel
HSDPA	High speed downlink packet access
IC	Interference cancellation
IP	Internet protocol
ITU	International telecommunications union
MAI	Multiple access interference
Mbps	Mega bits per second
Mcps	Mega chips per second
MIMO	Multiple-input multiple-output
MISO	Multiple-input single-output
MMSE	Minimum mean square error

MRC	Maximal ratio combining
NACK	Negative acknowledgement
OL	Open-loop
OOS	On-off scheduling
PC	Power control
P-CPICH	Primary common pilot channel
PDF	Probability density function
PIC	Parallel interference cancellation
QAM	Quadrature amplitude modulation
QoS	Quality of service
QPSK	Quadrature phase shift keying
RACH	Random access channel
RLB	Radio link budget
S-CPICH	Secondary common pilot channel
SIC	Serial interference cancellation
SIMO	Single-input multiple-output
SINR	Signal to interference and noise ratio
SISO	Single input single output
SNR	Signal to noise ratio
STBC	Space-time block code
STTD	Space-time transmit diversity
TD	Transmit diversity
TFCI	Transport format combination indicator
TPC	Transmit power control (in UTRA FDD)
TSC	Transmitter selection combining
TTI	Transport time interval
USBF	User specific beam-forming
UTRA	Universal Terrestrial radio access
WCDMA	Wideband CDMA
WLAN	Wireless local area network

1 Introduction

The purpose of this thesis is to summarize the research work that the author carried out during 2000-2005 in Nokia Networks/Strategy and Technology and Helsinki University of Technology/Signal Processing Laboratory. Since the third generation (3G) universal terrestrial radio access (UTRA) frequency division duplex (FDD), referred to as wideband code division multiple access (WCDMA), has fueled the research, it has been natural to adopt the corresponding system framework as a starting point. We shortly recall this framework in Section 2.

Nevertheless, since the results of this thesis are obtained by employing generic models and analytical tools, they are not limited to 3G systems only. Research topics have closely followed the interests of industry containing transmit diversity (TD), physical layer scheduling and multiple-input multiple-output (MIMO). In the following we briefly introduce these topics and list the publications that have been used as a basis for the thesis. Detailed discussion is placed on Sections 3 - 6 containing a more extensive list of references.

1.1 Transmit Diversity

Multiantenna transceivers have great potential to improve the performance of wireless systems. Compared to wireline systems, the inferior capacity of wireless cellular systems is caused by several different physical constraints like co-channel and adjacent channel interference, channel propagation loss, and flat or multi-path fading channels. Multi-antenna transmission and reception techniques are currently seen as one of the most promising approaches for significantly increasing the coverage, capacity and spectral efficiency of wireless systems.

Traditionally, multi-antenna techniques have mainly been considered within base stations (BS), because deploying multiple antennas in the user terminal is not straightforward due to cost, complexity of signal processing, and power consumption. Diversity reception, for example, is a mature technology and it has been successfully applied in base stations to increase cell coverage. Another well-known technique is the beamforming (BF) where highly correlated BS antennas are used. In beamforming, downlink beam is formed using the direction of arrival (DoA) information that is estimated based on uplink measurements. Such estimates can be carried out also in frequency division duplex (FDD) systems when the difference between uplink and downlink frequencies is small with respect to the carrier frequency.

Conventional BF is attractive if BS antennas are placed well above the rooftop level where angular spread (AS) of the received radio signal is usually small. If BS antennas are placed below the rooftop level or angular spread is large due to some other reason, the efficient use of conventional BF may

become difficult since uncertainty of user DoA increases and there might be several strong DoAs corresponding to different signal paths.

In contrast to beamforming, for transmit diversity techniques rich scattering environment is advantageous and most of the TD methods assume from the beginning that transmit antenna correlation is low. It is usual to divide TD techniques into two basic classes, namely into closed-loop (CL) methods, where short term channel state information (CSI) is available in the transmitter, and into open-loop (OL) methods where such information does not exist but, on the other hand, some space-time processing is used in order to improve the radio performance. Nevertheless, this classification is artificial because there exist also hybrid methods where both short-term CSI and OL space-time processing is applied.

With CL techniques, quantized CSI is transmitted to the BS via a control channel. The side information can then be used to weight the transmitted signals such that they combine constructively in the antennas of mobile station increasing the received signal power and consequently range and capacity. In case of uncorrelated signal paths, CL TD techniques can provide diversity benefit and increase the signal to noise ratio (SNR) in the receiver. When uplink and downlink operate in different frequency bands the side information related to the downlink channel requires additional signaling, and the design of signaling formats optimizing some performance measure in the mobile terminal while simultaneously minimizing the amount of uplink signaling makes the problem challenging.

Besides CL methods, several different OL TD diversity techniques based on space-time coding have been developed intensively in recent years, and the simplest space-time block code, referred to as space-time transmit diversity (STTD), has been adopted into UTRA FDD as an OL transmit diversity method for two transmit antennas. Space-time codes are blind in the sense that they do not exploit CSI in the transmitter. The codes are able to provide diversity gain but no antenna gain, and the diversity gain decreases as a function of correlation between the antenna elements.

Closed-loop techniques typically outperform the OL ones particularly within low-mobility environments where the delay of the feedback signaling does not exceed channel coherence time. The short-term CSI in the transmitter requires a control channel from the receiver to the transmitter and design of different quantization strategies is an important task. One of the goals of this thesis is to analyze the relation between feedback quantization and system performance for CL methods similar to UTRA FDD CL modes. Contrary to conventional BF the CL algorithms do not require accurate calibration of the transmit antennas. Only coarse calibration of antenna elements is necessary in order to avoid spurious antenna gain patterns and unexpected interference to the network.

Transmit diversity is considered in Section 3 where we introduce and analyze various CL methods. The main reference publications by the author

are [1] - [6] but useful information can be obtained also in [7] - [16].

1.2 Physical Layer Scheduling

Besides multi-antenna methods, also multi-user methods such as physical layer scheduling can be efficiently used in order to increase the system efficiency. When the transmission is not delay constrained, spectral efficiency of multi-user systems can be increased by employing shared channels and channel-aware schedulers, which divide the resources between multiple users. Such shared channels are already used in cdma2000 1xEV-DO and WCDMA high speed downlink packet access (HSDPA).

Efficient use of shared channels greatly depends on the available CSI in the transmitter. It is known that in case of single input single output (SISO) channel the capacity of the shared link can be maximized by giving all resources to the user with the strongest channel. When uplink and downlink employ different frequency bands as in WCDMA mode, scheduling requires a separate feedback channel, which may generate a lot of interference in the uplink. Furthermore, the capacity of control channels is necessarily limited, and large amounts of control information imply large latencies in feedback signaling, which limits the operation range of the system to slow mobile velocities.

In Section 4 we investigate this feedback problem by assuming a heavily quantized channel quality information (CQI). We consider a downlink on-off scheduling (OOS) where users report with one bit, whether their received SNRs fall below or above a predefined threshold. The scheduler then randomly picks one of the users above the threshold and transmits to the user with all available power. We compare OOS to round robin and maximum SNR schedulers that provide lower and upper bounds to the performance of OOS. Capacity gains of the three schedulers are derived together with transmitter selection combining (TSC) and Shannon capacity is used as a performance measure. Besides the shared channel capacity we also consider the bit-error-probability (BEP) of individual users in the presence of heavily quantized CQI. An important goal in Section 4 is to find out the effect of feedback errors.

With increasing load in the network, the uplink may also become a capacity bottleneck, and there is an increasing demand to improve coverage and throughput in the uplink as well. Feasibility study of UTRA FDD uplink enhancements introduces similar mechanisms as with HSDPA. On the contrary to HSDPA, uplink data and control channels employ fast transmit power control (PC), which is inherent characteristic of CDMA uplink. Accurate fast transmit PC is mandatory, because otherwise users in the vicinity of the base station would completely mask intra-cell users on cell edges.

Channel-aware scheduling improves the system performance also in uplink, but to this end the BS transmitter must somehow acquire channel state

information from different users. Thus, even if a user does not transmit any data in the dedicated data channel, it has to transmit some control information so that the scheduler is able to measure the channel state. Strict quality of service requirements are applied on continuously transmitted control channel, and therefore scheduling can be only applied on the dedicated channel. Scheduling may increase the system efficiency if the total number of users in the system is larger than the number of transmitting users, *i.e.* there are backlogged users waiting in the queue for transmission and the scheduler allows users with strongest channels to transmit. However, the larger is the number of users in the system the larger is the overhead caused by users' control channels. Thus, the increased interference due to control signaling and decreased interference due to scheduling should be jointly considered in algorithm design.

In Section 5 we study the effect of OOS to the required transmit power when PC is on. On-off scheduling is compared to two reference systems. The first one applies discontinuous transmission on data channel but the scheduler does not take into account channel state information. The second reference system transmits continuously on data and control channels. We will show that control channel overhead may limit the performance of OOS although users could tolerate unbounded delays.

Section 4 is based on articles [17] - [19] while references [20] - [24] provide additional information. Discussion on the uplink scheduling of Section 5 is mainly adopted from [25].

1.3 Uplink MIMO

Multiple degrees of freedom offered by multiple transmit and receive antennas can be used for diversity or for spatial multiplexing. In the former case, a single data stream is transmitted and multiple antennas are used to decrease the variance of the received signal and thereby improve the quality of the radio link. In the latter case, multiple transceiver antennas are used for parallel multiplexing, *i.e.* to transmit several data streams simultaneously to a user to increase peak data rates. In Section 6, these two approaches will be referred to as diversity MIMO and information MIMO, respectively.

In terms of channel capacity, information MIMO is a much more impressive concept than diversity MIMO. It is known that with parallel multiplexing, the capacity increases linearly with the number of transmit and receive antennas when the number of transmit antennas equals the number of receive antennas and when the channels between the antennas are independent and identically distributed. This observation has stimulated large interest toward MIMO transceivers, and in addition to academic research MIMO is actively being studied in standardization fora of different wireless systems, like UTRA, IEEE 802.11n and IEEE 802.16e.

The first release of UTRA FDD was completed in 1999. At that time, re-

search on information MIMO techniques was at initial stage, but the release already specified two-antenna open-loop and closed-loop transmit diversity modes that are part of the most recent Release 6 as well[1]. With multiple receive antennas these modes form basis for diversity MIMO. The introduction of more advanced MIMO techniques to WCDMA has not been straightforward. A lot of standardization effort in 3GPP has been dedicated to extend the specification of diversity MIMO to more than two transmit antennas, and information MIMO techniques to HSDPA have been extensively studied as well. However, at the time of writing no MIMO techniques have been accepted to technical specifications yet.

The basic idea of MIMO is useful in both downlink and uplink of a cellular system. Recently, the discussion has mainly focused on downlink because it is expected that capacity demanding services will be first applied in downlink. Nevertheless, the introduction of new services such as videophones will make it extremely important to reach high spectral efficiency also in the uplink direction. In Section 6 we consider two simple MIMO approaches that are suitable for UTRA FDD uplink. Discussion is based on [26] - [29].

1.4 Research Problems

The first goal of this thesis is to model and analyze some closed-loop transmit diversity methods that are of practical interest. We note that if quantized feedback is assumed in closed-loop transmit diversity the distribution of the sum channel SNR becomes cumbersome to compute in most cases. Therefore it is important to find suitable means in order to circumvent this difficulty and carry out closed-form analysis. Thus, the main research problems are:

- Develop analytical tools by which closed-loop transmit diversity methods can be analyzed.
- Carry out the analysis of the studied methods by using the developed tools and appropriate performance measures.

Channel-aware schedulers in FDD systems require fast feedback from receiver. In order to keep the signaling overhead as small as possible it is attractive to use heavy channel feedback quantisation. In such systems it is of great importance to find the impact of quantization to the scheduler performance. Also system specific aspects should be carefully considered. Main research questions in connection with physical layer scheduling are:

- Analyze the impact of channel feedback quantization. What is the performance of multi-user scheduling when channel feedback is minimized versus the systems with ideal feedback and no feedback?

[1]Recently, the second closed-loop mode was removed from Release'5 onwards in the campaign of simplifying the specifications

- Model and determine the effect of system specific aspects like feedback errors and increased control overhead.

The benefits of uplink MIMO in practical systems need to be characterized. For that purpose the UTRA FDD uplink provides an interesting framework. Research problems are:

- Determine simple and practical way to deploy MIMO in UTRA FDD uplink.
- Investigate the system level gain of uplink MIMO in UTRA FDD system.

1.5 Author's Contribution and Other Work

Publications have been coauthored in close cooperation and decomposing the publications into separate parts contributed by different authors is not feasible. Author's contribution to the publications [1] - [13], [15] - [21], [25] - [28] has been essential in general, and he has assumed the main responsibility in deriving mathematical analysis. In [26] - [28] simulations were carried out by Esa Tiirola (Nokia Networks), Kari Pajukoski (Nokia Networks) and Markku Kuusela (Nokia Research Center).

It is well acknowledged that the performance of various multi-antenna techniques depends on the assumed channel model. Therefore development and analysis of channel models is an important task. While this task is not in the focus of this thesis we only note that the author of the thesis has recently made some publications on this topic [30] - [34].

2 UTRA Framework

In WCDMA, narrowband user information is spread over a wide bandwidth by modulating a low-rate user data sequence with a high-rate spreading code (channelization code). The length of the spreading codes varies from 4 to 512 chips (in the uplink the maximum code length is 256 chips) and the chip rate is 3.84 Mcps (Mega chips per second) which together with transmit pulse shape filter leads to the carrier bandwidth of approximately 5 MHz. Variable spreading factors and multi-code transmission are used in order to support a wide scale of different data rates [35].

Scrambling codes of length 38400 chips are employed on top of channelization codes. In the downlink channelization codes are used to separate different intra-cell users and separation of inter-cell users is based on different scrambling codes. In the uplink the scrambling codes separate different users and channelization codes separate different physical data and control channels of a user [36]. This difference between the code usage in the downlink and uplink is essential: The limited number of orthogonal channelization codes imposes a strict upper bound to the achievable downlink capacity unless information MIMO technique reusing the channelization codes are used. The limitation is not strict in the uplink, because one user may use all channelization codes and the set of long scrambling codes contains several millions of codes.

The basic UTRA FDD mode supports user data rates up to 2.3 Mbps both in uplink and downlink. In downlink, transmission on the peak data rate requires the usage of 3 parallel channelization codes with spreading factor 4 which allocates 75% of code resources to a single user [37]. In uplink, terminal transmitting with the peak data rate is seen as a large interference source in the network but available code resources of other intra-cell users are not affected. High peak-to-average ratio of multi-code signals sets stringent requirements to transmitters, which are particularly critical to mobile stations.

2.1 UTRA FDD Downlink

Figure 1 presents a simplified downlink channel and frame structure. Each frame is divided into 15 time slots the frame length being 10 ms. The radio frame carries a dedicated physical channel (DPCH) that further divides into dedicated physical data channel (DPDCH) and dedicated physical control channel (DPCCH). The control channel contains transmit power control (TPC) bits for fast power control, transport format combination indicator (TFCI) bits that inform the receiver which transport channels are active and pilot bits enabling the channel and signal to interference and noise ratio (SINR) estimation from DPCH [38].

Figure 1 further shows the primary common pilot channel (P-CPICH)

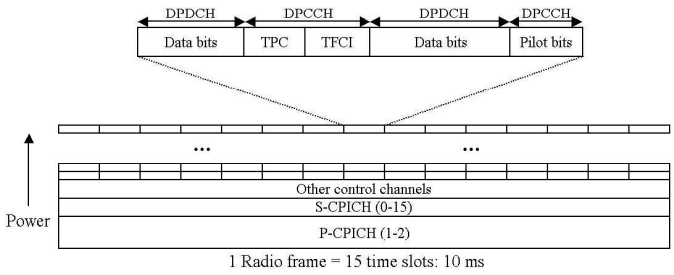

Figure 1: Downlink frame structure for dedicated physical channel.

and the secondary common pilot channel (S-CPICH) without time slot structure, where the numbers in brackets indicate the numbers of different pilot channels. While receiver may estimate the channel from the dedicated channel, better result is usually obtained when employing P-CPICH or S-CPICH, because these common pilot channels, especially P-CPICH, have higher transmit power. In practice, P-CPICH usually takes approximately 10% of transmit power resources of the base station while power on S-CPICHs is lower. This high transmit power on P-CPICH is due to the fact that P-CPICH is always transmitted to the whole cell enabling handover and cell selection/reselection measurements. By adjusting power differences between P-CPICHs of adjacent cells the network load can be balanced. The power on S-CPICH can be lower because it has to cover only part of the cell [38]. Usually S-CPICH is applied in connection with beamforming.

According to the present UTRA FDD specification only two P-CPICHs are available at maximum while multiple S-CPICHs can be introduced, for example, for beamforming purposes. This introduces a serious backward compatibility problem for the design of multi-antenna algorithms with more than two transmit antennas. If the power in P-CPICH is kept fixed but the power is divided to more than two transmit antennas, the channel estimation in legacy mobile terminals is deteriorated. If the power of P-CPICH is increased, interference to network increases as well.

2.2 High-Speed Downlink Packet Access

Starting from Release 5, WCDMA contains a highly optimized downlink data transmission concept referred to as high speed downlink packet access (HSDPA) [39], [40]. The HSDPA concept applies several advanced physical layer solutions, listed below, to enable high throughput and reduced service delays. The HSDPA concept introduces a new type of transport channel, referred to as the high speed downlink shared channel (HS-DSCH), with a fixed spreading factor of length 16. In addition, HSDPA utilizes

- adaptive modulation and coding (link adaptation)

- high order modulation
- hybrid automatic repeat request (HARQ) solution
- reduced length (2 ms) transport time interval (TTI)
- fast cell selection (FCS)
- physical layer scheduler located in base station

The control of HS-DSCH is terminated in the base station in order to adapt rapidly to changing channel conditions. Adaptation rate is increased by shortening transport time interval (TTI) from 10 ms in Release '99 and Release 4 to 2 ms. The same TTI can be used to transmit with multiple channelization codes to the same user depending on terminal capability. In addition, it is possible to multiplex multiple users in the code domain within one HS-DSCH TTI.

Link adaptation is implemented with a large set of possible transport format combinations, each associated with a unique combination of modulation, coding and block size parameters. Release '99 and Release 4 support only QPSK modulation, but an HSDPA terminal also supports 16-QAM. This increases the peak data rates in good channel conditions. Fast power control, which aims to keep the received signal to interference and noise ratio (SINR) constant, is not applied. This is because with non-real time data transmission it is more efficient to allow the received SINR to vary and change modulation and coding according to the channel state. Furthermore, fast power control used together with a high data rate and high power transport channel would generate large interference peaks to neighboring cells.

Data rates are assigned to a user based on CQI that is measured at the terminal and signalled to the base station in the form of a channel quality indicator. Thus, CQI feedback provides the necessary information for efficient real-time link adaptation and this enables a form of multi-user diversity when applied together with physical layer scheduling. It is known that in SISO scenario, throughput is maximized by maximum SNR scheduler transmitting to the user that reports the best SNR to the base station [41], [42]. Yet, when the distances of the users from the serving base station are different, such a scheduler is not fair, because the users on cell edge rarely get any transmission. Therefore, different fair schedulers have been developed, which aim to equalize transmission periods among the users. The physical layer scheduling mechanism is part of the WCDMA HSDPA specification but its implementation is vendor specific option. Instead of SNR, it is also possible to signal data rates or capacities by mapping the SNR values appropriately.

Fast cell selection is used to select the transmitting base station from the set of active base stations. Hybrid ARQ combines retransmission with

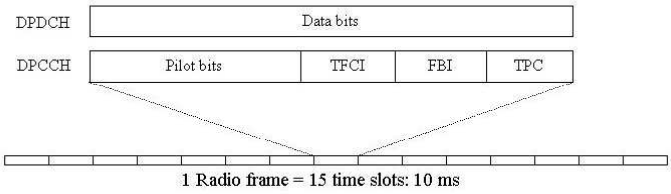

Figure 2: Uplink frame structure for DPDCH/DPCCH.

the previous transmissions to improve reliability, while ARQ ignores erroneously received packets. HARQ provides implicit rate matching, while adaptive modulation and coding (AMC) is used to maximize instantaneous throughput given the instantaneous CQI.

2.3 UTRA FDD Uplink

Figure 2 presents uplink frame and time slot structures for DPDCH and DPCCH. In uplink, user and control data are I/Q code multiplexed and several DPDCHs can be associated to a single DPCCH. In addition to pilot bits, TFCI and TPC uplink DPCCH slot contains feedback information bits (FBI) used to convey partial channel state information when UTRA two-antenna closed-loop transmit diversity modes are applied. Only user-specific dedicated pilot channels are available in uplink [38].

Uplink users are not synchronized and due to non-orthogonality of users' channelization codes, multi-user interference cannot be avoided. Accurate and fast PC is indispensable to uplink performance, because otherwise users in the vicinity of the base station would completely mask intra-cell users on cell edges.

2.4 Present Multi-antenna Methods in UTRA FDD

Conventionally, multi-antenna techniques have mainly been considered within base stations, because deploying multiple antennas in the user equipment is not straightforward due to cost, complexity of signal processing, and power consumption. This is still true in the present terminals that may support several radios like WCDMA, GSM, GPS, Bluetooth, WLAN. Thus, handsets that support only SISO processing may still require several antennas for different frequency bands, although the current trend is to handle the different frequencies with a single multi-frequency antenna.

Multi-antenna signal processing is useful in base station receivers, but the use of multiple antennas for transmission requires a careful study. All precoding methods that modify the transmitted signal constellation must be standardized to ensure that all mobile receivers are able to estimate and

detect the signals from different antennas. An extensive standardization process has been required even in case of transmit beamforming.

Present UTRA FDD specification supports two-antenna transmit diversity and transmit beamforming. Such multiple input single output (MISO) systems for downlink have been intensively studied, because at the time when the 3rd generation partnership project (3GPP) standardization was initiated most scenarios predicted that the capacity of wireless networks would be limited by the downlink connection. Although diversity MISO does not promise as high peak data rates as information MIMO, transmit diversity improves fading resistance and beamforming increases the system capacity while its impact to individual user data rates is small. Information MIMO techniques are not included in the UTRA FDD specification, mostly because the initial standardization work was carried out during the 1990's when the development of practical information MIMO algorithms was still in the beginning.

Conventional transmit beamforming provides the simplest approach to increase system capacity and coverage in downlink. The current 3GPP specification supports both fixed beamforming (FBF) and user specific beamforming (USBF) modes in downlink. Fixed beamforming introduces additional sectors to the cell, because the short term variation of the beams is small and a handover between the beams is required for mobile users. Each beam is associated with a unique S-CPICH while P-CPICH is transmitted to the whole cell.

Fixed beamforming is able to relax the code limitation in downlink, because orthogonal spreading codes can be reused within the same cell due to spatial filtering. It is also possible to use different scrambling codes in different beams. In the presence of flat fading the channelization codes of different users within the same beam remain orthogonal, because they are scrambled with the same code. Different beams interfere with each other and increase intra-cell interference, but when angular spread (AS) is reasonably small as in macro-cells, this interference remains acceptable. In addition to larger interference levels, control signaling overhead increases due to inter-beam handovers, because logically the fixed beams behave in the same way as different sectors in base stations. The overall effect to system capacity is positive though, and according to [43], a 2.4-fold system capacity gain can be achieved with a four-element antenna array when compared to a single antenna cell.

Instead of fixed transmit beams, USBF generates individual beams to each user. More sophisticated signal processing algorithms can be used, and consequently, USBF is able to provide higher individual data rates than FBF. In practice, USBF cannot be utilized in most cases within UTRA FDD downlink, because it prevents the user from employing the P-CPICH as a phase reference and according to the current specification S-CPICH cannot be employed in individual beams. Thus, channel estimation must

be based on dedicated pilot channels whose transmit power is low which may seriously corrupt channel estimation in terminal. Then only high data rate users near the base station may take full advantage from USBF. User-specific beamforming is optional for terminals in HS-DSCH and therefore network cannot assume that all users are able to support it.

Downlink beamforming changes the statistics of the fading signal, and in environments with small angular spread array gain dominates diversity gain. Therefore, the estimation of downlink beamforming gain over single antenna transmission is rather straightforward: The gain is approximately the same as the array gain. In uplink this is not as simple, though.

In uplink, both UTRA FDD beamforming techniques can be implemented in a straightforward manner in the receiver. The simplest approach is to combine the selected signal paths using maximal ratio combining (MRC) in the beam space. This leads to a standard Rake-receiver concept. The most challenging practical problems are related to beam selection (DoA estimation in USBF) and cost-efficient receiver structures. The former problem is related to the large variety of physical environments with different channel profiles. Furthermore, mobile's transmit power is typically low for low data rate connections making the channel estimation difficult. The latter problem arises from the fact that baseband complexity increases rapidly when spatio-temporal estimation processes are introduced. For example, preambles of random access channel (RACH) need to be monitored simultaneously for each beam in order to avoid additional delays in connection setup time.

Transmit beamforming improves the downlink capacity in UTRA FDD, but it is important to notice that receive beamforming is not necessarily the best solution in uplink because of its lack of diversity gain [44]. This gives rise to a trade-off between uplink and downlink design targets. If downlink capacity is the bottleneck, FBF provides a good solution in macro-cells. On the other hand, if good uplink coverage is the primary target, uncorrelated antennas with suitable receiver algorithms provide a better solution.

According to [44] basic receive diversity solution outperforms receive beamforming performance even when angular spread is small. Moreover, transmit beamforming in downlink looses its good performance in terms of capacity and coverage when AS becomes large so that beams cannot be accurately pointed to users any more. Hence, there is a need for a multi-antenna transmission method in downlink that performs well when correlation between the transmit antennas is low. In general, low correlation can be achieved when the distance between antenna elements in base station is several wavelengths. Conventional beamforming algorithms do not apply any more, and to this end, several open-loop transmit diversity techniques have been developed in recent years. The simplest space-time block code [45], has been adopted into 3GPP specification as a two-antenna open-loop transmit diversity method.

Space–time codes provide diversity reducing the variance of the received signal which further translates into reduced transmit power in downlink. However, space–time codes do not increase the received SNR when compared to single antenna transmission. With uncorrelated transmit antennas received SNR can be improved when short-term CSI is made available in the transmitter. Until Release 4 UTRA FDD technical specifications contained two closed-loop modes [46] where the relative phase and power between the two transmit antennas were adjusted according to feedback information bits signaled from mobile to a base station through a dedicated control channel. Later releases contain only the closed-loop mode in which relative phase between two transmit antennas is adjusted and both antennas transmit with the same power.

UTRA FDD supports two P-CPICHs in order to enable efficient channel estimation of the two channels when transmit diversity is in use. In case of closed-loop modes, feedback commands are determined from the P-CPICHs and transmit weights are applied on dedicated traffic channels. Common pilots are transmitted with higher power than dedicated pilots and therefore common pilots should be used for channel estimation whenever possible. With closed-loop modes, dedicated pilots are used for the verification of the transmit weights (feedback commands may be erroneously decoded in the base station and the mobile cannot automatically assume that the transmitter uses the weights that the mobile has instructed) and channel estimates can still be calculated from P-CPICHs.

The discussion on transmit diversity extensions to more than two transmit antenna systems was active in 3GPP for a long time [47]. The main concern was that the benefits from additional transmit antennas may not justify the additional complexity of transceiver and system design. A difficult backward compatibility with former releases is also encountered if the transmit power of common pilot channels is divided between, say, four transmit antennas to support channel estimation in mobile receivers. Then legacy terminals that are able to receive only two pilot channels loose performance, because they loose half of the available power of the common pilot signals. At the time of writing, proposed extensions of transmit diversity techniques have been withdrawn and the focus has been shifted to the specification of information MIMO techniques.

3 Closed-Loop Transmit Diversity

Beginning from [45], [48] and [49] a huge amount of papers on open-loop transmit diversity methods such as space-time block and trellis codes have been published. At the same time the number of publications that focus on closed-loop methods with partial CSI has been smaller. It seems that only transmit antenna selection is widely studied in the literature. For closed-loop methods with partial CSI a good quantization is needed which leads to a difficult problem that usually allows only numerical solutions. This problem makes the general analysis of closed-loop methods very difficult.

In spite of above-mentioned problem the analysis of closed-loop methods can be carried out in some interesting and practically viable cases. Besides the well-known transmit antenna selection we introduce and analyze two basic types of suboptimal closed-loop transmit diversity methods. The design of these methods is motivated by the UTRA FDD closed-loop transmit diversity mode 1 and 2. Therefore we will call them in the following as extended mode 1 (e-mode 1) and extended mode 2 (e-mode 2).

After introducing the system model in Section 3.1 we represent SNR gain analysis of e-mode 1 and 2 in Section 3.2. The content of Section 3.2 is based on [1], [2] and [3] while [7], [9] and [12] provide some additional information. Previously, SNR gain analysis for some closed-loop methods was also represented in [50] and [51].

The capacity analysis of Section 3.3 relies on [6], see also [11]. Previously, a generic capacity analysis for methods with CSI at the transmitter has been given in [53] while [54] provides explicit capacity formulas in case of receiver selection combining and MRC. As such the results in [54] can be also used for the analysis of transmitter selection combining and orthogonal space-time block codes.

Method for the BEP computation in Section 3.4 is due [5]. Also [55], [56] and [57] represent similar results in terms of bit error probability but [55] provides mainly simulation results, [56] assumes delayed ideal feedback while analysis of [57] focuses on corrupted feedback. The effect of feedback bit errors is considered in Section 3.5 based on results of [4]. The effect of feedback errors has also been studied in [15] where the site selection diversity transmission is investigated and in [57] where feedback system model is different from the model used in [4].

Finally, we note that also the effect of channel polarization to the performance of TD can be studied as is done in [14] where the performance of some simple TD techniques was considered assuming a channel model which takes into account the channel polarization [30]. Besides the conventional OL TD methods of [14], polarization matching (or polarization steering) has been investigated [10]. In polarization matching base station employs the information concerning the uplink channel polarization when selecting downlink transmit weights. This method was demonstrated in [59] and [60] showing

that the polarization matching can be feasible in mobile environments.

3.1 System Model, Algorithms and Performance Measures

System model for the CL TD methods is given in Figure 3. We denote by M_t the number of transmit antennas and by L we refer to the number of channel paths. Corresponding impulse responses are denoted by $h_{m,l}$, where l is the channel path number and m defines the channel between mth transmit and receive antenna. It is assumed that impulse responses are uncorrelated complex zero-mean Gaussian. If M_t or L is 1 we simply neglect the corresponding index.

Signal Model

We have only a single receive antenna in the mobile and the columns $\mathbf{h}_m$ of channel matrix $\mathbf{H}$ consist of channel taps $h_{m,l}$. in the presence of closed-loop transmit diversity the received signal in the mobile station is of the form

$$\mathbf{r} = (\mathbf{H}\mathbf{w})s + \mathbf{n},$$

where s is the transmitted symbol, $\mathbf{n}$ contains zero-mean Gaussian noise samples and $\mathbf{w} \in \mathbb{C}^{M_t}$ consists of complex transmit weights such that $\|\mathbf{w}\| = 1$. We assume that the channel matrix $\mathbf{H}$ is perfectly known in the receiver. In UTRA FDD two-antenna CL modes $\mathbf{H}$ is estimated from P-CPICH and transmit weights are applied on DPDCH or HS-DSCH.

Provided that quantized set $\mathbf{W}$ of feedback weights is given, the selection of the most suitable transmit weight vector $\hat{\mathbf{w}}$ can be based on the received SNR, *i.e.* we solve the problem

$$\text{Find } \hat{\mathbf{w}} \in \mathbf{W}: \qquad \|\mathbf{H}\hat{\mathbf{w}}\| = \max_{\mathbf{w}\in\mathbf{W}} \|\mathbf{H}\mathbf{w}\|. \tag{1}$$

Instead of SNR other measures such as channel capacity or bit-error rate could be used. However, SNR provides the simplest practical measure.

Instead of defining an explicit quantization scheme as in (1), CSI feedback can be modelled statistically, giving rise to mean feedback and covariance feedback schemes [58]. With mean feedback the transmitter assumes that the channel coefficients are distributed according to multivariate complex Gaussian distribution $N(\mathbf{w}, \delta^2\mathbf{I})$, where $\mathbf{w}$ and δ^2 can be interpreted as the estimate of the channel based on the feedback and the variance of the estimate, respectively. In covariance feedback, the channel (known at the transmitter) is distributed as $N(\mathbf{0}, \mathbf{R})$. This can be interpreted to model a case where the channel is changing very rapidly and the mean feedback is unable to track or model the instantaneous channel dynamics. However, the geometrical properties of the channel change slowly, and it is in many cases realistic to assume that the transmitter may know the channel covariance matrix $\mathbf{R}$.

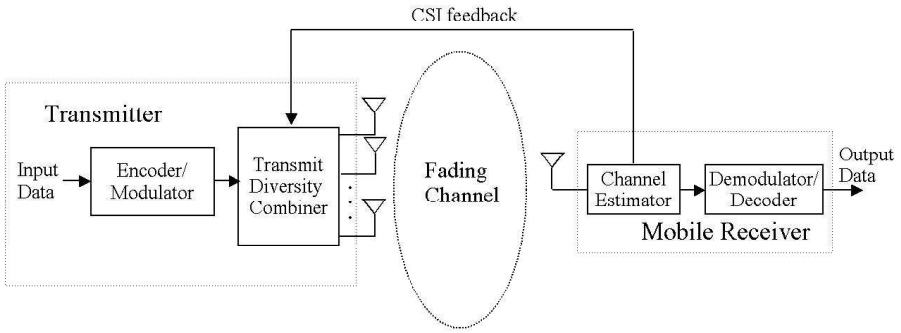

Figure 3: General system structure for CL TD.

In WCDMA, quantization of CSI is coarse and the capacity of the finite-rate feedback channel is defined explicitly. Thus, in this context it is more natural to study deterministic feedback strategies and characterize their performance given the number of quantization bits.

Feedback Channel

We begin by noticing that in the forthcoming discussion we will use 'feedback word' and 'transmit weight' interchangeably. In practice they are not the same but there is a one-to-one mapping between the quantization set and the set of feedback words.

Fundamental issues of control channels carrying short-term channel information are the very strict time delay and control overhead limits as well as the high robustness requirements. The use of strong error-correcting codes on the feedback channel is not a favorable solution, because coding increases signaling overhead and system may become complex, because the short-term feedback information needs to be decoded within a very short time frame. In the analysis of transmit diversity methods we assume a similar feedback channel structure as with the UTRA FDD closed-loop transmit diversity modes, where uncoded control information is transmitted to BS at each TTI in a dedicated control channel. Fast PC is applied to the uplink control channel so that the control information is received with approximately constant SNR and feedback bit errors can be assumed to be uniformly distributed in time. Hence, fast PC increases the robustness, because error bursts can be avoided and probability of feedback bit errors can be controlled with a proper transmit power.

Finally, we note that the effect of feedback latency is neglected in this study, which is approximately valid within low mobility environments. The effect of feedback delay to the performance of closed-loop transmit diversity is studied in [8], [56], [57] and [61].

Feedback Algorithms

With a given quantization (1) defines the weight that maximizes the SNR in the set of all weight vectors. When the number of antennas is small this approach can be viable, but in general case such an exhaustive search is not a good solution because computational complexity in mobile station is growing exponentially with respect to the number of transmit antennas. Furthermore, since feedback capacity is usually strictly limited, it is advantageous if feedback words can be divided flexibly into independent subwords that can be used in the transmitter before the whole feedback word is received. If continuous feedback update is not possible, then either feedback delay is long — which means that algorithm is sensitive to mobile speed — or the required feedback capacity is high.

Keeping in mind the problems above we introduce three suboptimal algorithms. First we introduce the well-known selection algorithm

Transmitter Selection Combining (TSC). In this case the set of transmit weights consists of vectors $\mathbf{w} = (0, \ldots, 0, 1, 0, \ldots, 0)$, where the nonzero component indicates the best channel in terms of received SNR. Hence

$$\|\mathbf{H}\hat{\mathbf{w}}\| = \max\{\|\mathbf{h}_m\| : 1 \leq m \leq M_t\}.$$

Since the quantization set has M_t points, $\lceil \log_2(M_t) \rceil$ feedback bits are needed. TSC is very simple and it requires a low feedback capacity but later on we will see that its performance is not very good and it is sensitive to feedback errors.

As another example of a suboptimal algorithm we introduce extended mode 1 in which only the relative phases between signals from separate antennas are adjusted. This special form of the co-phasing algorithm has been addressed previously in [50], where it was assumed that a feedback word of length $M_t - 1$ bits is provided to the base station having M_t antenna elements. Thus, the feedback word consists of information about the state of each relative phase between reference antenna and other $M_t - 1$ antennas. A generalization utilizing N_{rp} feedback bits/relative phase is given by the following algorithm.

Extended Mode 1 (e-mode 1). Here feedback bits are selected antenna wise using the condition

$$\|\mathbf{h}_1 + \hat{v}_m \mathbf{h}_m\| = \max\{\|\mathbf{h}_1 + v_m \mathbf{h}_m\| : v_m = e^{j2\pi(n-1)/2^{N_{\mathrm{rp}}}},\ 1 \leq n \leq 2^{N_{\mathrm{rp}}}\}.$$

The components of the final transmit weight $\hat{\mathbf{w}}$ are of the form

$$\hat{w}_m = \frac{1}{\sqrt{M_t}} \begin{cases} 1, & m = 1, \\ \hat{v}_m, & m > 1. \end{cases}$$

That is, each phase is adjusted independently against the phase of the first channel. It should be noticed that the complexity of the example algorithm increases linearly with additional antennas, *i.e.*, complexity is proportional to $(M_t - 1)2^{N_{\mathrm{rp}}}$. The feedback word in e-mode 1 can be divided into $M_t - 1$ subwords which all can be used independently in the transmitter. Therefore the required feedback overhead is not very high and computational work in mobile terminal can be spread to a longer time interval. We also note that since e-mode 1 applies only phase adjustments, the transmit antennas can maintain power balance which is advantageous in some practical systems.

A natural generalization to the above scheme is to weight transmit amplitudes in addition to adjusting phase differences. Intuitively, the stronger the channel, the more power should be transmitted through it. Bearing this in mind we give the following more feedback scheme, which provides a generalization for e-mode 1.

Extended Mode 2 (e-mode 2). In this algorithm receiver ranks some or all $\{\|h_m\|\}_{m=1}^{M_t}$ and selects the phase feedback by applying e-mode 1. Order and phase difference information is signaled to the transmitter which then chooses appropriate amplitude and phase weights from a finite set of transmit weights.

A crucial question when applying e-mode 2 is the selection of a suitable quantizer. This problem will be studied in detail in Section 3.2. Here we only briefly note that uniform quantizer suffices for the quantization of the phase differences, but finding a good quantizer for transmit powers is not any more a trivial task. If the number of transmit antennas is small then the quantization for amplitude weights can be found using simulations but when the number of transmit antennas is large, it can become a cumbersome task.

The length of the feedback word in e-mode 2 depends on the design, but if full order information is signaled, then at least $\lceil \log_2(M_t!) \rceil$ order bits are needed in addition to $(M_t - 1)N_{\mathrm{rp}}$ phase bits. The design that uses separate subwords corresponding to each antenna requires $M_t \lceil \log_2(M_t) \rceil$ order bits.

We remark that when $M_t = 2$ and $N_{\mathrm{rp}} = 2$ e-mode 1 resembles UTRA FDD closed-loop transmit diversity mode 1. The only difference between UTRA mode 1 and e-mode 1 is that in UTRA mode 1 the feedback word results from the interpolation between two consecutive one–bit feedback words. However, the difference is irrelevant here because feedback delay is not taken into account. Similarly, when $M_t = 2$ and $N_{\mathrm{rp}} = 3$ e-mode 2 coincides with UTRA closed-loop transmit diversity mode 2.

Both e-modes are clearly suboptimal and their performance could be improved without changing the quantization by determining the feedback word jointly across transmit antennas instead of independently for each transmit antenna. However, derivation of analytical results for joint quantization

when $M > 2$ becomes significantly more involved that with independent quantization. Furthermore, joint quantization would make the computational complexity exponential with respect to the number of transmit antennas. Another approach to reduce the computational complexity is to update feedback word iteratively exploiting the memory of the fading channel, and restrict the search of a new transmit weight vector to the neighborhood of the current weight [62]. The performance of such a scheme depends intimately on the fading rate of the channel and feedback delay which complicates the analysis.

In addition to independent quantization of transmit weights with respect to a reference antenna, e-mode is suboptimal, because amplitude and phase difference of transmit weights are adjusted independently, which is similar to polar quantization [103]. In [63, 64], a design criterion for quantization is developed that is based on the minimization of maximum correlation between the codewords. Codebooks for different number of transmit antennas and feedback bits are then determined by computer search given the design criterion. In these codebooks, amplitude and phase are quantized jointly.

Codebooks developed in [63, 64] do not facilitate continuous update of feedback word, because bits in the feedback words do not correspond directly to transmit antennas. On the other hand, without feedback latency and feedback errors, performance of the codebooks [63, 64] is necessary better than that of the suboptimal e-modes — provided that the computer search resulted in a good codebook. However, in practical wireless communication systems differences between the two approaches are small, because the number of codewords and the number of transmit antennas is limited.

SNR Gain and Fading Figure

The performance of various diversity methods is usually studied by using expected receiver bit-error probability or link capacity as a measure. Besides these approaches the computation of expected SNR in the receiver provides a simple and useful indicator that illustrates the benefit of closed-loop transmit diversity. This is based on the fact that SNR gain provides information concerning the coherent combining, or beamforming, benefit inherent to successful closed-loop processing of the transmitted signal. We define the SNR gain simply by

$$\mathcal{G} = \mathrm{E}\{\|\mathbf{H}\hat{\mathbf{w}}\|^2\}, \quad \|\hat{\mathbf{w}}\| = 1, \quad \mathrm{E}\{\|\mathbf{h}_m\|^2\} = 1, \tag{2}$$

where $\hat{\mathbf{w}}$ is the transmit weight vector defined by the feedback algorithm. At this stage we introduce notations

$$\gamma_m = \|\mathbf{h}_m\|^2, \quad z = \|\mathbf{H}\mathbf{w}\|^2 \tag{3}$$

that will be found useful later. We note that the former notation of (3) is applied only when the scaling in (2) is valid.

By using Schwarz inequality we find that

$$\mathcal{G} \leq \mathrm{E}\{\|\mathbf{H}\|^2\} \cdot \|\hat{\mathbf{w}}\|^2 = M_t. \tag{4}$$

Hence, maximum achievable SNR gain is given by the number of transmit antennas. On the other hand, if feedback information is not available and transmit weights are randomly selected, then there is no coherent combining gain and $\mathcal{G} = 1$. In flat Rayleigh fading channel the bound (4) is obtained by ideal feedback $\hat{w}_m = \bar{h}_m / \|\mathbf{H}\|$.

The drawback of SNR gain is that it does not indicate the diversity benefit that can be better illustrated through the fading figure defined by

$$\mathcal{F} = \frac{\mathcal{G}^2}{\mathrm{E}\{(\|\mathbf{H}\hat{\mathbf{w}}\|^2 - \mathcal{G})^2\}} = \frac{\mathcal{G}^2}{\mathrm{E}\{\|\mathbf{H}\hat{\mathbf{w}}\|^4\} - \mathcal{G}^2} \tag{5}$$

that takes into account also the second moment of SNR. For a flat Rayleigh fading channel $\mathcal{F} = 1$. When a closed-loop transmit diversity method is used the value of the fading figure becomes larger than one indicating the decrease in signal variation. If the variation of the signal power is fully compensated, then the channel seen by the receiver is static and $\mathcal{F} = \infty$.

Figure 4 displays the received SNR as a function of time for SISO and eight-antenna MISO with ideal feedback. It is found that besides the SNR gain the signal variation is remarkably reduced in case of closed-loop MISO. The 90% probability thresholds for SNRs are plotted using dashed lines while the expected SNRs are expressed using solid lines.

Link Capacity

Link capacity is probably the most popular analytical performance measure. In Section 3.3 we focus on two cases. First we consider the channel capacity in the presence of constant transmit power and receiver CSI only. Then capacity is of the form

$$C_{\mathrm{ora}}(\bar{\gamma}) = B \cdot \mathrm{E}\{\log_2(1 + \bar{\gamma} z)\}, \tag{6}$$

where B [Hz] is the channel bandwidth, $\bar{\gamma}$ is the mean SNR and z refers to the instantaneous received SNR [52], [53]. This expression is also referred to as average channel capacity [52], because it is obtained by averaging over the channel states. In case of closed-loop transmit diversity methods $z = \|\mathbf{H}\hat{\mathbf{w}}\|^2$.

Capacity (6) is a suitable performance measure in HSDPA where power control is not applied on shared channel. In dedicated data channels fast power control aims to invert the channel and a more appropriate performance measure is given by the capacity

$$C_{\mathrm{cifr}}(\bar{\gamma}) = B \cdot \log_2 \Big(1 + \bar{\gamma} / \mathrm{E}\{1/z\}\Big) \tag{7}$$

that is valid when transmitter adapts its power to maintain a constant SNR at the receiver and fixed coding and modulation is applied [53].

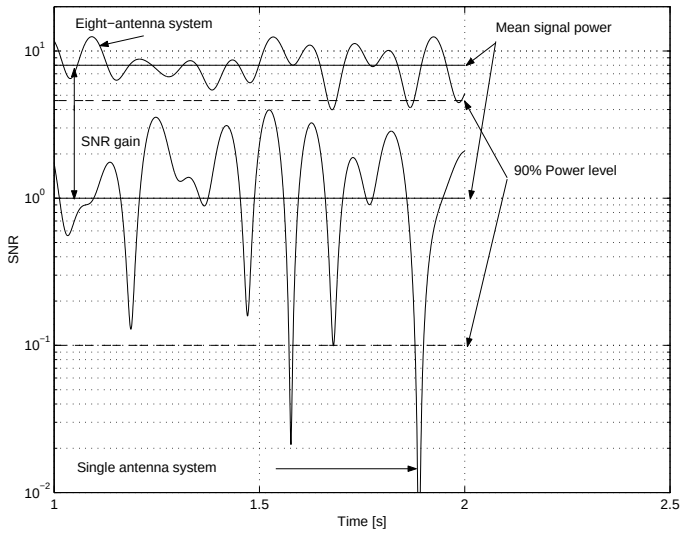

Figure 4: Received SNR for SISO (lower curve) and eight-antenna MISO (upper curve) with ideal feedback. Dashed lines: 90% level of SNR. Solid lines: mean SNR. Single path Rayleigh fading channel is assumed.

Bit-Error Probability (BEP)

The SNR gain and fading figure are valuable *relative* measures for the link performance and capacity gives good fundamental performance information. The BEP, however, provides a concrete and practical performance measure that can be directly used in system design. In general, BEP is defined by

$$P_{\mathrm{e}}(\bar{\gamma}) = \mathrm{E}\{P_{\mathrm{mod}}(\bar{\gamma} \cdot z)\}, \tag{8}$$

where P_{mod} is the error rate of the applied modulation in terms of received SNR. Similarly with the capacity this approach leads to very difficult equations when certain feedback algorithms are studied. In Section 3.4 we deduce an asymptotic formula for (8) in two-antenna case and provide an accurate approximation that is valid in the whole SNR scale.

3.2 Analysis Based on SNR Gain and Fading Figure

In the analysis we first compute the SNR gain for e-mode 1 and 2. During the analysis we deduce an amplitude weight quantization for e-mode 2 that is based on the order information. After showing general results that are valid in case $M_t > 1$ we give an extended analysis in two-antenna case. With this limitation the computation of fading figure is simplified and, on the other hand, we are able to extend the analysis to the case of multi-path fading. Besides the SNR gain computation we show that amplitude quantization for

e-mode 2 does not depend on the temporal channel profile as long as channel taps are uncorrelated complex zero-mean Gaussian.

Analysis of SNR Gain in Flat Rayleigh Fading

The simplest example of a closed-loop algorithm is provided by TSC. Since we use the performance of this algorithm as a baseline reference we recall that SNR for TSC is given by

$$\mathcal{G} = \sum_{m=1}^{M_t} \frac{1}{m}.$$

This formula is known already from [65] and it indicates that SNR gain of the TSC against the single antenna system is proportional to $\log(M_t)$ for large M_t.

The main benefit of TSC is the small feedback overhead requirement that makes it attractive from practical implementation point of view. The main drawbacks of TCS are the poor performance - when compared against more sophisticated closed-loop algorithms - and sensitivity to feedback errors [4].

The computation of SNR gain for e-mode 1 and 2 can be carried out following [1] and [2]. We note that SNR gain for e-mode 1 in case $N_{\mathrm{rp}} = 1$ was also given in [50]. Since e-mode 1 is a special case of e-mode 2 we consider first e-mode 2. Then we can write $\mathbf{Hw} = \tilde{\mathbf{H}}\mathbf{u}$, where $\mathbf{u}$ consists of real amplitude weights and $\tilde{\mathbf{H}}$ contains channel coefficients after the phase adjustments. The expectation of the received SNR in the mobile is now of the form

$$\mathrm{E}\{z\} = \mathbf{u}^T \mathrm{E}\{\tilde{\mathbf{H}}^H \tilde{\mathbf{H}}\}\mathbf{u} = \mathbf{u}^T \mathbf{R}_{\mathrm{fb}} \mathbf{u}, \tag{9}$$

where $\mathbf{R}_{\mathrm{fb}}$ is the covariance matrix corresponding to the adjusted channels. Hence, the use of short-term feedback introduces beneficial long-term correlation. The elements of $\mathbf{R}_{\mathrm{fb}}$ are given by

$$(\mathbf{R}_{\mathrm{fb}})_{m,k} = \mathrm{Re}\big\{\mathrm{E}\{\sqrt{\gamma_m \gamma_k} \cdot e^{j\psi_{m,k}}\}\big\} = \mathrm{E}\{\sqrt{\gamma_m \gamma_k}\}\mathrm{Re}\big\{\mathrm{E}\{e^{j\psi_{m,k}}\}\big\}, \tag{10}$$

where $\psi_{m,k} = \phi_m - \phi_k$ is the difference between mth and kth adjusted phases. If there are $(M_t - 1)N_{\mathrm{rp}}$ phase bits available, then $\phi_1 = 0$ and ϕ_m, $m > 1$, is uniformly distributed on $(-\pi/2^{N_{\mathrm{rp}}}, \pi/2^{N_{\mathrm{rp}}})$. In (10) the second equality holds because phase and order information are applied independently and phase and amplitude of a zero-mean Gaussian variable are uncorrelated. Let us compute the latter expectation. If $m > 1$ we have

$$\mathrm{E}\{\cos\psi_{m,1}\} = \frac{2^{N_{\mathrm{rp}}-1}}{\pi} \int_{-\pi/2^{N_{\mathrm{rp}}}}^{\pi/2^{N_{\mathrm{rp}}}} \cos\psi \, d\psi = \frac{2^{N_{\mathrm{rp}}}}{\pi} \sin\left(\frac{\pi}{2^{N_{\mathrm{rp}}}}\right) =: c_{N_{\mathrm{rp}}}. \tag{11}$$

The expectation for $\cos\psi_{m,k}$, $m, k > 1$, $m \neq k$ is computed by applying the identity $\psi_{m,k} = \psi_{m,1} - \psi_{k,1}$ and cosine summation formula. Since $\psi_{m,1}$ and

$\psi_{k,1}$ are independent if $m \neq k$ we obtain

$$\mathrm{E}\{\cos\psi_{m,k}\} = \mathrm{E}\{\cos\psi_{m,1}\}\mathrm{E}\{\cos\psi_{k,1}\} = c_{N_{\mathrm{rp}}}^2. \tag{12}$$

In case of e-mode 1 there is only phase information available and we set $u_m = 1/\sqrt{M_t}$. Furthermore, since amplitudes are uncorrelated and follow Rayleigh distribution, there holds

$$\mathrm{E}\{\sqrt{\gamma_m\gamma_k}\} = \mathrm{E}\{\sqrt{\gamma_m}\}\mathrm{E}\{\sqrt{\gamma_k}\} = \frac{\pi}{4},\ m \neq k. \tag{13}$$

After combining (10)-(13) we find that

$$\begin{aligned} &(\mathbf{R}_{\mathrm{fb}})_{m,m} = 1,\ (\mathbf{R}_{\mathrm{fb}})_{m,1} = (\mathbf{R}_{\mathrm{fb}})_{1,m} = \frac{\pi c_{N_{\mathrm{rp}}}}{4},\ m > 1, \\ &(\mathbf{R}_{\mathrm{fb}})_{m,k} = (\mathbf{R}_{\mathrm{fb}})_{k,m} = \frac{\pi c_{N_{\mathrm{rp}}}^2}{4},\ m \neq k,\ k \neq 1. \end{aligned} \tag{14}$$

The SNR gain of e-mode 1 is obtained by using elements (14) in (9). After some elementary manipulations it is found that

$$\mathcal{G} = 1 + \frac{M_t - 1}{2M_t}\Big(1 + \frac{M_t - 2}{2} \cdot c_{N_{\mathrm{rp}}}\Big) \cdot \pi c_{N_{\mathrm{rp}}}. \tag{15}$$

Hence, in contrast to TSC the SNR gain grows linearly with respect to the number of antennas. In the presence of ideal phasing information in the transmitter we have

$$c_\infty = \lim_{N_{\mathrm{rp}} \to \infty} c_{N_{\mathrm{rp}}} = 1.$$

Then the upper bound for the SNR gain due to the phasing is given by

$$\mathcal{G} = 1 + \frac{\pi}{4}(M_t - 1).$$

Figure 5 shows the SNR gain for e-mode 1 and TSC in terms of the number of transmit antennas. The results show that most of the achievable SNR gain from phase adjustments is obtained when $N_{\mathrm{rp}} = 3$. Antenna selection is clearly inferior to e-mode 1 when $N_{\mathrm{rp}} > 1$ but if $N_{\mathrm{rp}} = 1$ there is not much difference in performance provided that the number of transmit antennas is small.

If order information is available in the transmitter we indicate it by brackets around the channel index. Then $\gamma_{(m)} \geq \gamma_{(k)}$ if $m > k$ and equation (13) is not valid any more because ordered amplitudes are not uncorrelated. By using (10)-(12) we find that

$$(\mathbf{R}_{\mathrm{fb}})_{m,k} = \mathrm{E}\{\sqrt{\gamma_{(m)}\gamma_{(k)}}\}\epsilon_{m,k} = \varrho_{m,k}\epsilon_{m,k},$$

where $\varrho_{m,k}$ is a correlation due to the order statistics and $\epsilon_{m,k} = c_{N_{\mathrm{rp}}}$ if $k = 1$ or $m = 1$ and $\epsilon_{m,k} = c_{N_{\mathrm{rp}}}^2$ otherwise. Phasing and ordering together

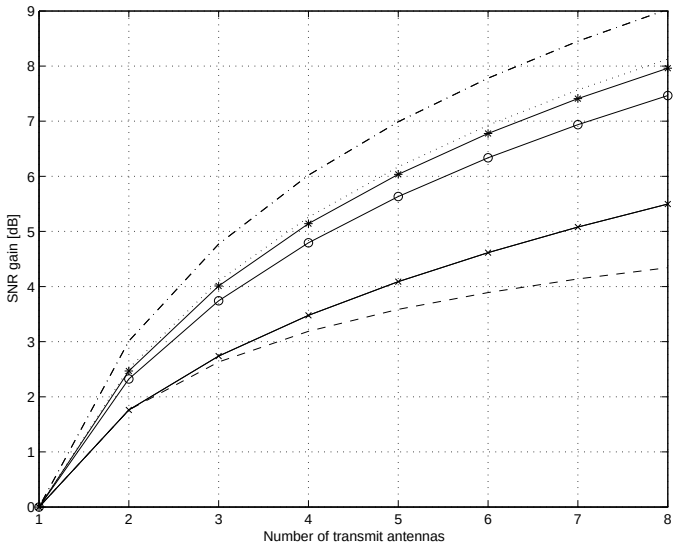

Figure 5: SNR gain for e-mode 1 as a function of the number of transmit antennas when $N_{\mathrm{rp}} = 1$ (x), $N_{\mathrm{rp}} = 2$ (o) and $N_{\mathrm{rp}} = 3$ (*). Dashed curve refers to the SNR gain of TSC, dotted curve defines the SNR gain of e-mode 1 when $N_{\mathrm{rp}} \to \infty$ and dashed and dotted curve shows the SNR gain in case of ideal CSI.

introduce a certain long-term signal statistics that defines an amplitude weight quantization through the eigenvectors of $\mathbf{R}_{\mathrm{fb}}$. Then, the SNR gain for e-mode 2 is given by

$$\mathcal{G} = \lambda_{\max} = \max\{\lambda : \mathbf{R}_{\mathrm{fb}}\mathbf{u} = \lambda\mathbf{u}\}.$$

Thus, the SNR gain is defined by the largest eigenvalue of $\mathbf{R}_{\mathrm{fb}}$. Since all channel orderings are equally probable the amplitude weight quantization consists of permutations of the eigenvector corresponding to the largest eigenvalue. Then

$$\mathbf{U} = \{\sigma_{\mathrm{p}}(\mathbf{u}) : \mathbf{R}_{\mathrm{fb}}\mathbf{u} = \lambda_{\max}\mathbf{u},\ \|\mathbf{u}\| = 1\}, \tag{16}$$

where $\sigma_{\mathrm{p}}(\mathbf{u})$ refers to a permutation of $\mathbf{u}$. In general the computation of moments $\varrho_{m,k}$ is difficult. Closed-form expressions for $\varrho_{m,k}$ in the presence of flat Rayleigh fading are given in [1] and [2] based on previous results in [66]. In case of Rice and Nakagami fading and two transmit antennas moments $\varrho_{m,k}$ are evaluated in [9] and [12]. In [7] multi-path Rayleigh fading is assumed and moments $\varrho_{m,k}$ are obtained by simulations.

Figure 6 displays SNR gain for e-mode 2 when $N_{\mathrm{rp}} = 1$, 2 and 3. By comparing Figures 5 and 6 it is seen that additional gain from order information is noticeable but since the signalling overhead is rapidly increasing with

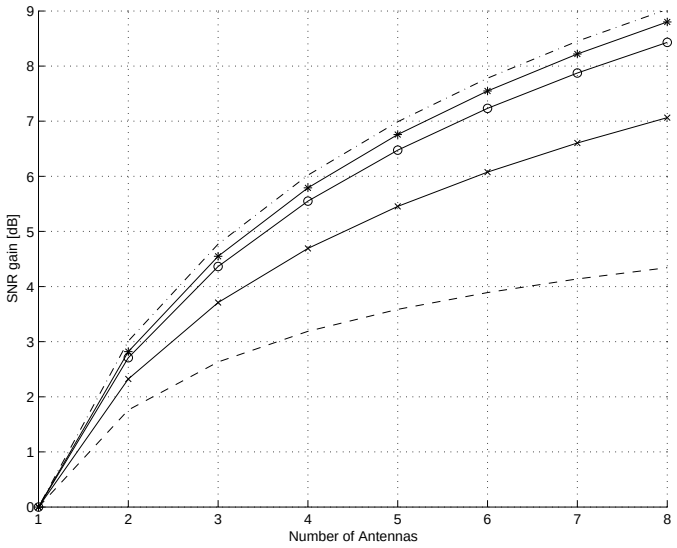

Figure 6: SNR gain for e-mode 2 as a function of the number of transmit antennas when $N_{\mathrm{rp}} = 1$ (x), $N_{\mathrm{rp}} = 2$ (o) and $N_{\mathrm{rp}} = 3$ (*). Dashed curve refers to the SNR gain of TSC and dashed and dotted curve shows the SNR gain in case of ideal CSI.

additional antennas, the use of full order may be practically viable only if the number of antennas is small. Figure 6 also indicates that e-mode 2 with full order and 3-bit phasing information is able to provide almost optimal SNR gain if the number of transmit antennas is small.

For the e-mode 2 the main problem is the feedback overhead $\lceil \log_2(M_t! \cdot 2^{(M_t-1)N_{\mathrm{rp}}}) \rceil$ which grows rapidly with additional antennas. An other problem that is of great practical importance is that the amplitude statistics may vary in different environments and weight quantization that is suitable, for example, in Rayleigh fading environment is not optimal in the presence of LOS where channel gain follows Rician distribution [9], [12]. Former problem can be solved by applying a reduced order information where only the order of few best channels are signalled to the base station [1]. Concerning the latter problem we will later show that in case of two antennas the weight quantization does not depend on the multi-path profile if channel path impulse responses are uncorrelated zero-mean Gaussian.

Fading Figures for Two-Antenna System

The two-antenna case is important, because UTRA FDD specifications includes closed-loop mode 1 and 2 that are special cases of e-mode 1 and 2. While previous discussion provides means for SNR gain computation our

goal here is to illustrate the diversity benefit of e-mode 1 and 2 through fading figure. This measure was first introduced in [67] and [68] and conventionally it is used as a fading parameter in Nakagami fading distribution that gives one-sided Gaussian distribution if $\mathcal{F} = 1/2$ and Rayleigh distribution if $\mathcal{F} = 1$. Values $\mathcal{F} < 1$ correspond to deeper fading than the Rayleigh while values $\mathcal{F} > 1$ represent shallower fading than the Rayleigh.

As a reference we use the fading figure of TSC and, on the other hand, the fading figure in case of ideal feedback. We begin with TSC. The probability density function (PDF) of maximum taken over M_t exponentially distributed variables is of the form

$$f(\gamma) = M_t e^{-\gamma}(1 - e^{-\gamma})^{M_t - 1} = \sum_{m=1}^{M_t} \binom{M_t}{m} (-1)^{m+1} m \cdot e^{-m\gamma},$$

where the latter equality is obtained by using the binomial expansion. Furthermore, after substituting $t = m\gamma$ and applying the definition of Gamma function ((6.1.1) of [69]) we find that

$$\int_0^\infty \gamma^n e^{-m\gamma} d\gamma = \frac{n!}{m^{n+1}}. \tag{17}$$

Hence,for TSC the moments of SNR are found to be

$$\mathrm{E}\{\gamma^n\} = \sum_{m=1}^{M_t} \binom{M_t}{m} \frac{(-1)^{m+1} n!}{m^n}, \qquad n \in \mathbb{N}. \tag{18}$$

If ideal CSI is available in the transmitter, SNR $\gamma = \|\mathbf{H}\|^2$ follows the χ^2 distribution with $2M_t$ degrees of freedom,

$$f(\gamma) = \frac{1}{\Gamma(M_t)} \gamma^{M_t - 1} e^{-\gamma}, \tag{19}$$

where Γ refers to the gamma-function. By (6.1.1) of [69] we find that the moments in case of ideal feedback are given by

$$\mathrm{E}\{\gamma^n\} = \Gamma(M_t + n)/\Gamma(M_t). \tag{20}$$

The fading figure for TSC can be computed by using (18) and for system with ideal feedback we can use (20). In the latter case it is easily seen that $\mathcal{F} = M_t$. Hence, in the presence of flat Rayleigh fading and partial feedback, the value of fading figure for any closed-loop algorithm is upper bounded by the number of transmit antennas.

Let us next consider the fading figure for e-mode 1 and 2 in case of two transmit antennas. The second moment of SNR for e-mode 1 and 2 can be computed from

$$\mathrm{E}\{z^2\} = \mathrm{E}\{\big(u_1^2 \gamma_{(1)} + u_2^2 \gamma_{(2)} + 2u_1 u_2 \sqrt{\gamma_{(1)}\gamma_{(2)}} \cos\phi\big)^2\}. \tag{21}$$

By expanding this formula we find that the required second moment is obtained provided that expectations

$$\mathrm{E}\{\cos^k\phi\},\ k\in\{1,2\},\quad \mathrm{E}\{\gamma_{(1)}^{2-\delta}\gamma_{(2)}^{\delta}\},\ \delta\in\{0,1/2,1,3/2,2\} \tag{22}$$

can be computed. The former expectation for $k=1$ is known from (11) and after a similar computation we find that

$$\mathrm{E}\{\cos^2\phi\} = 1/2\cdot(1+c_{N_{\mathrm{rp}}-1}). \tag{23}$$

It remains to compute the latter expectation in (22). We first note that the joint distribution of $\gamma_{(1)}$ and $\gamma_{(2)}$ is given by

$$f(\gamma_{(1)},\gamma_{(2)}) = 2\cdot\begin{cases} e^{-|\gamma|}, & \gamma_1\geq\gamma_2,\\ 0, & \text{otherwise,}\end{cases} \tag{24}$$

where we have denoted $\gamma=(\gamma_1,\gamma_2)$ and $|\gamma|=\gamma_1+\gamma_2$. Second expectation in (22) is not difficult to compute directly but instead we apply substitution, $\gamma_2=t\gamma_1$, change the order of the integration and then substitute $s=\gamma_1(1+t)$. Then we find that

$$\mathrm{E}\{\gamma_{(1)}^{2-\delta}\gamma_{(2)}^{\delta}\} = \int_0^\infty s^3e^{-s}ds\cdot\int_0^1\frac{2t^\delta dt}{(1+t)^4} = 6\cdot\int_0^1\frac{2t^\delta dt}{(1+t)^4} =: 6\cdot I_\delta. \tag{25}$$

We use this computation method because its idea is found useful later in the analysis of link capacity. The integral I_δ can be computed by using elementary means. Resulting formulas are

$$I_0=\frac{7}{12},\ I_{\frac{1}{2}}=\frac{1}{12}+\frac{\pi}{16},\ I_1=\frac{1}{6},\ I_{\frac{3}{2}}=-\frac{1}{12}+\frac{\pi}{16},\ I_2=\frac{1}{12}. \tag{26}$$

Based on (21), (11), (23), (25) and (26) we can compute the second moment of SNR in case of e-mode 1 and 2. Then, using the SNR gains that were computed in the previous section we obtain fading figures. Table 1 gives the fading figures for TSC, and e-mode 1 and 2. The results show that e-mode 1 and 2 provide clearly better fading figures than TSC but differences are small indicating that all studied methods provide good diversity gain. Since the fading figure for the Alamouti code [45] and for ideal CSI in the transmitter is 2, we note that closed-loop methods with partial side information are not able to provide full diversity benefit if it is measured in terms of fading figure.

SNR Gain in Multi-path Fading

Here we adopt a multi-path Rayleigh fading model and assume Rake combining over signal paths. Now $\mathbf{H}$ is a matrix with columns $\mathbf{h}_m$ that consists of the channel impulse responses $h_{m,l}$ corresponding to L channel paths.

TSC	e-mode 1, (2)	e-mode 1, (3)	e-mode 2, (2)	e-mode 2, (3)
1.8000	1.9104	1.9123	1.9867	1.9913

Table 1: Fading figures for TSC and two-antenna e-mode 1 and 2. The number of phase bits is given in brackets.

In multi-path Rayleigh fading model coefficients $h_{m,l}$ are independent zero-mean Gaussian random variables. Furthermore, we denote $\mathrm{E}\{|h_{m,l}|^2\} = 2\sigma_l^2$, $l = 1, 2, \ldots, L$ and use scaling

$$\mathrm{E}\{\|\mathbf{h}_m\|^2\} = 2\sum_{l=1}^{L} \sigma_l^2 = 1.$$

Consider the feedback quantization in a detailed manner. In two antenna case transmit weights are of the form $w_1 = u_1$, $w_2 = u_2 e^{j\phi}$, where $0 \leq u_1, u_2 \leq 1$ and uniform quantization of the phase ϕ is clearly a good choice if transmit antennas are uncorrelated. In the following we show that optimal amplitude weights are of the form

$$\hat{u}_{1,2} = \left\{ \frac{1}{2}\left(1 \pm \left(1 + \frac{\pi^2 c_{N_{\mathrm{rp}}}^2}{4}\right)^{-1/2}\right)\right\}^{1/2}, \tag{27}$$

where the '+' sign corresponds to the weight $\hat{u}_1$ of the stronger channel while the '-' sign corresponds to the weight $\hat{u}_2$ of the weaker channel. For flat fading this result is known already from [1]. However, it is not immediately clear that weights (27) represent the best choice also in the presence of multi-path Rayleigh fading. In fact, from [9] and [12] it is known that weights (27) are *not* optimal in Rice and Nakagami fading channels. This question on optimal weights is of interest because UTRA FDD standards specify fixed amplitude weights while applied 3GPP test channels use various profiles [70]. At this stage we note that specified amplitude weights in UTRA FDD are given by $u_1, u_2 \in \{\sqrt{0.8}, \sqrt{0.2}\}$ while numeric values of optimal weights according to (27) are $\sqrt{0.7735}$ and $\sqrt{0.2265}$. In flat Rayleigh fading channel the difference in obtained SNR gains when applying these different weights is of no practical meaning - it os less than 0.005 dB - but the squares of the specified weights admit a simple digital expression.

Let us consider the equation

$$\|u_1\mathbf{h}_{(1)} + u_2 e^{j\phi}\mathbf{h}_{(2)}\|^2 - \|u_2\mathbf{h}_{(1)} + u_1 e^{j\phi}\mathbf{h}_{(2)}\|^2 = (u_1^2 - u_2^2)\Big(\|\mathbf{h}_{(1)}\|^2 - \|\mathbf{h}_{(2)}\|^2\Big).$$

From this equation we find that independently from ϕ, the better SNR is always achieved if more power is allocated into the transmit antenna

providing larger received power. Based on this observation we assume that $u_1 > u_2$ in the following discussion. Further, we obtain

$$\|\mathbf{Hw}\|^2 = u_1^2\|\mathbf{h}_{(1)}\|^2 + u_2^2\|\mathbf{h}_{(2)}\|^2 + 2u_1u_2|\mathbf{h}_{(1)}^H\mathbf{h}_{(2)}|\cos\psi, \tag{28}$$

where $\psi = \phi + \theta$ and $\theta = \arg(\mathbf{h}_{(1)}^H\mathbf{h}_{(2)})$ is uniformly distributed on $(-\pi, \pi)$. We note that ψ and $|\mathbf{h}_{(1)}^H\mathbf{h}_{(2)}|$ are independent. Moreover, the order of channel vectors has no effect to the absolute value of the inner product between $\mathbf{h}_{(1)}$ and $\mathbf{h}_{(2)}$. After the adjustments the relative phase ψ is uniformly distributed on $(-\pi/2^{N_{\mathrm{rp}}}, \pi/2^{N_{\mathrm{rp}}})$. Then we have

$$\mathrm{E}\{z\} = \mathbf{u}^T\mathbf{R}_{\mathrm{fb}}\mathbf{u}, \quad \mathbf{R}_{\mathrm{fb}} = \begin{pmatrix} \mathrm{E}\{\|\mathbf{h}_{(1)}\|^2\} & c_{N_{\mathrm{rp}}}\mathrm{E}\{|\mathbf{h}_{(1)}^H\mathbf{h}_{(2)}|\} \\ c_{N_{\mathrm{rp}}}\mathrm{E}\{|\mathbf{h}_{(1)}^H\mathbf{h}_{(2)}|\} & \mathrm{E}\{\|\mathbf{h}_{(2)}\|^2\} \end{pmatrix}. \tag{29}$$

After these preparations we are ready to prove that (27) defines optimal weights also in case of multi-path Rayleigh fading when the paths are uncorrelated. Note this is also true for ideal CSI feedback and for Grassmanian codebooks [63, 64] as observed in [64].

Let $\hat{u}_1$ and $\hat{u}_2$ be the components of the eigenvector of the largest eigenvalue of $\mathbf{R}_{\mathrm{fb}}$, defined in (29). After solving the corresponding eigenvalue problem it is found that

$$\hat{u}_{1,2} = \left\{\frac{1}{2}\Big(1 \pm \Big(1+\rho^2\Big)^{-1/2}\Big)\right\}^{1/2} \tag{30}$$

where ρ is given by

$$\rho = \frac{2c_{N_{\mathrm{rp}}}\mathrm{E}\{|\mathbf{h}_{(1)}^H\mathbf{h}_{(2)}|\}}{\mathrm{E}\{\|\mathbf{h}_{(1)}\|^2\} - \mathrm{E}\{\|\mathbf{h}_{(2)}\|^2\}}. \tag{31}$$

Hence, by (27) it remains to show that $\rho = \pi c_{N_{\mathrm{rp}}}/2$. Since $\mathbf{h}_{(1)}$ and $\mathbf{h}_{(2)}$ consists of uncorrelated Gaussian zero-mean variables the following trick can be used: Assume e-mode 1 with $N_{\mathrm{rp}} = 1$ and define

$$\tilde{\mathbf{h}}_1 = \frac{1}{\sqrt{2}}\Big(\mathbf{h}_1 + \mathbf{h}_2\Big), \quad \tilde{\mathbf{h}}_2 = \frac{1}{\sqrt{2}}\Big(\mathbf{h}_1 - \mathbf{h}_2\Big). \tag{32}$$

Then it is evident that the SNR gain of e-mode 1 with $N_{\mathrm{rp}} = 1$ can be obtained from the formula

$$\mathcal{G} = \mathrm{E}\{\|\tilde{\mathbf{h}}_{(1)}\|^2\}. \tag{33}$$

Furthermore, it is not difficult to see that the elements of the vectors $\tilde{\mathbf{h}}_1$ and $\tilde{\mathbf{h}}_2$ are distributed identically with the elements of vectors $\mathbf{h}_1$ and $\mathbf{h}_2$. Thus,

$$\mathrm{E}\{\|\tilde{\mathbf{h}}_{(1)}\|^2\} = \mathrm{E}\{\|\mathbf{h}_{(1)}\|^2\}. \tag{34}$$

On the other hand, when computing the SNR gain of 1-bit phasing from (28) it is found that

$$\mathcal{G} = \frac{1}{2}\big(\mathrm{E}\{\|\mathbf{h}_{(1)}\|^2\} + \mathrm{E}\{\|\mathbf{h}_{(2)}\|^2\}\big) + c_1 \mathrm{E}\{|\mathbf{h}_{(1)}^H \mathbf{h}_{(2)}|\}. \tag{35}$$

By combining (33), (34), (35) and equality $c_1 = 2/\pi$ we find that

$$\mathrm{E}\{\|\mathbf{h}_{(1)}\|^2\} = \frac{1}{2}\big(\mathrm{E}\{\|\mathbf{h}_{(1)}\|^2\} + \mathrm{E}\{\|\mathbf{h}_{(2)}\|^2\}\big) + \frac{2}{\pi} \cdot \mathrm{E}\{|\mathbf{h}_{(1)}^H \mathbf{h}_{(2)}|\}. \tag{36}$$

From (31) and (36) it is seen that $\rho = \pi c_{N_{\mathrm{rp}}}/2$ in (30) and thus, the shape of the delay profile does not effect the value of the optimal weights as far as channel paths are uncorrelated and Rayleigh fading is assumed.

Let us next consider the SNR gain for two-antenna e-mode 1 and 2 in the presence of multi-path fading. For e-mode 1 it is seen from (28) that

$$\mathcal{G} = 1 + c_{N_{\mathrm{rp}}} \mathrm{E}\{|\mathbf{h}_{(1)}^H \mathbf{h}_{(2)}|\}. \tag{37}$$

Before giving the expectation in (37) we deduce a similar expression for the SNR gain of mode 2. By computing the largest eigenvalue of $\mathbf{R}_{\mathrm{fb}}$, defined in (29), we obtain

$$\mathcal{G} = 1 + \Big(1 - \mathrm{E}\{\|\mathbf{h}_{(1)}\|^2\}\mathrm{E}\{\|\mathbf{h}_{(2)}\|^2\} + c_{N_{\mathrm{rp}}}^2 E\{|\mathbf{h}_{(1)}^H \mathbf{h}_{(2)}|\}^2\Big)^{\frac{1}{2}}. \tag{38}$$

Keeping in mind the scaling

$$\mathrm{E}\{\|\mathbf{H}\|^2\} = \mathrm{E}\{\|\mathbf{h}_{(1)}\|^2\} + \mathrm{E}\{\|\mathbf{h}_{(2)}\|^2\} = 2 \tag{39}$$

we find from (36) that

$$\mathrm{E}\{\|\mathbf{h}_{(1)}\|^2\} = 1 + \frac{2}{\pi} E\{|\mathbf{h}_{(1)}^H \mathbf{h}_{(2)}|\},\ \mathrm{E}\{\|\mathbf{h}_{(2)}\|^2\} = 1 - \frac{2}{\pi} E\{|\mathbf{h}_{(1)}^H \mathbf{h}_{(2)}|\}. \tag{40}$$

After combining (38) and (40) we finally obtain the following form for the SNR gain of e-mode 2,

$$\mathcal{G} = 1 + \Big(\frac{4}{\pi^2} + c_{N_{\mathrm{rp}}}^2\Big)^{\frac{1}{2}} \mathrm{E}\{|\mathbf{h}_{(1)}^H \mathbf{h}_{(2)}|\}. \tag{41}$$

Thus, for final SNR gain formulas of e-mode 1 and 2 it remains to compute $\mathrm{E}\{|\mathbf{h}_{(1)}^H \mathbf{h}_{(2)}|\}$. This has been done in [3] where it was shown that

$$\mathrm{E}\{|\mathbf{h}_{(1)}^H \mathbf{h}_{(2)}|\} = \frac{\pi}{2} \sum_{l=1}^{L} \sigma_l^2 \prod_{k=1, k\neq l}^{L} \frac{\sigma_l^4}{\sigma_l^4 - \sigma_k^4}. \tag{42}$$

This formula is valid provided that mean path powers are distinct. In the presence of multiple receive antennas and single path channel we can use Lemma 2 of [3],

$$\mathrm{E}\{|\mathbf{h}_{(1)}^H \mathbf{h}_{(2)}|\} = \sqrt{\pi} \cdot \Gamma(M_r + 1/2).$$

Channel profile	Rayleigh	Ped. A	Ped. B	Veh. A
e-mode 1, $N_{\mathrm{rp}} = 1$	1.7609 dB	1.7446 dB	1.3012 dB	1.3839 dB
e-mode 1, $N_{\mathrm{rp}} = 2$	2.3226 dB	2.3024 dB	1.7436 dB	1.8489 dB
e-mode 1, $N_{\mathrm{rp}} = 3$	2.4683 dB	2.4472 dB	1.8603 dB	1.9712 dB
e-mode 2, $N_{\mathrm{rp}} = 1$	2.3226 dB	2.3024 dB	1.7436 dB	1.8489 dB
e-mode 2, $N_{\mathrm{rp}} = 2$	2.7092 dB	2.6865 dB	2.0549 dB	2.1748 dB
e-mode 2, $N_{\mathrm{rp}} = 3$	2.8199 dB	2.7966 dB	2.1450 dB	2.2690 dB

Table 2: SNR gains for two-antenna e-mode 1 and 2 assuming different channel profiles of [70].

The formula in general case, where the number M_r of receive antennas is larger than one and multi-path channel is assumed, can be deduced similarly with (42).

Table 2 depicts the obtained SNR gains for e-mode 1 and 2 when $M_r = 1$ and different channel profiles are assumed. Results show that SNR gains of e-mode 1 and 2 are noticeably corrupted due to the multi-path fading. Finally, we note that the SNR gain in the presence of multi-path Rayleigh fading is also studied in [7] where the case $M_t > 2$ is considered.

3.3 Computation of Link Capacity

Here we consider the link capacity for e-mode 1 and 2. First we focus on capacity (6) that assumes constant transmit power and optimal rate adaptation to the channel fading. As mentioned, capacity (6) is an appropriate performance measure in HSDPA where power control is not applied on the shared channel.

It will turn out, however, that the computation of exact closed-form expression for (6) is extremely difficult in case of closed-loop transmit diversity methods. Contrary to exact expression a simple upper bound can be obtained through the estimate

$$C_{\mathrm{ora}}(\bar{\gamma}) \leq B \cdot \log_2\left(1 + \bar{\gamma} \cdot \mathrm{E}\{z\}\right) = B \cdot \log_2\left(1 + \bar{\gamma} \cdot \mathcal{G}\right) \tag{43}$$

that applies the fact that logarithm is a concave function. Hence the capacity of a closed-loop transmit diversity method is upper bounded by the capacity of AWGN channel where mean SNR is scaled by the SNR gain $\mathcal{G}$. Since (43) provides only a loose bound it is of interest to find a better estimate for capacity (6). In this section we introduce such a simple and accurate approximation and also provide an error analysis for the given approximation in case of two transmit antennas.

We recall that by (3) the instantaneous received SNR for a closed-loop

transmit diversity method can be expressed in the form

$$z(\gamma,\phi) = \Big| \sum_{m=1}^{M_t} \hat{u}_m \sqrt{\gamma_m} \cdot e^{j\phi_m} \Big|^2, \quad \gamma_m = |h_m|^2, \tag{44}$$

where $\phi_1 = 0$ and adjusted phases ϕ_m, $m = 2, 3, \ldots, M_t$ are uniformly distributed on the interval $(-\pi/2^{N_{\mathrm{rp}}}, \pi/2^{N_{\mathrm{rp}}})$. In general the distribution of z is difficult to deduce but (44) indicates that SNR gain can be computed provided that distributions of γ and ϕ are known. Since channel coefficients are uncorrelated and phase and amplitude adjustments are done independently we find that

$$f(\gamma,\phi) = f(\gamma)f(\phi) = f(\gamma) \prod_{m=2}^{M_t} f_m(\phi_m), \quad |\gamma| = \sum_{m=1}^{M_t} \gamma_m, \tag{45}$$

where f_m refer to the uniform distribution function corresponding to ϕ_m, resulting from the N_{rp}-bit phase adjustments. The distribution of γ depends on the amplitude information. In case of e-mode 1 there is no such information and $f(\gamma) = e^{-|\gamma|}$.

Computation of capacity (6) can be based on the conditional distribution. Then

$$C_{\mathrm{ora}}(\bar{\gamma}) = B \int \log_2(1 + \bar{\gamma} \cdot z(\gamma,\phi)) f(\gamma,\phi) d\gamma d\phi, \tag{46}$$

where $d\gamma = d\gamma_1 d\gamma_2 \ldots d\gamma_{M_t}$ and $d\phi = d\phi_2 \ldots d\phi_{M_t}$. We introduce an approximation by which the computation of (46) can be greatly simplified. By using the basic properties of the logarithm we find that

$$\log_2(1 + \bar{\gamma} \cdot z(\gamma,\phi)) = \log_2(1 + \bar{\gamma} \cdot \mathcal{G}|\gamma|/M_t) + \log_2(1 + \rho(\gamma,\phi)), \tag{47}$$

where ρ is given by

$$\rho(\gamma,\phi) = \bar{\gamma} \cdot \frac{z(\gamma,\phi) - \mathcal{G}|\gamma|/M_t}{1 + \bar{\gamma} \cdot \mathcal{G}|\gamma|/M_t}. \tag{48}$$

According to the decomposition (47) we can write

$$C_{\mathrm{ora}}(\bar{\gamma}) = \tilde{C}_{\mathrm{ora}}(\bar{\gamma}) + \epsilon(\bar{\gamma}), \tag{49}$$

where ϵ represents the error of the approximation

$$\begin{aligned} \tilde{C}_{\mathrm{ora}}(\bar{\gamma}) &= B \int \log_2(1 + \bar{\gamma} \cdot \mathcal{G}|\gamma|/M_t) f(\gamma,\phi) d\gamma d\phi \\ &= B \int \log_2\big(1 + \bar{\gamma} \cdot \mathcal{G}|\gamma|/M_t\big) f(\gamma) d\gamma \approx C_{\mathrm{ora}}(\bar{\gamma}). \end{aligned} \tag{50}$$

Let us briefly explain the idea leading to this approximation. Since $\mathcal{G} = \mathrm{E}\{z\}$ and $\mathrm{E}\{|\gamma|/M_t\} = 1$ we find that the expectation in the numerator of (48) vanishes. Then it can be expected that the error

$$\epsilon(\bar{\gamma}) = B \cdot \mathrm{E}\{\log_2(1+\rho)\}$$

is small. Furthermore, we note that if $\mathcal{G} = 1$ then $\tilde{C}_{\mathrm{ora}}$ represents the link capacity in the presence of orthogonal design such as rate 1 space-time block code. Such a system provides full diversity benefit but no coherent combining gain. In (50) this additional gain from coherent combining is embedded into the SNR gain $\mathcal{G}$. On the other hand, if perfect CSI is available in the transmitter, then $\mathcal{G} = M_t$ and $\tilde{C}_{\mathrm{ora}}$ gives the exact capacity of M_t antenna receiver maximal ratio combining. The closed-form expression for the capacity of receiver maximal ratio combining is deduced in [54],

$$C_{\mathrm{ora,MRC}}(\bar{\gamma}) = B\log_2(e)\Big(\mathcal{P}_{M_t}\Big(-\frac{1}{\bar{\gamma}}\Big)E_1\Big(\frac{1}{\bar{\gamma}}\Big)+\sum_{k=1}^{M_t-1}\frac{1}{k}\mathcal{P}_k\Big(\frac{1}{\bar{\gamma}}\Big)\mathcal{P}_{M_t-k}\Big(-\frac{1}{\bar{\gamma}}\Big)\Big), \quad (51)$$

where $\mathcal{P}_{M_t}$ is the Poisson distribution function, defined by

$$\mathcal{P}_{M_t}(x) = e^{-x} \cdot \sum_{m=0}^{M_t-1}\frac{x^m}{m!}. \quad (52)$$

From (50) and (51) we find that our approximation reads as

$$\tilde{C}_{\mathrm{ora}} = C_{\mathrm{ora,MRC}}\Big(\frac{\mathcal{G}}{M_t}\cdot\bar{\gamma}\Big). \quad (53)$$

Hence, the applied approximation reduces the computation of the link capacity to the computation of SNR gain that is a much more straightforward operation. Figure 7 depicts the link capacity (6) as a function of mean SNR for two-antenna e-mode 1 ($N_{\mathrm{rp}} = 2$) and e-mode 2 ($N_{\mathrm{rp}} = 3$) corresponding to UTRA FDD mode 1 and 2 respectively. The results show that e-mode 1 and 2 provide better capacity than TSC while the performance difference between e-mode 1 and 2 is small. The performance difference between e-mode 2 and ideal case is very small as well. For single antenna system, TSC, and ideal case the exact closed-form expressions are applied and for e-mode 1 and 2 the approximation (53) is employed. Point values (x) and (o) corresponding to e-mode 1 and 2 were simulated by using 10^6 samples. As found from Figure 7 there is no visible error between simulated point values and approximation curves.

Although simulations hint that error ϵ in (49) is small, it is worth of studying the error more carefully. In general, an appropriate error analysis should contain the following stages:

- Confirm that the given approximation is well defined.

• Find an upper bound for the approximation error.

Clearly, approximation (49) is well defined if $\rho > -1$. Let us show that this condition is valid provided that $\mathcal{G} > 1$ and $N_{\rm rp} > 1$. For that purpose we expand (44). In the resulting formula cross-terms containing $\cos(\phi_m - \phi_k)$, $m \neq k$, are non-negative because $|\phi_m - \phi_k| \leq \pi/2$. We note that in two-antenna case cross-term is non-negative also in case $N_{\rm rp} = 1$. We attain a lower bound

$$z(\gamma, \phi) \geq \sum_{m=1}^{M_t} \hat{u}_m^2 \gamma_m \geq |\gamma|/M_t, \tag{54}$$

where the second inequality is trivially true for e-mode 1 and in case of e-mode 2 it reflects the fact that it is always a better strategy to put more power on the stronger channel than to share transmit power evenly between channels. By applying (54) to (48) we find that

$$\rho(\gamma, \phi) \geq -\frac{\bar{\gamma} \cdot \mathcal{G}|\gamma|/M_t}{1 + \bar{\gamma} \cdot \mathcal{G}|\gamma|/M_t} \Big(\frac{\mathcal{G} - 1}{\mathcal{G}} \Big) \geq -\frac{\mathcal{G} - 1}{\mathcal{G}}. \tag{55}$$

Hence, if $\mathcal{G} > 1$ then $\rho > -1$. Condition $\mathcal{G} > 1$ is not restrictive because it is valid always when closed-loop method gives SNR gain.

It remains to find an upper bound for the approximation error. In the forthcoming error analysis we apply the formula

$$\log_2(1 + \rho) = \log_2(e) \Big(\rho - \frac{\rho^2}{2(1 + \zeta)^2} \Big), \ \min\{0, \rho\} \leq \zeta \leq \max\{0, \rho\}, \tag{56}$$

that is obtained by using Taylor's expansion with respect to ρ. To avoid intolerable complexity we assume from this on that $M_t = 2$. Next we show that the expectation of ρ vanishes. We begin this proof by writing

$$\rho(\gamma, \phi) = z(\xi, \phi) - \mathcal{G}|\xi|/2, \ \xi_m = \frac{\gamma_m}{1/\bar{\gamma} + \mathcal{G}|\gamma|/2}.$$

By taking the expectation with respect to γ and ϕ we obtain

$$\mathrm{E}\{z(\xi, \phi)\} = u_1^2 \mathrm{E}\{\xi_{(1)}\} + u_2^2 \mathrm{E}\{\xi_{(2)}\} + 2u_1 u_2 \mathrm{E}\{\sqrt{\xi_{(1)} \xi_{(2)}}\} c_{N_{\rm rp}}. \tag{57}$$

The required expectations are computed similarly with (25). First we substitute $\gamma_2 = t\gamma_1$. Then

$$\mathrm{E}\{\xi_{(1)}^{1-\delta} \xi_{(2)}^{\delta}\} = \int_0^{\infty} \int_0^1 \frac{2\gamma_1^2 t^{\delta} e^{-\gamma_1(1+t)}}{1/\bar{\gamma} + \mathcal{G}\gamma_1(1 + t)/2} dt \, d\gamma_1. \tag{58}$$

In the second stage we change the integration order and substitute $s = \gamma_1(1 + t)$. The resulting formula reads as

$$\mathrm{E}\{\xi_{(1)}^{1-\delta} \xi_{(2)}^{\delta}\} = \Big\{ \int_0^1 \frac{2t^{\delta} dt}{(1 + t)^3} \Big\} \Big\{ \int_0^{\infty} \frac{s^2 e^{-s}}{1/\bar{\gamma} + \mathcal{G}s/2} ds \Big\} = \tilde{I}_{\delta} \cdot I_{\xi}. \tag{59}$$

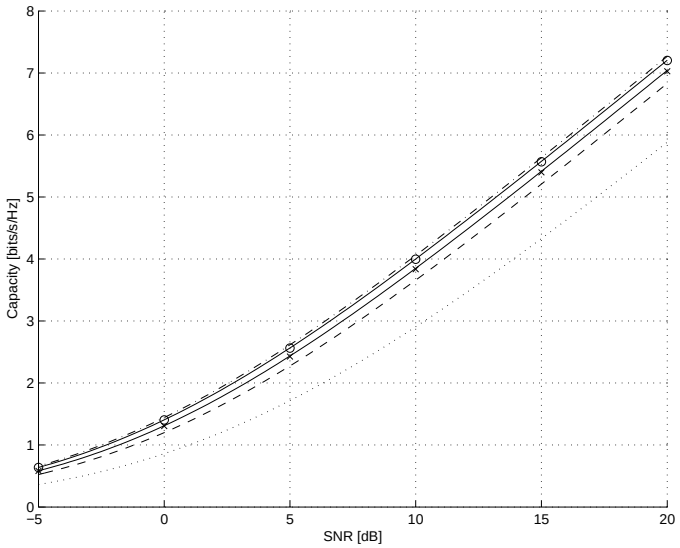

Figure 7: Link capacity for two-antenna e-mode 1 when $N_{\mathrm{rp}} = 2$ (x) and e-mode 2 when $N_{\mathrm{rp}} = 3$ (o) in the presence of Rayleigh fading, constant transmit power and optimal rate adaptation. Dotted curve refers to the capacity of single antenna transmission, dashed curve indicates the capacity given by TSC and dashed and dotted curve refers to the capacity in case of ideal CSI.

For (57) we need $\tilde{I}_0$, $\tilde{I}_{1/2}$ and $\tilde{I}_1$. The computation of these integrals is a straightforward task and results in

$$\tilde{I}_0 = 3/4, \quad \tilde{I}_{1/2} = \pi/8, \quad \tilde{I}_1 = 1/4. \tag{60}$$

Hence, we have

$$\mathrm{E}\{z(\xi,\phi)\} = \Big(\frac{3}{4}\hat{u}_1^2 + \frac{1}{4}\hat{u}_2^2 + \frac{\pi c_{N_{\mathrm{rp}}}}{4}\hat{u}_1\hat{u}_2\Big) I_\xi = \frac{\mathcal{G}}{2}\cdot I_\xi. \tag{61}$$

On the other hand, using the same substitutions as in (58) and (59) we obtain

$$\mathrm{E}\Big\{\frac{\mathcal{G}}{2}|\xi|\Big\} = \frac{\mathcal{G}}{2}\big(\mathrm{E}\{\xi_{(1)}\} + \mathrm{E}\{\xi_{(2)}\}\big) = \frac{\mathcal{G}}{2}\cdot I_\xi.$$

By combining the last two equations we find that $\mathrm{E}\{\rho\} = 0$.

Now we know that the distribution of ρ is concentrated on 0 in which point the error ϵ vanishes. For the final error bound we need the second moment of ρ. This is due to the estimate

$$|\epsilon| = B\log_2(e)\Big|\mathrm{E}\Big\{\frac{\rho^2}{2(1+\zeta)^2}\Big\}\Big| \le B\log_2(e)\max\Big\{\frac{1}{2(1+\zeta)^2}\Big\}\mathrm{E}\{\rho^2\}, \tag{62}$$

that is obtained from (56). By (55) it is found that

$$1+\zeta \geq 1+\min\{0,\rho\} \geq 1-\frac{\mathcal{G}-1}{\mathcal{G}} = \frac{1}{\mathcal{G}}. \tag{63}$$

Then (62) implies

$$|\epsilon| \leq B\log_2(e)\cdot\frac{1}{2}\cdot\mathcal{G}^2\cdot\mathrm{E}\{\rho^2\} =: \hat{\epsilon} \tag{64}$$

and it remains to deduce the second moment of ρ.

It is not difficult to see that $\mathrm{E}\{\rho^2\}$ attains a closed-form expression. Since the resulting formula is relatively complex we only compute a bound for the asymptotic error ϵ_∞ that is defined by

$$\epsilon_\infty = B\cdot\mathrm{E}\{\log_2(1+\rho_\infty)\},\ \rho_\infty = \lim_{\bar{\gamma}\to\infty}\rho.$$

We begin by expanding ρ_∞^2 as follows

$$\mathrm{E}\{\rho_\infty^2\} = \mathrm{E}\{z(\xi,\phi)^2\} - 2\mathrm{E}\{z(\xi,\phi)\} + 1. \tag{65}$$

Hence, we need to compute the first and the second moment of $z(\xi,\phi)$ with respect to γ and ϕ. For the first moment there holds by (61)

$$\lim_{\bar{\gamma}\to\infty}\mathrm{E}\{z(\xi,\phi)\} = \frac{\mathcal{G}}{2}\lim_{\bar{\gamma}\to\infty} I_\xi = \int_0^\infty se^{-s}ds = 1. \tag{66}$$

In a similar manner as in (21) and (22) the evaluation of the second moment of $z(\xi,\phi)$ is reduced to the computation of moments

$$\mathrm{E}\{\xi_{(1)}^{2-\delta}\xi_{(2)}^{\delta}\},\quad \delta\in\Big\{0,1/2,1,3/2,2\Big\}.$$

Furthermore, by using the method of (58) and (59) we find that

$$\lim_{\bar{\gamma}\to\infty}\mathrm{E}\{\xi_{(1)}^{2-\delta}\xi_{(2)}^{\delta}\} = I_\delta, \tag{67}$$

where values of I_δ are available from (26). Thus, by combining (64) and (65)-(67) we can compute an upper bound $\hat{\epsilon}_\infty$ for the error ϵ_∞. The resulting error bounds for our capacity approximations are given in Table 3 showing that asymptotic approximation errors are small.

Fast power control approximately inverts the dedicated channels in UTRA FDD, and a suitable form of capacity is given by (7), where $\mathrm{E}\{1/z\}$ represents the power that is required to compensate the fading. In the computation of $\mathrm{E}\{1/z\}$ we apply the approximation

$$\mathrm{E}\Big\{\frac{1}{z}\Big\} = \frac{M_t}{\mathcal{G}}\mathrm{E}\Big\{\frac{1}{|\gamma|}\Big\} - \varepsilon \approx \frac{M_t}{\mathcal{G}}\mathrm{E}\Big\{\frac{1}{|\gamma|}\Big\}, \tag{68}$$

$\hat{\epsilon}_\infty$ [bps/Hz]	$N_{\mathrm{rp}} = 1$	$N_{\mathrm{rp}} = 2$	$N_{\mathrm{rp}} = 3$
e-mode 1	0.0601	0.0329	0.0344
e-mode 2	0.0329	0.0056	0.0039

Table 3: Upper bounds for capacity approximation error in case of two transmit antennas.

where ε is the corresponding error. Since $|\gamma|$ follows the χ^2-distribution with $2M_t$ degrees of freedom it is easily found that [54]

$$\mathrm{E}\{1/|\gamma|\} = 1/(M_t - 1). \tag{69}$$

The approximation $\tilde{C}_{\mathrm{inv}}$ of C_{inv} is then given by

$$\tilde{C}_{\mathrm{inv}} = B \cdot \log_2 \Big(1 + \frac{(M_t - 1)\mathcal{G}}{M_t} \cdot \bar{\gamma}\Big). \tag{70}$$

When $\mathcal{G} = 1$ Equation (70) provides the capacity of a rate 1 space-time block code that applies orthogonal design.

As an additional reference we consider the capacity of TSC. From [54] it is known that for TSC

$$\mathrm{E}\Big\{\frac{1}{\gamma_{(1)}}\Big\} = \lim_{\omega \to 0+} M_t \sum_{k=0}^{M_t-1} (-1)^k \binom{M_t - 1}{k} E_1((1+k)\omega), \tag{71}$$

where E_1 is the first order exponential integral function defined by

$$E_n(x) = \int_1^\infty \frac{e^{-xt}}{t^n} dt, \quad \arg(x) < \pi, \ n \in \mathbb{N}_0. \tag{72}$$

The computation of the rather complex-looking limit (71) is not carried out in [54], and therefore we will do it here. Let $\bar{\gamma}$ be arbitrary but fixed positive number. Then, if ω is small we have by (5.1.11) of [69]

$$E_1((1+k)\omega) = -e_0 - \log((1+k)\omega) = -e_0 - \log\omega - \log(1+k),$$

where e_0 is Euler's constant. Moreover, by Binomial Theorem there holds

$$0 = (1-1)^{M_t - 1} = \sum_{k=0}^{M_t-1} (-1)^k \binom{M_t - 1}{k}.$$

Hence we find that the term containing ω vanishes in (71) and

$$\begin{aligned} \mathrm{E}\Big\{\frac{1}{\gamma_{(1)}}\Big\} &= M_t \sum_{k=0}^{M_t-1} (-1)^{k+1} \binom{M_t - 1}{k} \log(1+k) \\ &= \sum_{k=1}^{M_t} \binom{M_t}{k} k \cdot \log(k). \end{aligned}$$

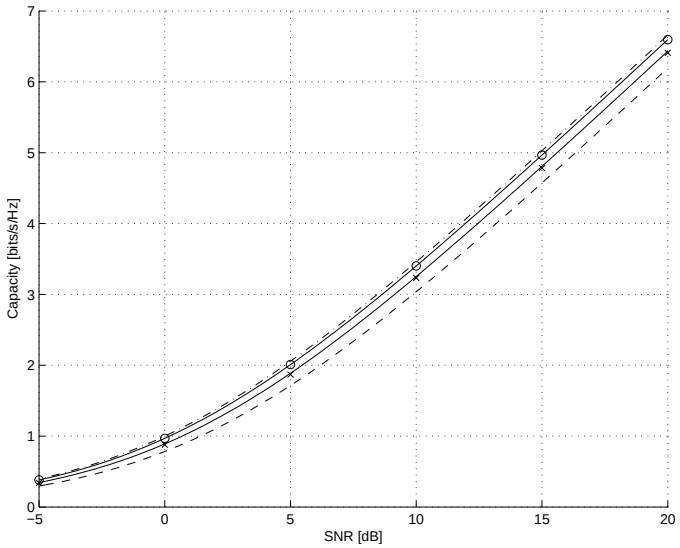

Figure 8: Link capacity for e-mode 1 when $N_{\rm rp} = 2$ (x) and for e-mode 2 when $N_{\rm rp} = 3$ (o) in the presence of Rayleigh fading, ideal PC, and fixed-rate modulation and coding. Dashed curve refers to the capacity given by TSC and dashed and dotted curve refers to the capacity in case of ideal CSI.

Figure 8 shows $\tilde{C}_{\rm inv}$ for two-antenna e-mode 1 ($N_{\rm rp} = 2$) and e-mode 2 ($N_{\rm rp} = 3$). The corresponding discrete values (x) and (o) were simulated by using 10^6 samples. The results show that UTRA FDD closed-loop modes provide better capacity than TSC also in case of PC and fixed-rate modulation and coding. Again the gap between e-mode 2 and ideal case is small.

According to Figure 8 the approximation error is again very small. In the following we show this also analytically. We deduce the error bound for the approximation (70) in case of two antennas. There holds

$$\epsilon(\bar{\gamma}) = C_{\rm inv}(\bar{\gamma}) - \tilde{C}_{\rm inv}(\bar{\gamma}) = B \cdot \log_2 \Big(\frac{1 + \bar{\gamma}/\mathrm{E}\{1/z\}}{1 + \mathcal{G}(M_t - 1)\bar{\gamma}/M_t} \Big). \qquad (73)$$

Let us substitute the approximation (68) in (73) and use (69). Then we find that

$$\epsilon(\bar{\gamma}) = B \cdot \log_2 \Big(\frac{1 + \bar{\gamma}/\big(M_t/\mathcal{G}(M_t - 1) - \varepsilon\big)}{1 + \mathcal{G}(M_t - 1)\bar{\gamma}/M_t} \Big). \qquad (74)$$

Again we concentrate on the asymptotic SNR region. Then by (74) there holds

$$\epsilon_\infty = B \cdot \log_2 \Big(\frac{1}{1 - \varepsilon \cdot \mathcal{G}(M_t - 1)/M_t} \Big). \qquad (75)$$

Furthermore, since ε is small, we get

$$\epsilon_\infty \approx B \cdot \log_2(e) \cdot \frac{\mathcal{G}(M_t - 1)}{M_t} \cdot \varepsilon$$

and it remains to find the error ε. To this end we can apply the identity

$$\frac{1}{z(\gamma,\phi)} = \frac{M_t}{\mathcal{G}|\gamma|} \cdot \frac{1}{1+\rho_\infty(\gamma,\phi)}, \quad \rho_\infty(\gamma,\phi) = \frac{z(\gamma,\phi) - \mathcal{G}|\gamma|/M_t}{\mathcal{G}|\gamma|/M_t}$$

and Taylor's expansion

$$\frac{1}{1+\rho_\infty} = 1 - \rho_\infty + \frac{\rho_\infty^2}{(1+\zeta)^3}, \ \min\{0,\rho_\infty\} \le \zeta \le \max\{0,\rho_\infty\}.$$

After combining (68) and the last two equations we find that

$$\varepsilon = \frac{M_t}{\mathcal{G}} \Big(\mathrm{E}\Big\{ \frac{\rho_\infty(\gamma,\phi)}{|\gamma|} \Big\} - \mathrm{E}\Big\{ \frac{\rho_\infty(\gamma,\phi)^2}{(1+\zeta)^3|\gamma|} \Big\} \Big). \tag{76}$$

Here the first expectation on the right-hand side vanishes. To show this, we need to compute expectations $\mathrm{E}\{\xi_{(1)}^{1-\delta}\xi_{(2)}^{\delta}\}$, $\delta \in \{0, 1/2, 1\}$, where $\xi_m = M_t\gamma_m/\mathcal{G}|\gamma|^2$. By using the same substitutions as in previous cases we obtain

$$\mathrm{E}\{\xi_{(1)}^{1-\delta}\xi_{(2)}^{\delta}\} = \frac{2}{\mathcal{G}} \int_0^1 \frac{2t^\delta dt}{(1+t)^3} = \frac{2}{\mathcal{G}} \cdot \tilde{I}_\delta.$$

The values of $\tilde{I}_\delta$ were given in (60). Hence, similarly with (57) and (61) we find that

$$\mathrm{E}\big\{ z(\gamma,\phi)/|\gamma|^2 \big\} = \mathcal{G}/2. \tag{77}$$

Then, after applying the definition of ρ_∞ and equality $\mathrm{E}\{1/|\gamma|\} = 1$ by (69) we see that the first expectation on the right-hand side of (76) vanishes. Now, by (76) and the estimate (63) we find that

$$|\varepsilon| \le M_t \cdot \mathcal{G}^2 \cdot \mathrm{E}\big\{ \rho_\infty(\gamma,\phi)^2/|\gamma| \big\} =: \hat{\varepsilon}.$$

In the computation of bound $\hat{\varepsilon}$ we need the expression

$$\rho_\infty(\gamma,\phi)^2/|\gamma| = \big((2/\mathcal{G})^2 z(\gamma,\phi)^2/|\gamma|^3 - 4z(\gamma,\phi)/\mathcal{G}|\gamma|^2 + 1/|\gamma| \big).$$

Using this equality, the result (77) and equality $\mathrm{E}\{1/|\gamma|\} = 1$ we obtain

$$\hat{\varepsilon} = \mathcal{G}^2 \cdot \big((2/\mathcal{G})^2 \mathrm{E}\{ z(\gamma,\phi)^2/|\gamma|^3 \} - 1 \big).$$

After suitable substitutions it is seen that the expectation on the right can be expressed in terms of I_δ for which numeric values were given in (26). Now we are able to compute the values of $\hat{\varepsilon}$.

Table 4 gives analytical upper bounds for the error of the approximation (70) in two-antenna case.

$\hat{\varepsilon}[bps/Hz]$	$N_{\mathrm{rp}}=1$	$N_{\mathrm{rp}}=2$	$N_{\mathrm{rp}}=3$
e-mode 1	0.0902	0.0561	0.0607
e-mode 2	0.0561	0.0104	0.0074

Table 4: Analytic upper bounds for approximation error $\hat{\varepsilon}$ in case of two transmit antennas.

3.4 Computation of BEP

In the conventional approach the bit error probability P_{e} for a certain SNR is computed by using the formula

$$P_{\mathrm{e}}(\bar{\gamma}) = \mathrm{E}\{P_{\mathrm{mod}}(\bar{\gamma}\cdot z)\} = \int P_{\mathrm{mod}}\big(\bar{\gamma}\cdot z(\gamma,\phi)\big) f(\gamma,\phi) d\gamma d\phi, \qquad (78)$$

where P_{mod} is the error rate of the modulation. We consider e-mode 1 in general case while e-mode 2 is discussed only in case $M_t = 2$. In the presentation we follow [5].

For single antenna transmission as well as for MRC and TSC closed-form expressions of (78) are known for various modulation techniques. On the contrary, BEP formulas for advanced closed-loop transmit diversity methods such as e-mode 1 and e-mode 2 — that apply partial CSI — are widely unknown. Recently, lower bounds for symbol error probabilities of closed-loop feedback schemes were formulated in [75]. These bounds are tight for good codebooks derived according to design principles in [63, 64]. Here we concentrate on e-mode 1 and 2 and show a method to compute BEP in asymptotic SNR region. Furthermore, we recall an approximation which admits an accurate BEP estimate for e-mode 1 and 2 in the whole SNR scale. For simplicity we assume BPSK modulation.

We begin with e-mode 1 and write

$$P_{\mathrm{e}}(\bar{\gamma}) = \int_{\Omega_\phi} f(\phi)\Big(\int_{\mathbb{R}_+^{M_t}} P_{\mathrm{mod}}\big(\bar{\gamma}\cdot z(\gamma,\phi)\big) e^{-|\gamma|} d\gamma\Big) d\phi, \qquad (79)$$

where $f(\phi)$ is the PDF of adjusted relative phases and Ω_ϕ is given by

$$\Omega_\phi = \{\phi \in \mathbb{R}^{M_t-1} : -\pi/2^{N_{\mathrm{rp}}} \le \phi_m \le \pi/2^{N_{\mathrm{rp}}},\ m = 1,2,\ldots,M_t-1\}.$$

We first modify the formula (79) through the substitution $\gamma = s\mathbf{r}$,

$$s>0,\ \mathbf{r} = (r_1,\ldots,r_{M_t-1},1),\ d\gamma = s^{M_t-1} dr_1\ldots dr_{M_t-1} ds = s^{M_t-1} d\mathbf{r} ds.$$

The resulting expression reads as

$$P_{\mathrm{e}}(\bar{\gamma}) = \int_{\Omega_\phi} f(\phi)\Big(\int_{\mathbb{R}_+}\Big(\int_{\mathbb{R}_+^{M_t-1}} P_{\mathrm{mod}}\big(\bar{\gamma}\cdot s\cdot z(\mathbf{r},\phi)\big) s^{M_t-1} e^{-s|\mathbf{r}|} d\mathbf{r}\Big) ds\Big) d\phi.$$

To find a suitable expression for asymptotic BEP we change the integration order and set $t = \bar{\gamma} \cdot s \cdot z(\mathbf{r}, \phi)$. Then

$$P_{\mathrm{e}}(\bar{\gamma}) = \Big(\frac{1}{\bar{\gamma}}\Big)^{M_t} \int_{\Omega_\phi} \int_{\mathbb{R}_+^{M_t-1}} \frac{f(\phi)}{z(\mathbf{r},\phi)^{M_t}} \Big(\int_{\mathbb{R}_+} P_{\mathrm{mod}}(t) t^{M_t-1} e^{-\frac{t|\mathbf{r}|}{\bar{\gamma}\cdot z(\mathbf{r},\phi)}} dt \Big) d\mathbf{r} d\phi.$$

Let us compute the integral in the brackets when SNR grows without limit. For that purpose we use the equation

$$\int_{\mathbb{R}_+} P_{\mathrm{mod}}(t) t^{M_t-1} e^{-at} dt = \Big(-\frac{d}{da} \Big)^{M_t-1} \int_{\mathbb{R}_+} P_{\mathrm{mod}}(t) e^{-at} dt, \qquad (80)$$

that is valid provided that integral on the right is finite. Since BPSK modulation is employed we have by (7.4.19) of [69]

$$\int_{\mathbb{R}_+} P_{\mathrm{mod}}(t) e^{-at} dt = \frac{1}{2} \int_{\mathbb{R}_+} \mathrm{erfc}(\sqrt{t}) e^{-at} dt = \frac{1}{2a} \Big(1 - \sqrt{\frac{1}{1+a}} \Big).$$

After applying Taylor's expansion to $(1+a)^{-1/2}$ we further obtain

$$\int_{\mathbb{R}_+} P_{\mathrm{mod}}(t) e^{-at} dt = \sum_{k=0}^{\infty} d_k a^k, \quad d_k = \frac{(-1)^k (2k+1)!}{2^{2k+2} k! (k+1)!}.$$

Now it is a simple task to compute the limit in (80). We have

$$\begin{aligned} \lim_{\bar{\gamma}\to\infty} \int_{\mathbb{R}_+} P_{\mathrm{mod}}(t) t^{M_t-1} e^{-at} dt &= \lim_{\bar{\gamma}\to\infty} \Big\{ \Big(-\frac{d}{da} \Big)^{M_t-1} \sum_{k=0}^{\infty} d_k a^k \Big\} \\ &= (-1)^{M_t-1} (M_t-1)! \cdot d_{M_t-1} = \frac{(2M_t-1)!}{2^{2M_t} M_t!}. \end{aligned} \qquad (81)$$

By using the equation (81) we attain an asymptotic formula

$$P_{\mathrm{e}}(\bar{\gamma}) = \Big(\frac{1}{\bar{\gamma}}\Big)^{M_t} \frac{(2M_t-1)!}{2^{2M_t} M_t!} \int_{\Omega_\phi} \int_{\mathbb{R}_+^{M_t-1}} \frac{f(\phi) d\mathbf{r} d\phi}{z(\mathbf{r},\phi)^{M_t}}$$

that is valid when $\bar{\gamma} >> 1$ and BPSK modulation is assumed. For comparison purposes we write

$$P_{\mathrm{e}}(\bar{\gamma}) = \binom{2M_t-1}{M_t} \Big(\frac{A_{M_t,N_{\mathrm{rp}}}}{4(\bar{\gamma}/M_t)} \Big)^{M_t}, \quad \bar{\gamma} >> 1, \qquad (82)$$

where $\bar{\gamma}/M_t$ is the SNR per transmit antenna and $A_{M_t,N_{\mathrm{rp}}}$ is defined by

$$A_{M_t r,N_{\mathrm{rp}}} = \Big\{ \frac{(M_t-1)!}{M_t^{M_t}} \int_{\Omega_\phi} \int_{\mathbb{R}_+^{M_t-1}} \frac{f(\phi) d\mathbf{r} d\phi}{z(\mathbf{r},\phi)^{M_t}} \Big\}^{\frac{1}{M_t}}. \qquad (83)$$

Formula (82) is handy because it is similar to the well-known asymptotic BEP formula of M_t-antenna MRC [71]. By setting $A_{M_t,N_{\mathrm{rp}}} = M_t$ in (82) we

$N_{\rm rp}$	1	2	3	∞
$A_{2,N_{\rm rp}}$[dB]	1.505	2.198	2.340	2.386
$B_{2,N_{\rm rp}}$[dB]	2.198	2.694	2.810	2.847

Table 5: Asymptotic BEP gains of e-mode 1 and 2 against rate=1 space-time orthogonal design when $M_t = 2$.

obtain the BEP of receiver MRC while with $A_{M_t,N_{\rm rp}} = 1$ Equation (82) provides the BEP for rate 1 space-time orthogonal design. Hence, the constant $A_{M_t,N_{\rm rp}}$ in (82) indicates the coherent combining gain due to closed-loop adjustments.

In [5] it was shown — by a straightforward integration — that for two-antenna e-mode 1 there holds

$$A_{2,N_{\rm rp}} = \Big\{ \frac{1 - \frac{2^{N_{\rm rp}-1}}{\pi} \sin \frac{\pi}{2^{N_{\rm rp}-1}}}{2 \sin^2 \frac{\pi}{2^{N_{\rm rp}}}} \Big\}^{\frac{1}{2}}.$$

Following the reasoning of [5] we find that formula (82) is valid also for two-antenna e-mode 2 provided that $A_{M_t,N_{\rm rp}}$ is replaced with

$$B_{2,N_{\rm rp}} = \Big\{ \frac{2^{N_{\rm rp}}}{\pi} \int_0^1 \int_0^{\pi/2^{N_{\rm rp}}} \frac{d\phi dr}{(\hat{u}_1^2 + \hat{u}_2^2 r + 2\hat{u}_1\hat{u}_2\sqrt{r}\cos\phi)^2} \Big\}^{\frac{1}{2}}.$$

Closed-form expression for $B_{2,N_{\rm rp}}$ exists but it is omitted because it is rather complex. Table 5 gives values of $A_{2,N_{\rm rp}}$ and $B_{2,N_{\rm rp}}$ when $N_{\rm rp} = 1, 2, 3, \infty$. We recall that in two-antenna case e-mode 1 with $N_{\rm rp} = 1$ coincides with TSC. According to the results in Table 5 the UTRA FDD mode 1 and 2 provide 0.693 dB and 1.305 dB gain against TSC in asymptotic BEP respectively.

In [5] it was also shown that for e-mode 1 with M_t antennas there holds

$$A_{M_t,\infty} = \Big\{ \frac{2^{M_t-1}(M_t-1)!}{(2M_t-1)!} \Big\}^{\frac{1}{M_t}}.$$

Since e-mode 1 with ideal phasing is equivalent with receiver equal gain combining, the computation of $A_{M_t,\infty}$ provides also means to deduce the BEP of equal gain combining. If $M_t > 2$ and $N_{\rm rp}$ is finite, the computation of $A_{M_t,N_{\rm rp}}$ and $B_{M_t,N_{\rm rp}}$ is an open problem.

While (82) is valid when $\bar{\gamma}$ is large, it is of great importance to find also a BEP formula that is valid through the whole SNR range. This task is solved in [5] showing that a good approximation in two-antenna case is given by

$$\tilde{P}_{\rm e}(\bar{\gamma}) = \frac{1}{4}\Big(1 - \sqrt{\frac{\bar{\gamma}/2}{C_{2,N_{\rm rp}} + \bar{\gamma}/2}}\Big)^2 \Big(2 + \sqrt{\frac{\bar{\gamma}/2}{C_{2,N_{\rm rp}} + \bar{\gamma}/2}}\Big), \qquad (84)$$

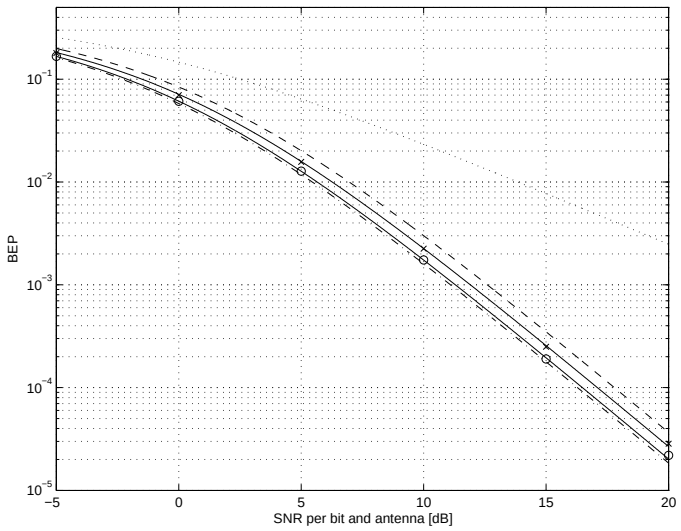

Figure 9: BEP curves as a function of SNR for e-mode 1 when $N_{\mathrm{rp}} = 2$ (x) and for e-mode 2 when $N_{\mathrm{rp}} = 3$ (o). Dotted curve refers to the single antenna transmission, dashed curve depicts the BEP of TSC and dashed and dotted curve refers to the case with ideal CSI.

where $C_{2,N_{\mathrm{rp}}} \in \{A_{2,N_{\mathrm{rp}}}, B_{2,N_{\mathrm{rp}}}\}$. This approximation is obtained from BEP of MRC by setting

$$\tilde{P}_{\mathrm{e}}(\bar{\gamma}) = P_{\mathrm{e}}^{\mathrm{MRC}}\big(\bar{\gamma}/2C_{2,N_{\mathrm{rp}}}\big).$$

Then $\tilde{P}_{\mathrm{e}} \to P_{\mathrm{e}}$ if $\bar{\gamma} \to \infty$. A more detailed error analysis can be found from [5].

Figure 9 displays the bit error curves as a function of SNR when $M_t = 2$. BEP curves for e-mode 1 and 2 (solid curves) are plotted using the approximation (84) while point values (x) and (o) are obtained through simulating 10^7 sample cases. It is found that the approximation is accurate. The performance of e-mode 1 and 2 is superior to single antenna transmission while the gain against TSC is smaller.

3.5 Effect of Feedback Errors

As shown in the previous sections, closed-loop transmit diversity techniques provide both diversity and coherent combining gain when compared to single antenna transmission. Previous results, however, are valid only if error-free feedback information is available in the transmitter. This is usually not the case in practice because it is difficult to design such a high performance reverse channel within reasonable capacity and delay limits. Hence, the negative effect of feedback errors should be taken into account in the system design phase.

We show here that in the presence of feedback errors the asymptotic diversity of the feedback schemes is equal to one which is similar to a single antenna transmission. The same observation has been made in [57] assuming Gaussian distributed quantization error. This may seem to be a severe drawback of feedback schemes, but with proper feedback requirements system can be designed in such a way that feedback errors will not dominate the performance.

In analysis we assume that the feedback bit error probability is constant - it is denoted by p - and bit errors are uniformly distributed in time. This model can be considered to be approximately valid in UTRA FDD because the fast uplink power control is applied to the control channel carrying the feedback information. Of course, this assumption does not hold any more with high mobile speeds when the delay of the feedback loop exceeds the coherence time of the channel. Nevertheless, assumption is well justified within low mobility environments.

We begin with a simple example. Consider the two-antenna TSC where a single feedback bit is available in the transmitter. Let $P_{\mathrm{e},2}(\bar{\gamma}|p)$ be the BEP on the condition that feedback bit error probability is p. Then

$$P_{\mathrm{e},2}(\bar{\gamma}|p) = (1-p) \cdot P_{\mathrm{e},2}(\bar{\gamma}|w = \hat{w}) + p \cdot P_{\mathrm{e},2}(\bar{\gamma}|w \neq \hat{w}), \tag{85}$$

where $\hat{w}$ is the correct feedback word, and $P_{\mathrm{e},2}(\bar{\gamma}|w = \hat{w})$ and $P_{\mathrm{e},2}(\bar{\gamma}|w \neq \hat{w})$ refer to the BEP in the presence of error–free and erroneously received feedback, respectively.

It would not be difficult to compute a closed-form expression to formula (85). Instead of doing that we adopt a more general approach where we apply the expression

$$P_{\mathrm{e},1}(\bar{\gamma}) = \frac{1}{2} \cdot P_{\mathrm{e},2}(\bar{\gamma}|w = \hat{w}) + \frac{1}{2} \cdot P_{\mathrm{e},2}(\bar{\gamma}|w \neq \hat{w}). \tag{86}$$

This expression states that the BEP of two-antenna TSC is equal to BEP of single antenna transmission - denoted by $P_{\mathrm{e},1}(\bar{\gamma})$ - provided that feedback is random, *i.e.* feedback bit error probability is 1/2. By combining equations (85) and (86) we obtain an expression

$$P_{\mathrm{e},2}(\bar{\gamma}|p) = (1-2p) \cdot P_{\mathrm{e},2}(\bar{\gamma}|w = \hat{w}) + 2p \cdot P_{\mathrm{e},1}(\bar{\gamma}). \tag{87}$$

Figure 10 displays the BEP curve of two-antenna TSC. It is seen that the term $2p$ in (87) defines the asymptotic difference between the single antenna and the two–antenna bit error probabilities. In practice, the loss of asymptotic diversity need not be critical, because the requirements of feedback error rate can be designed in such a way that performance losses are small in the SNR region where the system operates.

The approach extends to a general case as follows: Assume that $P_{\mathrm{e},M_t}(\bar{\gamma}|p)$ is a BEP of any M_t-antenna closed-loop transmit diversity method

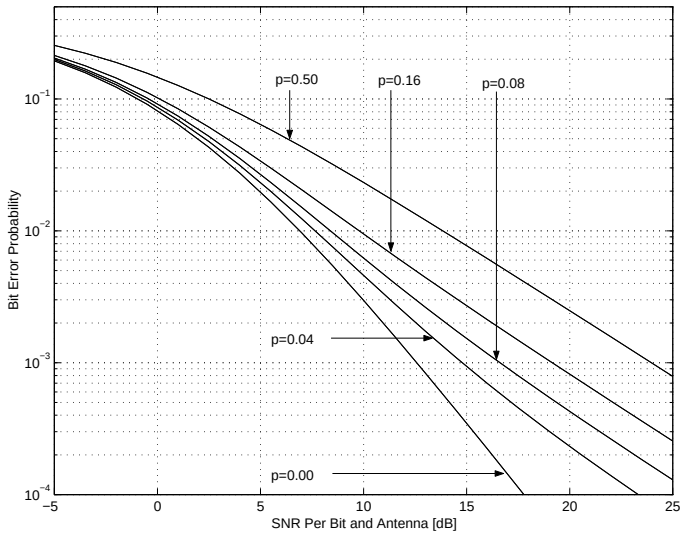

Figure 10: Bit error probability curves as a function of SNR for two-antenna TSC when $p = 0.00$, 0.04, 0.08, 0.16, 0.50.

when quantization $\mathbf{W}$ is employed and feedback bit error probability is p. Furthermore, assume that any transmit weight $\mathbf{w}$ represents the best choice $\hat{\mathbf{w}}$ equally likely. Then we can write

$$P_{\mathrm{e},M_t}(\bar{\gamma}|p) = \sum_{\mathbf{v}\in\mathbf{W}} q(\mathbf{w}=\mathbf{v}) P_{\mathrm{e},M_t}(\bar{\gamma}|\mathbf{w}=\mathbf{v}), \tag{88}$$

where $q(\mathbf{w}=\mathbf{v})$ is the probability that transmit weight $\mathbf{w}$ is applied in transmission on the condition that $\hat{\mathbf{w}}$ is the optimal transmit weight and $P_{\mathrm{e},M_t}(\bar{\gamma}|\mathbf{w}=\mathbf{v})$ is the corresponding BEP. On the other hand, the BEP of single antenna transmission can be expressed in the form

$$P_{\mathrm{e},1}(\bar{\gamma}) = \frac{1}{|\mathbf{W}|} \sum_{\mathbf{v}\in\mathbf{W}} P_{\mathrm{e},M_t}(\bar{\gamma}|\mathbf{w}=\mathbf{v}), \tag{89}$$

where $|\mathbf{W}|$ refers to the number of quantization points. Hence, irrespective of the optimal feedback word, the performance of the closed-loop transmit diversity system is equal to the performance of a single antenna system when the feedback word is randomly selected.

Let $\check{\mathbf{w}}$ be a weight - not necessarily unique - that gives the minimum of $q(\mathbf{w}=\mathbf{v})$. Then we obtain by (88) and (89) an expression

$$\begin{aligned} P_{\mathrm{e},M_t}(\bar{\gamma}|p) = {} & |\mathbf{W}| \cdot q(\mathbf{w}=\check{\mathbf{w}}) \cdot P_{\mathrm{e},1}(\bar{\gamma}) \\ & + \sum_{\mathbf{v}\in\mathbf{W}} \big(q(\mathbf{w}=\mathbf{v}) - q(\mathbf{w}=\check{\mathbf{w}})\big) P_{\mathrm{e},M_t}(\bar{\gamma}|\mathbf{w}=\mathbf{v}). \end{aligned} \tag{90}$$

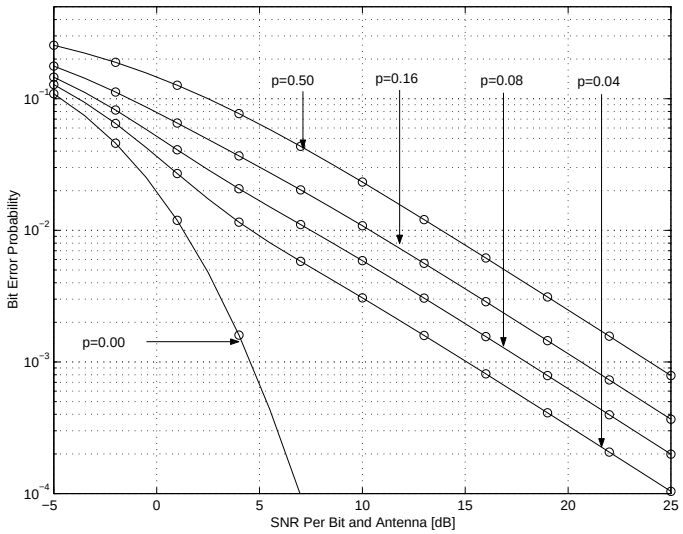

Figure 11: BEP as a function of SNR for TSC when $M_t = 8$ and $p = 0.00, 0.04, 0.08, 0.16, 0.50$.

Since the difference in the sum of formula (90) is non-negative, we obtain a lower bound

$$P_{\mathrm{e},M_t}(\bar{\gamma}|p) \geq |\mathbf{W}| \cdot q(\mathbf{w} = \check{\mathbf{w}}) \cdot P_{\mathrm{e},1}(\bar{\gamma}). \tag{91}$$

This bound shows that the asymptotic BEP of a general feedback method is always reduced to one in the presence of feedback errors. Hence, *in practical systems with feedback errors closed-loop transmit diversity methods can never achieve full diversity benefit.*

Consider the bound (91) for TSC and e-mode 1. For simplicity we assume that $\log_2(M_t)$ is integer. Then there holds

$$P^{\mathrm{TSC}}_{\mathrm{e},M_t}(\bar{\gamma}) \geq M_t \cdot p^{\log_2(M_t)} P_{\mathrm{e},1}(\bar{\gamma}),$$
$$P^{\text{e-mode 1}}_{\mathrm{e},M_t}(\bar{\gamma}) \geq (2p)^{N_{\mathrm{rp}}(M_t-1)} P_{\mathrm{e},1}(\bar{\gamma}).$$

It is found that the bounds decay in a different manner when $p \to 0$. This difference gives only a hint on the asymptotic performance of the two algorithms, because these bounds do not necessarily give the accurate difference in asymptotic curves. Figure 11 displays the BEP of the selection algorithm in the presence of different feedback bit error probabilities when $M_t = 8$. It is seen that already at the feedback bit error level $p = 0.04$ the effect of errors is significant, and the slope is similar to that of a single transmit antenna ($p = 0.50$).

Figure 12 displays the BEP of the e-mode 1 when $N_{\mathrm{rp}} = 1$, $M_t = 8$ and $p = 0.00, 0.04, 0.08, 0.16, 0, 50$. Comparing Figures 11 and 12 shows that in

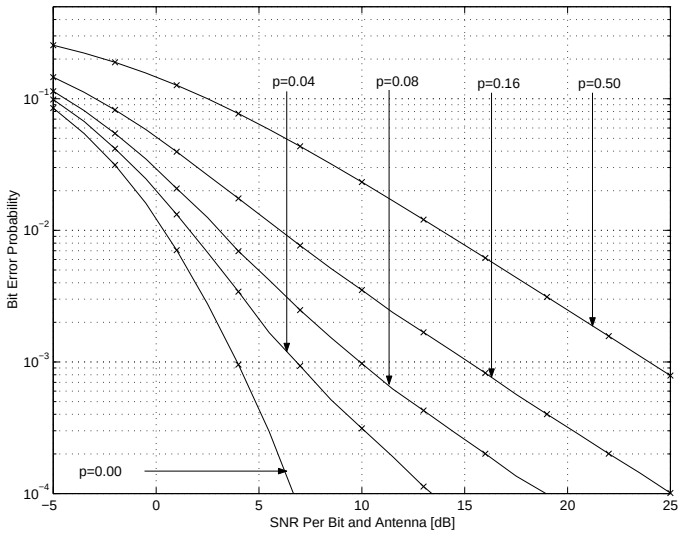

Figure 12: BEP as a function of SNR for e-mode 1 when $N_{\mathrm{rp}} = 1$, $M_t = 8$ and $p = 0.00, 0.04, 0.08, 0.16, 0.50$.

the presence of erroneous feedback e-mode 1 clearly outperforms TSC. We remark that the comparison is not necessarily fair because the number of feedback bits is 3 for selection and 7 for e-mode 1.

Consider next the case where transmit weights corresponding to different feedback words are orthogonal. Then there are at most M_t transmit weights and we have

$$\mathrm{E}\{(\mathbf{H}\mathbf{w}_m)^H(\mathbf{H}\mathbf{w}_k)\} = \mathbf{w}_m^H \mathrm{E}\{\mathbf{H}^H\mathbf{H}\}\mathbf{w}_k = \mathbf{w}_m^H\mathbf{w}_k = 0, \quad m \neq k.$$

Hence, the sum channels obtained through different transmit weights are uncorrelated. But if the channels resulting from different adjustments are uncorrelated, then the mapping between feedback words and transmit weights does not affect the system performance as it does if Gray coding — or other feedback coding — can be used as in case of e-mode 1 and 2. In fact, if erroneous feedback is applied, then BEP is the same for all erroneous feedback words on average. The following result illustrates this fact. We may now write

$$\begin{aligned} P_{\mathrm{e},M_t}(\bar{\gamma}|p) = \big(1-(1-p)^{\log_2(M_t)}\big) P_{\mathrm{e},M_t}(\bar{\gamma}|\mathbf{w} = \hat{\mathbf{w}}) \\ + (1-p)^{\log_2(M_t)} P_{\mathrm{e},M_t}(\bar{\gamma}|\mathbf{w} \neq \hat{\mathbf{w}}), \end{aligned} \tag{92}$$

where $P_{\mathrm{e},M_t}(\bar{\gamma}|\mathbf{w} \neq \hat{\mathbf{w}})$ is the BEP on the condition that erroneous feedback word is selected. We note that this formula is valid only if transmit weights are orthogonal. Furthermore, there holds

$$P_{\mathrm{e},1}(\bar{\gamma}) = \frac{1}{M_t} P_{\mathrm{e},M_t}(\bar{\gamma}|\mathbf{w} = \hat{\mathbf{w}}) + \frac{M_t - 1}{M_t} P_{\mathrm{e},M_t}(\bar{\gamma}|\mathbf{w} \neq \hat{\mathbf{w}}). \tag{93}$$

By combining (92) and (93) we obtain

$$\begin{aligned} P_{\mathrm{e},M_t}(\bar{\gamma}|p) = \Big(1 - \frac{M_t}{M_t - 1}(1-p)^{\log_2(M_t)}\Big) P_{\mathrm{e},M_t}(\bar{\gamma}|\mathbf{w} = \hat{\mathbf{w}}) \\ + \frac{M_t}{M_t - 1}(1-p)^{\log_2(M_t)} P_{\mathrm{e},1}(\bar{\gamma}). \end{aligned} \tag{94}$$

Thus, when feedback words are orthogonal BEP can be expressed in terms of the BEP of error-free system and BEP of a single antenna transmission. It is worth noticing that BEP of the single antenna transmission dominates when SNR is large. Then the term $M_t/(M_t - 1)(1-p)^{\log_2(M_t)}$ defines the asymptotic BEP gain of transmit diversity against the single antenna transmission.

4 Physical Layer Scheduling on a Shared Link

The research of multi-user diversity was initialized in [41], [42] and [72]. The goal in multi-user diversity is to provide diversity gain against channel fading through scheduled transmissions. Hence, access to the transmission resources is granted to users with good channel conditions. If the users are stationary, time selectivity can be introduced artificially as shown in [72].

In Sections 4.2 - 4.5 we compare the capacity of shared links that apply long-term fair scheduling strategies and focus on FDD downlink systems, where channel-aware schedulers require fast feedback channel from mobile to base to allocate transmit resources. The aim is to study practical systems that need little control signaling overhead and maintain a simple receiver implementation. We compare on-off scheduling (OOS) to round robin and maximum SNR schedulers which provide lower and upper bounds to the scheduling performance, respectively. On-off scheduling requires only one-bit channel quality indicator (CQI), which is a valuable feature, because it has been observed that the feedback required by maximum SNR scheduler can cause a significant interference, especially when the mobiles are located on cell edges [40]. Capacity gains of the three schedulers are derived together with transmitter selection combining (TSC). The effect of limited feedback has also been considered in [73], [74] and [76] while the interaction of transmit diversity and scheduling has been investigated in [77], [78] and [79].

Fairness is one of the main concerns in the design of scheduling algorithms. There is no unique definition for fairness, but usually it is defined for some low-level characteristic like throughput. Proportional fair scheduler achieves fairness by transmitting to a user whose instantaneous channel quality is high relative to its own average channel condition over the time scale t_c. Thus, in time slot t the proportional fair scheduler transmits to the user k^* given by

$$k^* = \arg\max_k \frac{R_k(t)}{T_k(t)}$$

where $R_k(t)$ is the requested data rate according to the CQI of user k in time slot t and $T_k(t)$ is the average throughput of user k in a past window of length t_c. Alternatively, it is possible to feed back some other metric than $R_k(t)$, such as the received SNR, describing the quality of the connection. Typically, the average throughput $T_k(t)$ is evaluated using an exponentially weighted low-pass filter

$$T_k(t+1) = \begin{cases} (1-1/t_c)T_k(t) + R_k(t)/t_c, & k = k^*, \\ (1-1/t_c)T_k(t), & k \neq k^*. \end{cases} \tag{95}$$

When t_c is large, the scheduler can wait a long time until transmitting to a user whose channel quality attains a peak. Unfortunately, it is difficult to

describe the performance of the proportional fair scheduler in closed-form, because of the filtering operation in (95).

Scheduling based on requested data rates only would be unfair, because it would strongly favor the users close to the base station. However, when requested data rates are normalized by their respective average throughputs, a scheduling algorithm is fair. In comparisons of Sections 4.2 - 4.5 the long-term fairness is achieved by reporting a SNR threshold relative to mean received SNR, which removes the effect of different path losses due to different locations of users. We derive asymptotic expression for capacity gains of the three systems together with TSC and study the effect of feedback errors. Such errors could be avoided with strong forward error correcting codes, but this is not a favorable solution when small overheads and feedback latencies are desired.

Capacity of OOS is studied in Sections 4.2 - 4.5 based on the results in [17]. In Section 4.6, BEP in the presence of OOS is considered using results of [18] and in Section 4.7 the effect of feedback quantization is investigated [19]. References [20], [21], [22], [23] and [24] provide additional information.

4.1 System Model

The transmission system is shown in Figure 13, where a single data link, transmitted by the base station, is shared between K mobile users. Furthermore, a MISO system is assumed, where BS is equipped with M_t transmit antennas, each mobile station has a single receive antenna and it is assumed that mobile stations are able to estimate the M_t different channels from the common pilot signals multiplexed to the data. Such a common code multiplexed pilot structure is employed, for example, in FDD WCDMA system [35]. Moreover, we assume that the M_t channels are uncorrelated block flat Rayleigh fading channels which remain constant during each transmission time interval (TTI) and channel coefficients between separate TTIs are independent.

As with HSDPA fast PC is not applied. However, slow PC can be used to compensate shadow fading. Our analysis covers the following two alternative approaches:

PC1. Base station applies slow PC so that all K users experience identical long-term and short-term channel statistics.

PC2. Mean received SNR, denoted by $\bar{\gamma}$, of different users may vary but short-term statistics of relative SNR $\gamma/\bar{\gamma}$ is the same for all users.

The important common property for PC1 and PC2 is that the scheduling decision is based on the relative SNR in both approaches. In practice, the two approaches, however, will lead to systems of very different nature.

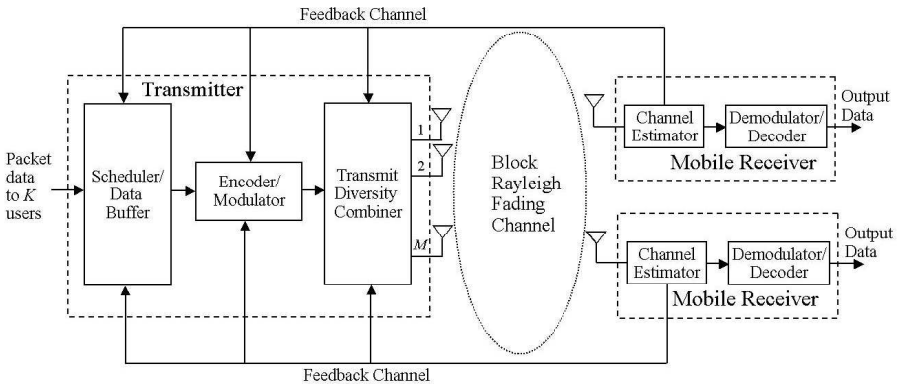

Figure 13: Model for the scheduling on a shared channel.

In PC1 long-term power control is applied to compensate path losses of users situated in different geographical locations. This results in different transmit powers, but all users may apply the same service independently of their mean path losses. The scheme provides temporal fairness in the sense that each user obtains an equal share of transmit resources over time. Furthermore, PC1 provides also throughput fairness, because the users obtain an equal share of the total system throughput as well. However, PC1 is suitable only when interference to neighboring cells is not an issue. Network expenses will be high due to small cell coverage if the system is expected to support high data rates.

Base station applies a fixed transmit power in PC2. This approach is a more capacity preserving solution from the whole network point of view than PC1. From user point of view it is not as fair as PC1, because users near the transmitter may have an access to higher data rates than users that are located on the cell edge. Thus, PC2 provides temporal fairness but not throughput fairness.

On-off Scheduling

On-off scheduling is defined as a method where transmitter selects the served user from the set of users for which the received SNR γ exceeds the predefined SNR threshold γ_0. If $\gamma < \gamma_0$ for all users, the served user is randomly selected to guarantee that all compared schedulers deliver the same total transmit power. Another possibility is to suspend the transmission when none of the SNRs are good enough, which would be a better solution from network point of view. Threshold $\gamma_0 = \xi\bar{\gamma}$ is set in the BS on long-term basis. During the setup process the mean received SNR is first estimated in mobile terminal and signaled to BS. Then the relative threshold ξ is chosen by BS and signaled to the terminal, see Figure 14. In practical systems,

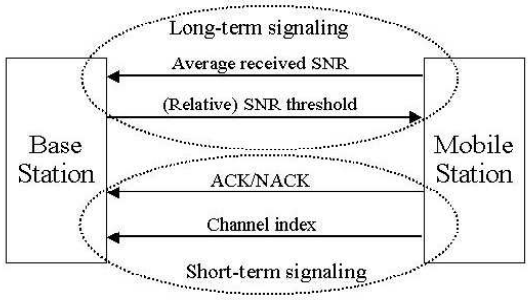

Figure 14: Signaling between base and mobile stations in on-off scheduling.

threshold ξ would be service-specific but since the range of different services may be large, which would lead to unnecessary system complexity, we will employ the same ξ for all users in examples.

Since $\bar{\gamma}$ and ξ are signaled on long-term basis, the corresponding signaling overhead is small. On the contrary the acknowledgement (ACK) that carries instantaneous OOS information needs to be signaled on short-term basis. Fortunately, the information consists of one bit per TTI and again, the signaling overhead is small when compared to full SNR feedback. If OOS is applied on top of TSC, terminal monitors M_t channels, defines the largest channel power and sends the corresponding antenna index together with the one-bit scheduling information to the BS, see Figure 14.

Only scarce channel information is available to BS in OOS. According to this information users can be divided into two groups and the served user is selected from the group of users for which $\gamma > \gamma_0$. We could also assume 2^κ-state quantization with κ-bit scheduling feedback. Then we could divide active users into 2^κ sets and select the user from the set with the highest received SNR. When the number of quantization sets grows to infinity we obtain an ideal case where SNR of each user is perfectly known in the BS. In the analysis we will consider only extreme cases where received SNR is not known in BS, there is one-bit scheduling information, or SNRs of all users are perfectly known in BS. The feedback channel is similar to that with the transmit diversity system in Section 3. Finally, we note that the effect of feedback latency is neglected, which is approximately valid within low mobility environments.

Analyzed Systems

We compare three adaptive systems where the channel is assumed to be perfectly known in the receiver, but the amount of CSI in the transmitter varies.

System 1) TSC and round robin. This is a baseline system where the served user is randomly selected among K active users, or the selection is performed according to a fixed sequence. The system does not take into account users' channel states, but there is a user-specific feedback concerning antenna selection. Feedback may be corrupted and the probability of feedback bit error is denoted by p. Antenna selection feedback consists of the index of the best transmit antenna only, and it is not useful from scheduling point of view.

System 2) TSC and OOS. In OOS, the served user is selected randomly or according to a fixed sequence among the users that have reported a positive ACK. If negative acknowledgement (NACK) is received from all users, the served user is randomly chosen among all active users. Hence, OOS takes into account the channel state between users in a very simple way: Users are divided into two groups according to one-bit feedback information and the served user is selected from the group of users with favorable feedback bit. The ACK/NACK decision is made in terminal based on the relative SNR $\gamma/\bar{\gamma}$. Probability of ACK/NACK error in OOS is denoted by q.

System 3) TSC and maximum SNR scheduling. Here we assume that BS knows the relative SNR of the best channel out of M_t alternatives. Thus, terminal reports unquantized relative SNR $\gamma/\bar{\gamma}$, where γ is the SNR of the strongest channel, to BS, and the user with the best relative SNR is served.

Comparison

The primary intention of the comparison is not to provide absolute performance results, but instead, we adopt the following two goals using capacity of the shared link as a performance measure:

- Investigate the effect of relative SNR feedback to the system performance.
- Track the effect of feedback errors.

For the first goal we make a comparison between systems 1-3, but for the second goal we only investigate systems 1 and 2. Although it is known that system capacity in SISO channels is maximized when all resources are given to the user with the best *absolute* SNR, we study systems where CSI in the transmitter is based on the *relative* SNR, because it provides a good starting point when designing practical and 'more fair' scheduling strategies than the conventional maximum SNR scheduling.

Fast power control is not applied on the shared channel and in performance comparisons we can apply the channel capacity assuming constant transmit power and optimal rate adaptation to the channel fading. Thus,

$$C_l(\bar{\gamma}) = B \cdot \mathrm{E}\{\log_2(1+\gamma)|\text{system } l\}. \tag{96}$$

Capacities of the different systems can then be obtained by using corresponding SNR distributions.

Finally, we note that the mean user capacities in systems 1-3 are simply given by C_l/K, $l = 1, 2, 3$, provided that there are K active users. While delay can be fixed in system 1 to K TTIs, in systems 2 and 3 the delay varies, the expectation being the same K TTIs. In practice, the variation of the delay depends on queueing principles of the schedulers and type of services.

4.2 Round Robin Scheduling with TSC

Closed-form capacity formulas for receiver selection combining have been previously considered in [54], and the results are directly applicable also to TSC provided that error-free feedback is available. Since this is not necessarily the case in system 1 we extend the capacity analysis to cover TSC with corrupted feedback.

Probability Density Function

We begin by recalling the distribution of the received SNR after error-free transmitter selection combining over M_t antennas,

$$f_{\text{TSC}}(\gamma) = \frac{M_t}{\bar{\gamma}} \cdot e^{-\gamma/\bar{\gamma}} \big(1 - e^{-\gamma/\bar{\gamma}}\big)^{M_t - 1}. \tag{97}$$

For the SNR distribution of system 1 it remains to model the effect of feedback errors. For this purpose we recall the model in Section 3.5, and assume for simplicity that $M_t = 2^\kappa$, $\kappa \in \mathbb{N}$ so that the uncoded feedback word in TSC contains κ bits. Following the reasoning of (92), (93) and (94) we find that the PDF of received SNR in system 1 - denoted by f_1 - can be written as

$$f_1(\gamma) = \Big(1 - \frac{M_t p_w}{M_t - 1}\Big) f_{\text{TSC}}(\gamma) + \frac{M_t p_w}{M_t - 1} f_{\text{SA}}(\gamma), \tag{98}$$

where $p_w = 1-(1-p)^\kappa$, $\kappa = \log_2(M_t)$, is the feedback word error probability and f_{SA} is the PDF corresponding to the single antenna transmission. Hence, the PDF of SNR for TSC with corrupted feedback can be expressed in terms of PDF of SNR for TSC without feedback errors and PDF corresponding to single antenna transmission.

Computation of Capacity

Capacity for system 1 can be computed using (96) and (98). For that purpose we recall from [54] the capacity formula for TSC over M_t antennas. We

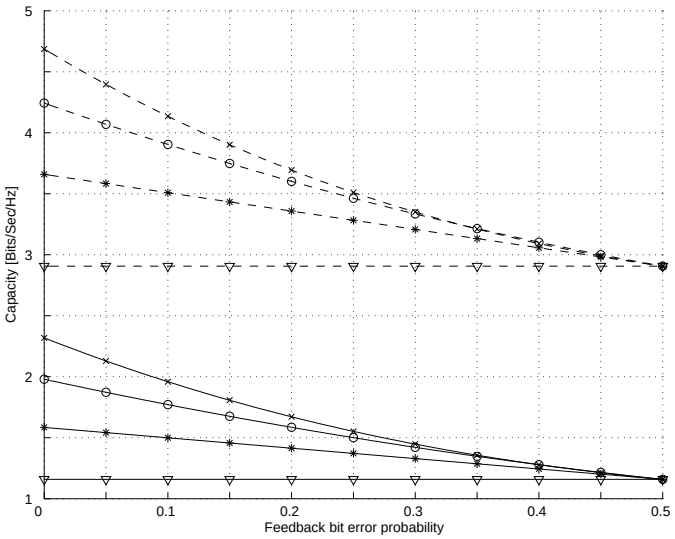

Figure 15: Capacity of system 1 as a function of feedback bit error probability when $SNR = 2$ dB (solid curves), $SNR = 10$ dB (dashed curves) and $M_t = 1$ (-∇-), $M_t = 2$ (-*-), $M_t = 4$ (-o-) and $M_t = 8$ (-x-).

have

$$C_{\mathrm{TSC}}(\bar{\gamma}) = B \cdot \log_2(e) \sum_{m=1}^{M_t} \binom{M_t}{m} (-1)^{m-1} e^{m/\bar{\gamma}} E_1\big(m/\bar{\gamma}\big). \tag{99}$$

The required capacity for single antenna transmission - denoted by C_{SA} - over Rayleigh fading channel is obtained from (99) by setting $M_t = 1$. By (98) and (99) we obtain

$$C_1(\bar{\gamma}) = \Big(1 - \frac{M_t p_w}{M_t - 1}\Big) C_{\mathrm{TSC}}(\bar{\gamma}) + \frac{M_t p_w}{M_t - 1} C_{\mathrm{SA}}(\bar{\gamma}). \tag{100}$$

Figure 15 depicts the capacity of system 1 as a function of feedback bit error probability when SNR is 2 and 10 dB, and $M_t = 1, 2, 4, 8$. It is found that the adverse effect of feedback errors increases with the number of transmit antennas. This is due to the fact that for fixed bit error probability the feedback word error probability increases rapidly when the length of the feedback word is growing. Hence, if the number of transmit antennas is large, uncoded feedback is a suitable choice only if the bit error probability on the feedback channel is small.

Figure 15 also hints that capacity gain from TSC increases with SNR. However, the gain will saturate when SNR becomes large. To show this we deduce the formula

$$C_1(\bar{\gamma}) = C_{\mathrm{SA}}(\bar{\gamma}) + \Big(1 - \frac{M_t p_w}{M_t - 1}\Big) \Delta_1(\bar{\gamma}), \tag{101}$$

where Δ_1 is the selection gain over M_t antennas, given by

$$\Delta_1(\bar{\gamma}) \approx B \cdot \sum_{m=1}^{M_t} \binom{M_t}{m} (-1)^m \log_2(m),\ \bar{\gamma} >> 1. \tag{102}$$

Through this formula it is found that in high SNR region selection gain depends only on the number of antennas. Furthermore, feedback errors reduce the achievable gain and the gain vanishes when $p = 0.5$.

Let us now show (101)– (102). From (100) we obtain

$$C_1(\bar{\gamma}) - C_{\text{SA}}(\bar{\gamma}) = \Big(1 - \frac{M_t p_w}{M_t - 1}\Big)\big(C_{\text{TSC}}(\bar{\gamma}) - C_{\text{SA}}(\bar{\gamma})\big). \tag{103}$$

The difference on the right hand side represents the gain of TSC when feedback is error-free. At this stage we recall that exponential integral function admits the expression [69]

$$E_1(x) = -e_0 - \log(x) - \sum_{n=1}^{\infty} \frac{(-x)^n}{n \cdot n!}, \tag{104}$$

where $e_0 = 0.5772156649$ refers to Euler constant. If x is small, we may neglect the sum term and approximate

$$E_1(x) \approx -e_0 - \log(x), \quad x << 1. \tag{105}$$

By (103) we have $\Delta_1 = C_{\text{TSC}}(\bar{\gamma}) - C_{\text{SA}}(\bar{\gamma})$ and if $\bar{\gamma} >> 1$, we find from (99) and (105) that

$$\begin{aligned} \Delta_1(\bar{\gamma}) \approx B \cdot \log_2(e) \sum_{m=1}^{M_t} \binom{M_t}{m} (-1)^m \big(e_0 + \log(m/\bar{\gamma})\big) \\ + B \log_2(e)\big(e_0 + \log(1/\bar{\gamma})\big). \end{aligned} \tag{106}$$

Here we can apply the equation

$$\sum_{m=1}^{M_t} \binom{M_t}{m} (-1)^m = -1 \tag{107}$$

that can be easily shown to be valid by binomial expansion. Equation (102) is now obtained by (106) and (107), and (101) follows by (103).

4.3 On-off Scheduling with TSC

In order to avoid unnecessary complexity in the analysis of system 2 we neglect the effect of TSC errors and concentrate on OOS errors. However, incorporating TSC errors to the analysis is a straightforward extension.

Probability Density Function

Assume first an error-free feedback and let P_+ be the probability that a user sends an ACK, and $P_+ = 1 - P_-$, where P_- is the probability of NACK. Then, in system 2 the PDF of SNR on the shared channel attains the form

$$f_2(\gamma) = (1 - P_-^K) f_2(\gamma|I_+) + P_-^K f_2(\gamma|I_-), \tag{108}$$

where $1 - P_-^K$ is the probability that $\gamma \in I_+ = (\gamma_0, \infty)$ for some of the users and P_-^K indicates that $\gamma \in I_- = (0, \gamma_0]$ for all users. Without feedback errors the conditional PDFs are of the form

$$f_2(\gamma|I_\pm) = u_\pm(\gamma) f_{\text{TSC}}(\gamma)/P_\pm, \tag{109}$$

where $u_\pm$ is the step function such that

$$u_+(\gamma) = \begin{cases} 1, & \gamma > \gamma_0 \\ 0, & \gamma \leq \gamma_0 \end{cases}, \; u_-(\gamma) = 1 - u_+(\gamma). \tag{110}$$

It will turn out that the capacity of system 2 can be expressed in terms of a certain ACK probability that is further related to threshold ξ through the equation

$$P_+ = 1 - F_{\text{TSC}}(\gamma_0) = 1 - (1 - e^{-\xi})^{M_t}, \tag{111}$$

where F_{TSC} refers to the cumulative distribution function (CDF) of TSC. Hence, it is found that

$$\xi = -\log\left(1 - (1 - P_+)^{1/M_t}\right). \tag{112}$$

This formula can be used when illustrating the capacity of system 2 as a function of ACK probability.

It is assumed that terminal compares the received SNR to a threshold without errors, but feedback errors may corrupt decisions made in the BS. If ACK/NACK information is corrupted, we have

$$f_{2,q}(\gamma|I_\pm) = \frac{(1-q) \cdot u_\pm(\gamma) + q \cdot u_\mp(\gamma)}{(1-q) \cdot P_\pm + q \cdot P_\mp} f_{\text{TSC}}(\gamma), \tag{113}$$

where q is the ACK/NACK error probability and the denominator gives the ACK/NACK probability in BS in the presence of feedback errors. There are two possible events leading to positive ACK decision in BS: The received SNR in terminal is above the given threshold and the received feedback in BS is correct, or the received SNR is below the threshold but the feedback is corrupted and BS receives ACK. Analogously, NACK decision in BS may precede two similar but complementary events. We write

$$P_{\pm,q} = (1-q) \cdot P_\pm + q \cdot P_\mp = q + (1 - 2q) \cdot P_\pm, \tag{114}$$

and after some simple manipulations we obtain

$$f_{2,q}(\gamma|I_{\pm}) = \frac{(1-2q)\cdot P_{\pm} f_2(\gamma|I_{\pm})}{P_{\pm,q}} + \frac{q\cdot f_{\mathrm{TSC}}(\gamma)}{P_{\pm,q}}. \tag{115}$$

The PDF of SNR in case of system 2 with corrupted feedback is given by

$$f_{2,q}(\gamma) = (1-P_{-,q}^K) f_{2,q}(\gamma|I_+) + P_{-,q}^K \cdot f_{2,q}(\gamma|I_-). \tag{116}$$

Computation of Capacity

From (115) it is found that capacity for system 2 can be deduced provided that conditional capacities can be computed. Using (109) we obtain

$$C_2(\bar{\gamma}|I_+) = \frac{B\cdot \log_2(e)}{P_+} \int_{\gamma_0}^{\infty} \log(1+\gamma) f_{\mathrm{TSC}}(\gamma) d\gamma. \tag{117}$$

After applying the integration by parts it is found that

$$C_2(\bar{\gamma}|I_+) = \frac{B\cdot \log_2(e)}{P_+} \Big(P_+ \log(1+\gamma_0) + \int_{\gamma_0}^{\infty} \frac{1-F_{\mathrm{TSC}}(\gamma)}{1+\gamma} d\gamma \Big). \tag{118}$$

In (118) we apply the equality

$$F_{\mathrm{TSC}}(\gamma) = \sum_{m=0}^{M_t} \binom{M_t}{m} (-1)^m e^{-m\gamma/\bar{\gamma}} \tag{119}$$

that is found by binomial expansion. Before combining the last two equations we give the formula

$$\int_{\gamma_0}^{\infty} \frac{e^{-m\gamma/\bar{\gamma}}}{1+\gamma} d\gamma = e^{m/\bar{\gamma}} E_1((1+\gamma_0)m/\bar{\gamma}) \tag{120}$$

that results after using the substitution $(1+\gamma)m/\bar{\gamma} \to \gamma$. The formula for conditional capacity (117) is achieved by combining (118), (119) and (120). We have

$$\begin{aligned} C_2(\bar{\gamma}|I_+) = \frac{B\cdot \log_2(e)}{P_+} \Big(& P_+ \log(1+\gamma_0) \\ & + \sum_{m=1}^{M_t} \binom{M_t}{m} (-1)^{m-1} e^{m/\bar{\gamma}} E_1\big((1+\gamma_0)m/\bar{\gamma}\big) \Big). \end{aligned} \tag{121}$$

Furthermore, in case of feedback errors there holds

$$C_{2,q}(\bar{\gamma}|I_{\pm}) = \frac{(1-2q)\cdot P_{\pm} C_2(\bar{\gamma}|I_{\pm})}{P_{\pm,q}} + \frac{q\cdot C_{\mathrm{TSC}}(\bar{\gamma})}{P_{\pm,q}}. \tag{122}$$

For the final capacity formula we also need the capacity on the condition that $\gamma \leq \gamma_0$. For that purpose we note that

$$C_2(\bar{\gamma}|I_-) = \frac{1}{P_-}\big(C_{\text{TSC}}(\bar{\gamma}) - P_+ C_2(\bar{\gamma}|I_+)\big). \tag{123}$$

Capacity of system 2 is obtained using (116), (115) and (121) - (123).

Let us suppose an extreme case where $K \to \infty$. This case is interesting because it provides an upper bound for the achievable capacity in system 2. Now, for any threshold γ_0 there exists a user with $\gamma > \gamma_0$. Hence, with '+' equation (122) defines the capacity of system 2. Moreover, we have

$$\begin{aligned} C_{2,q}(\bar{\gamma}|I_+) &\geq \frac{(1-2q)P_+}{q+(1-2q)P_+} C_2(\bar{\gamma}|I_+) \\ &\geq \frac{(1-2q)P_+}{q+(1-2q)P_+} C_{\text{AWGN}}(\xi\bar{\gamma}), \end{aligned} \tag{124}$$

where the latter estimate follows from (118) because the integral term in (118) is positive and can be dropped out from (124).

Assume for a while that the mean SNR is fixed. If $q \neq 0$, then (124) gives only a trivial bound when $P_+ \to 0$, but if there are no feedback errors, the lower bound in (124) grows without limit when $P_+ \to 0$. Although (124) hints that large capacity gains can be achieved on the shared channel if the number of active users is large, the capacities of individual users decay, because there is an increasing number of users competing simultaneously on the same shared channel resource.

This phenomenon is illustrated in Figure 16, which shows the capacity of system 2 as a function of ACK probability when $K \to \infty$. It is found that the effect of feedback errors is largest when ACK probability is small. This is due to the fact that the error event where BS transmits although terminal sent NACK begins to dominate when P_+ is small. Then it might even happen that most of the packets are transmitted at a wrong time. Hence, the expected P_+ should be taken into account in the design of the feedback channel. Finally, we note that the effect of scheduling errors is smaller in case of four transmit antennas than in case of one transmit antenna, because overall gain of OOS is smaller when also TSC is applied.

Assume next a finite number of users and a fixed probability of ACK. Then we may write

$$C_2(\bar{\gamma}) = C_{\text{SA}}(\bar{\gamma}) + \Delta_2(\bar{\gamma}), \tag{125}$$

where Δ_2 represents the gain of system 2 versus continuous single antenna transmission. Let us compute this gain. For simplicity we neglect the effect of feedback errors. Then, by using (123) we obtain

$$\begin{aligned} C_2(\bar{\gamma}) &= (1-P_-^K)C_2(\bar{\gamma}|I_+) + P_-^K C_2(\bar{\gamma}|I_-) \\ &= (1-P_-^{K-1})C_2(\bar{\gamma}|I_+) + P_-^{K-1} C_{\text{TSC}}(\bar{\gamma}). \end{aligned} \tag{126}$$

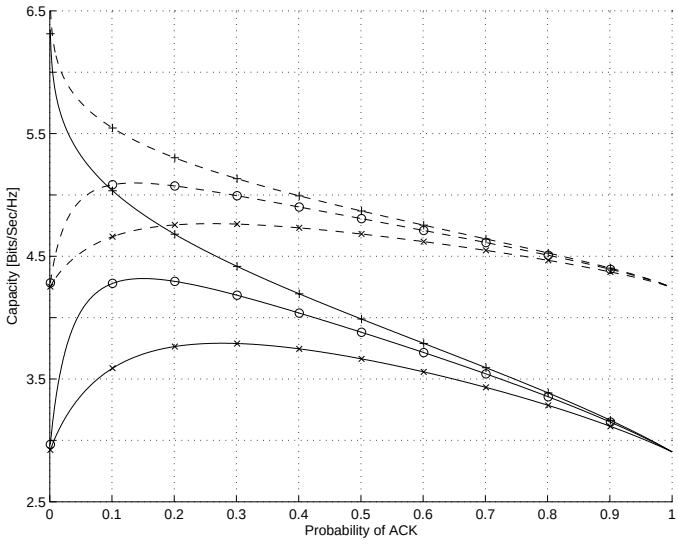

Figure 16: Capacity of system 2 as a function of ACK probability when $K \to \infty$, $SNR = 10$ dB, $M_t = 1$ (solid curves), $M_t = 4$ (dashed curves) and $q = 0.00$ (-+-), $q = 0.05$ (-o-) and $q = 0.15$ (-x-).

With the help of (126) we may further write

$$\begin{aligned} \Delta_2(\bar{\gamma}) &= C_2(\bar{\gamma}) - C_{\text{SA}}(\bar{\gamma}) \\ &= (1 - P_-^{K-1})\Delta_+(\bar{\gamma}) + P_-^{K-1}\Delta_1(\bar{\gamma}), \end{aligned} \tag{127}$$

where Δ_1 is the gain of system 1, given by (102) when $\bar{\gamma} >> 1$ and by (121) we have

$$\begin{aligned} \Delta_+(\bar{\gamma}) &= C_2(\bar{\gamma}|I_+) - C_{\text{SA}}(\bar{\gamma}) \\ &= B\log_2(e)\Big(\log(1+\xi\bar{\gamma}) - e^{1/\bar{\gamma}}E_1(1/\bar{\gamma}) \\ &+ \frac{1}{P_+}\sum_{m=1}^{M_t}\binom{M_t}{m}(-1)^{m-1}e^{m/\bar{\gamma}}E_1\big((1+\xi\bar{\gamma})m/\bar{\gamma}\big)\Big). \end{aligned}$$

If $\bar{\gamma} >> 1$, we can apply the approximation

$$\log(1+\xi\bar{\gamma}) - e^{1/\bar{\gamma}}E_1(1/\bar{\gamma}) \approx e_0 + \log(\xi). \tag{128}$$

Hence, Δ_+ attains the form

$$\begin{aligned} \Delta_+(\bar{\gamma}) \approx B \cdot \log_2(e)\Big(e_0 + \log(\xi) \\ + \sum_{m=1}^{M_t}\binom{M_t}{m}\frac{(-1)^{m-1}E_1(\xi m)}{1-(1-e^{-\xi})^{M_t}}\Big), \quad \bar{\gamma} >> 1. \end{aligned} \tag{129}$$

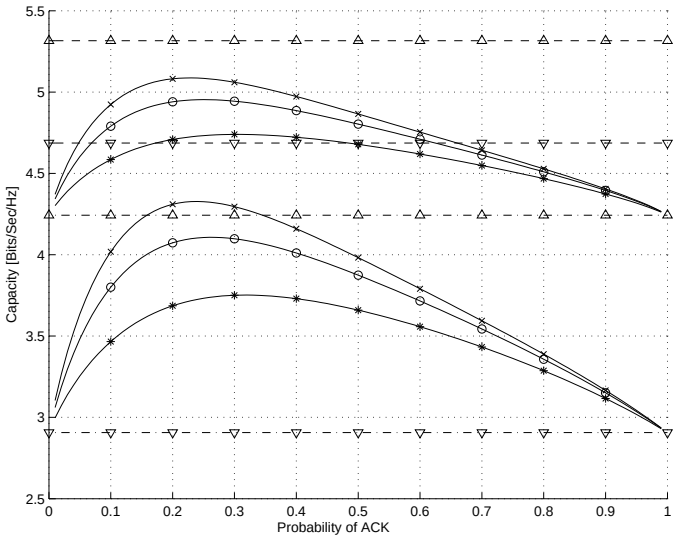

Figure 17: Capacity of system 1 (dash-dot lines), system 2 (solid curves) and system 3 (dashed lines) as a function of threshold exceeding probability when $SNR = 10$ dB and $K = 8$, $q = 0.00$ (-x-), $q = 0.05$ (-o-), $q = 0.15$ (-*-). Number of transmit antennas is $M_t = 1$ (symbols '∇' for systems 1 and 3, lower set of solid curves for system 2) and $M_t = 4$ (symbols 'Δ' for systems 1 and 3, upper set of solid curves for system 2).

It is found from (125), (127) and (129) that for a finite number of active users and fixed ACK probability the gain of system 2 against continuous single antenna transmission is constant in high SNR region. Moreover, if we increase the number of active users, ξ increases but using (5.1.51) of [69] it is found that the second term in (129) remains bounded. Then Δ_+ admits logarithmic growth with respect to ξ.

4.4 Maximum SNR Scheduling with TSC

In third system BS knows perfectly the relative SNR of K channels, each representing the largest relative SNR out of M_t alternatives. Based on this information BS then selects the served user among K active users.

Now SNR threshold is irrelevant, because the best channel out of $M_t \cdot K$ channels is always selected. However, we note that in practice, when SNR is applied as a decision basis in scheduling, some SNR quantization is always applied dividing active users into 2^κ groups where κ is the number of feedback bits. If the received SNR is the only parameter in the scheduling decision, the served user is selected from the group of users with the largest reported relative SNR. Increasing the number of quantization sets finally results in a system where relative SNR is perfectly known in BS. Then the

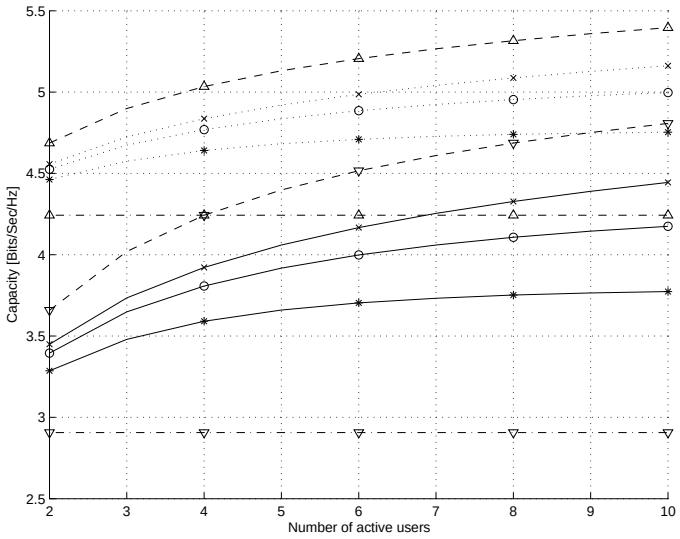

Figure 18: Capacity of system 1 (dash-dot lines), system 2 (solid and dotted curves) and system 3 (dashed curves) when $SNR = 10$ dB, $q = 0.00$ (-x-), $q = 0.05$ (-o-) and $q = 0.15$ (-*-) as a function of active users. The number of transmit antennas is $M_t = 1$ (symbols '∇' for systems 1 and 3, set of solid curves for system 2) and $M_t = 4$ (symbols 'Δ' for systems 1 and 3, set of dotted curves for system 2). System 2 applies optimal ACK probability.

PDF of SNR on the shared channel is given by

$$f_3(\gamma) = K \cdot f_{\mathrm{TSC}}(\gamma) F_{\mathrm{TSC}}(\gamma)^{K-1} = M_t \cdot K \cdot f_{\mathrm{SA}}(\gamma) F_{\mathrm{SA}}(\gamma)^{M_t \cdot K - 1}.$$

The capacity of the shared link is now obtained from (99) by substituting $M_t \cdot K$ to M_t. Feedback errors are not modelled because there is no quantization. Finally, we note that asymptotic formula similar to (101) and (102) can be easily deduced for system 3 as well. The corresponding gain of system 3 against continuous single antenna transmission is denoted by Δ_3 and according to (102) we have

$$\Delta_3(\bar{\gamma}) \approx B \cdot \sum_{m=1}^{M_t \cdot K} \binom{M_t \cdot K}{m} (-1)^m \log_2(m), \ \bar{\gamma} >> 1.$$

4.5 Comparisons and Conclusions

We begin the comparison from Figure 17, which shows the capacities of systems 1-3 as a function of ACK probability when SNR=10 dB, $K = 8$, and the curves are based on closed-form formulas of the previous sections.

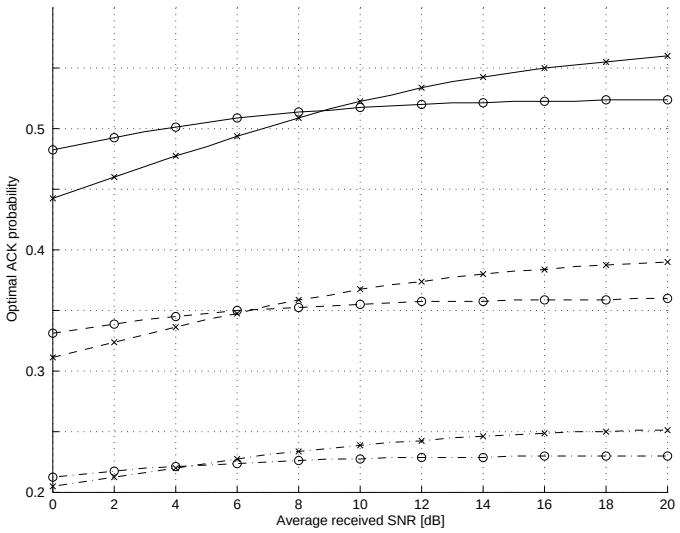

Figure 19: Optimal ACK probability in system 2 as a function of mean SNR when $M_t = 1$ (-x-), $M_t = 4$ (-o-) and the numbers of active users are 2 (solid curves), 4 (dashed curves) and 8 (dash-dot curves).

As was already noticed from the asymptotic formula of Δ_2, the capacity of system 2 varies with the ACK probability, and Figure 17 shows that there exists an ACK probability which maximizes capacity. With error-free feedback and single transmit antenna the difference between capacities of system 2 and 3 is only round 0.5 bits/sec/Hz when applying optimal ACK probability. On the other hand, at this optimal point the capacity difference between systems 1 and 2 is slightly less than 1.5 bits/sec/Hz. Hence, with OOS it is possible to achieve round $G = 75\%$ of the gain of relative SNR feedback, where the relative gain of OOS is defined as

$$G = \frac{C_2 - C_1}{C_3 - C_1} \cdot 100\%.$$

Note that we measure the gain of OOS with respect to round robin, while the 90% gain in [74] refers to percentage of the maximum SNR scheduling gain. Approximately the same ratio applies with four transmit antennas but the absolute gains are smaller. In fact, if the number of active users is fixed but the number of transmit antennas increases, the lower and upper bounds for the capacity of system 2, defined by capacities of systems 1 and 3, respectively, are closing and achievable scheduling gain is decreasing. In high SNR region, this difference can be computed from (102).

We also find from Figure 17 that the effect of scheduling errors is remarkable but not as dramatic as in Figure 16 where feedback errors become a dominating factor when ACK probability is small. Thus, the results point

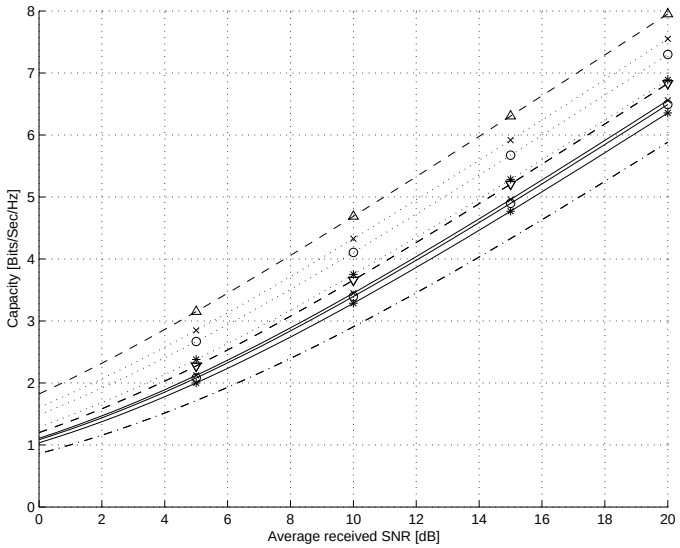

Figure 20: Capacity of system 1 (dash-dot curve), system 2 (solid and dotted curves) and system 3 (dashed curves) when $M_t = 1$ and $q = 0.00$ (-x-), $q = 0.05$ (-o-), $q = 0.15$ (-*-). The number of users is 2 (solid curves for system 2, symbols '∇' for system 3) and 8 (dotted curves for system 2, symbols 'Δ' for system 3). Optimal ACK probability is applied.

out that uncoded feedback is applicable if the feedback error ratio is low.

Figure 18 depicts the capacities of systems 1-3 as a function of the number of active users when SNR=10 dB. It shows that the capacities of systems 2 and 3 admit a logarithmic growth with additional users, as expected based on formulas of Δ_2 and Δ_3. This feature has also been observed in [72]. It is seen that the relative gain G increases with the number of users and thus, even more than 75% of the achievable gain can be obtained by OOS. The effect of feedback errors to the scheduling increases with the number of users, because errors reduce the slope of the capacity curves. We note that optimal ACK probability was applied when computing the capacity of system 2.

While the mean SNR is the same for all users with PC1, with PC2 the received mean SNR between users may greatly vary depending on the geographical distribution of the users. Thus, the optimal ACK probability is applicable when assuming PC1 but in case of PC2 the simplest choice is to use a fixed ACK probability although users' mean SNRs are different. Figure 19 shows the optimal ACK probability as a function of mean SNR. It is seen that the best ACK probability depends only slightly on the SNR and this weak dependency is even smaller when TSC is applied. Moreover, the best ACK probability is almost directly proportional to the inverse of the number of active users. The results of Figure 19 hint that there is no

large penalty when fixed ACK probability and the corresponding threshold ξ are applied to the whole SNR scale.

Figure 20 displays the capacities of systems 1-3 as a function of mean SNR when optimal ACK probability is applied. We note that the results would have been practically the same, up to figure resolution, if fixed ACK probability, optimal for SNR=10 dB, had been applied to the whole SNR scale. Hence the results of Figure 20 are valid for both PC1 and PC2. It is worth mentioning that the gains of systems 2 and 3 against system 1 remain noticeable also when SNR is low.

4.6 Computation of Bit Error Probabilities

The goal of this section is to investigate the receiver BEP when OOS is applied. Results will show that the effect of feedback errors is crucial to the system. Without feedback errors the asymptotic decay of BEP is exponential while in the presence of feedback errors the slope of the asymptotic decay of BEP is the same as in case of continuous transmission.

We have adopted the system model from Section 4.1. The only difference is that we now also consider the rate 1 orthogonal space–time block coded (STBC) transmission that is available for BPSK modulation when $M_t \in \{2, 4, 8\}$ [49]. In STBC, different code sequences are transmitted from separate antennas, and after decoding in the receiver, the received SNR is of the form

$$\gamma = \frac{1}{M_t} \sum_{m=1}^{M_t} \gamma_m.$$

We remark that the transmit power has been divided evenly between the M_t antennas.

General Formulas

The performance of the systems is studied using the bit error probability as a performance measure,

$$P_{\mathrm{e}}^{\mathrm{OOS}}(\bar{\gamma}) = \mathrm{E}\{P_{\mathrm{mod}}(\gamma) |\ \mathrm{OOS}\ \}.$$

We will concentrate in BPSK modulation, but the analysis can be extended to other MPSK and QAM schemes by utilizing the corresponding BEP approximations [71] or exact expressions [80] for P_{mod}. Furthermore, bit error probabilities for adaptive modulation schemes assuming different switching levels can be derived from the given expressions.

We recall that the PDF of SNR in the presence of OOS is defined by

$$f^{\mathrm{OOS}}(\gamma) = u_+(\gamma) f(\gamma) / P_+,$$

where u_+ is the step function of (110), P_+ is the probability of positive ACK in OOS and f refers to the PDF of SNR in the underlying unscheduled

system. In this section, f corresponds to single antenna transmission, TSC or STBC.

Assuming that the feedback bit error probability is q, we further recall that the PDF to be integrated is expressed in the form

$$f_q^{\mathrm{OOS}}(\gamma) = \frac{(1-q)\cdot u_+(\gamma) + q\cdot u_-(\gamma)}{(1-q)\cdot P_+ + q\cdot P_-} f(\gamma),$$

where the denominator gives the transmission probability in the presence of OOS feedback bit errors.

According to (114) and (115) the PDF attains the form

$$f_q^{\mathrm{OOS}}(\gamma) = \frac{(1-2q)\cdot P_+ f^{\mathrm{OOS}}(\gamma)}{P_{+,q}} + \frac{q\cdot f(\gamma)}{P_{+,q}}.$$

Hence, the PDF of the received SNR can be expressed in terms of the PDF of error-free transmission and continuous transmission. This implies the following interesting result on BEP. Namely, BEP in the presence of OOS and feedback bit errors can be written as

$$P_{\mathrm{e},q}^{\mathrm{OOS}}(\bar{\gamma}) = \frac{(1-2q)\cdot P_{\mathrm{e}}^{\mathrm{OOS}}(\bar{\gamma})}{P_{+,q}} + \frac{q\cdot P_{\mathrm{e}}(\bar{\gamma})}{P_{+,q}}, \tag{130}$$

where $P_{\mathrm{e}}^{\mathrm{OOS}}$ is the BEP without feedback errors and P_{e} is the BEP of continuous transmission.

Later we will see that the asymptotic decay of $P_{\mathrm{e}}^{\mathrm{OOS}}$ is exponential in the three example cases. Therefore, if $\bar{\gamma}$ is high, then P_{e} will dominate over $P_{\mathrm{e}}^{\mathrm{OOS}}$. This implies that the slope of the asymptotic BEP in the logarithmic scale is the same as in case of continuous transmission, but there is a constant BEP gain of magnitude $10\log_{10}(q/P_{+,q})$ at high SNR region. In system design q and P_+ should be selected such that feedback errors will not dominate in the SNR region where the system is operating.

Calculation of Bit Error Probabilities

We evaluate bit error probabilities by simply using the integration by parts. This is possible in the studied cases because the integral functions of distributions are known. Moreover, for the BPSK modulation we have

$$\frac{d}{d\gamma} P_{\mathrm{mod}}(\gamma) = -\frac{1}{\sqrt{4\pi\gamma}} e^{-\gamma} \tag{131}$$

(see [69] (6.5.17), (7.1.2) and (7.1.19)). This approach provides integral formulas that can be expressed using combinations of complementary incomplete gamma function

$$\Gamma(t,x) = \int_x^\infty e^{-s} s^{t-1} ds. \tag{132}$$

Single Antenna Transmission. Assume a single antenna transmission in flat Rayleigh fading environment. Then using (131), and integration by parts we find that the BEP is of the form

$$P_{\rm e}^{\rm OOS}(\bar{\gamma}) = \frac{1}{\sqrt{4\pi}}\Big(\Gamma\big(\frac{1}{2},\xi\bar{\gamma}\big) - \sqrt{\frac{\bar{\gamma}}{1+\bar{\gamma}}}e^{\xi}\Gamma\big(\frac{1}{2},\xi(1+\bar{\gamma})\big)\Big). \tag{133}$$

Before [18] a similar formula was presented in [42]. The formula for BEP in the presence of feedback errors can be found directly by using (130). Furthermore, employing (6.5.32) in [69] we obtain the asymptotic formula for large SNR

$$P_{\rm e}^{\rm OOS}(\bar{\gamma}) = \frac{e^{-\xi\bar{\gamma}}}{\sqrt{4\pi\xi\bar{\gamma}^3}}, \qquad \bar{\gamma} >> 1. \tag{134}$$

Hence, without feedback errors the asymptotic decay of BEP is exponential.

Figure 21 illustrates the performance of the single transmit antenna system when $P_{+,q} = 0.2$. This ACK probability of OOS is rather low and it can be used only if the number of active users is large. We note that in a K-user system with *i.i.d.* channels the system outage probability becomes $(1 - P_{+,q})^K$. The BEP results in this section are given for fixed $P_{+,q}$. For that purpose we solve ξ of (133) from equation

$$P_{+,q} = q + (1-2q)P_{+} = q + (1-2q)e^{-\xi}.$$

Then, after substituting the value of ξ into (133) we obtain by (130) BEP as a function of SNR for different values of $P_{+,q}$. It is seen that BEP decreases rapidly when SNR is high and there are no feedback errors. Moreover, it is noticed that feedback errors seriously degrade the performance at high SNR, and the asymptotic behavior of BEP in the presence of feedback errors is clearly visible.

OOS with TSC. In case of TSC, the PDF of SNR is given by (97) and the effect of antenna selection errors can be taken into account through formula (98). We note that the asymptotic diversity order is M_t when antenna selection is error-free and only OOS feedback is subject to errors. However, asymptotic diversity order becomes one when both feedback types are subject to feedback errors.

A closed-form expression for the BEP is deduced employing the integration by parts. This is possible because the integral function of $f_{\rm TSC}$ is known. Furthermore, applying the binomial expansion to the expression $(1 - e^{-\gamma/\bar{\gamma}})^M$ we obtain

$$P_{\rm e}^{\rm OOS}(\bar{\gamma}) = \frac{1}{\sqrt{4\pi}}\Big(\Gamma\big(\frac{1}{2},\xi\bar{\gamma}\big) + \sum_{m=1}^{M_t}\binom{M_t}{m}\sqrt{\frac{\bar{\gamma}}{m+\bar{\gamma}}}\frac{(-1)^m\Gamma\big(\frac{1}{2},\xi(m+\bar{\gamma})\big)}{1-(1-e^{-\xi})^{M_t}}\Big).$$

This equation provides the BEP of OOS when TSC is used and feedback information is error-free. Again, employing (6.5.32) in [69] we find that for

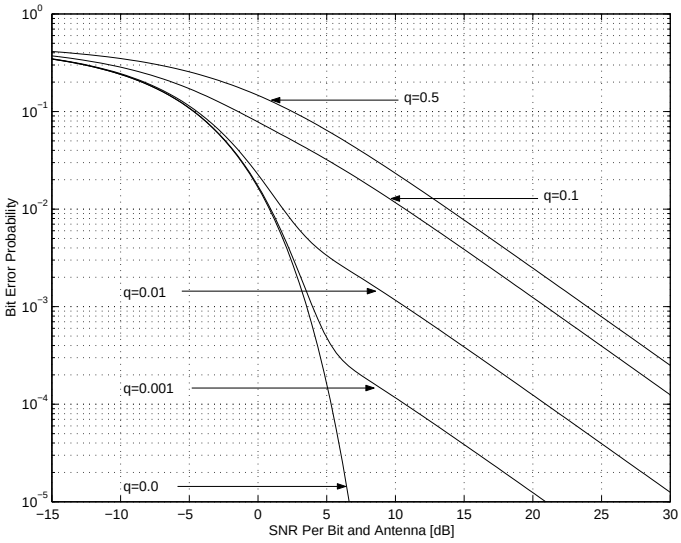

Figure 21: BEP of OOS when single antenna transmission is applied, $P_{+,q} = 0.2$ and OOS feedback bit error rate is 0%, 0.1%, 1%, 10% and 50%.

large SNR there holds

$$P_{\mathrm{e}}^{\mathrm{OOS}}(\bar{\gamma}) = \frac{e^{-\xi\bar{\gamma}}}{\sqrt{4\pi\xi\bar{\gamma}^3}}\Big(\frac{M_t e^{-\xi}(1-e^{-\xi})^{M_t-1}}{1-(1-e^{-\xi})^{M_t}}\Big).$$

We note that a fair comparison between TSC and single antenna transmission requires that bit error probabilities are calculated assuming the same ACK probability. This is possible, because ξ admit a closed–form expression as a solution of

$$P_{+,q} = q + (1-2q)(1-(1-e^{-\xi})^{M_t}).$$

Figure 22 displays the BEP performance of the antenna selection when $M_t = 4$ and $P_{+,q} = 0.2$. Antenna selection is assumed to be error-free in order to simplify the comparison between the methods. It is noticed that because of the diversity benefit of TSC, its performance is not as sensitive to feedback errors as that of the single transmit antenna system. Nevertheless, when feedback errors in the antenna selection are dominating, the performance gain from both antenna diversity and scheduling are lost. Again, asymptotic BEP gain is clearly seen.

Orthogonal Space–Time Coding. Now the PDF of the received SNR is the same as with M_t-antenna maximal ratio combining. Hence

$$f_{\mathrm{STBC}}(\gamma) = \frac{M_t}{\bar{\gamma}\cdot\Gamma(M_t)}\Big(\frac{M_t\gamma}{\bar{\gamma}}\Big)^{M_t-1}e^{-M_t\gamma/\bar{\gamma}}.$$

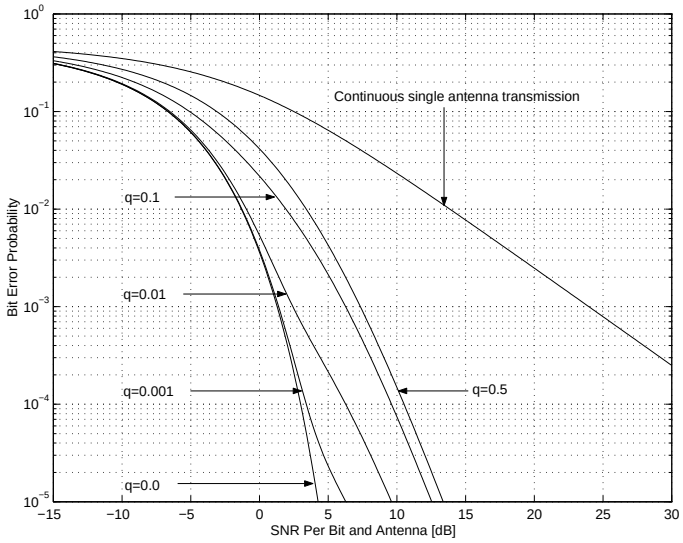

Figure 22: BEP of OOS when TSC is applied, $M_t = 4$, $P_{+,q} = 0.2$ and OOS feedback bit error rate is 0%, 0.1%, 1%, 10% and 50%.

The integral function of this PDF is found using (6.5.25) in [69],

$$f_{\mathrm{STBC}}(\gamma) = -\frac{M_t}{\bar{\gamma}\cdot\Gamma(M_t)}\frac{\partial\Gamma\big(M_t,t\big)}{\partial t}\Big|_{t=M_t\gamma/\bar{\gamma}}. \tag{135}$$

By (135) we find that ACK probability is of the form

$$P_+ = \frac{\Gamma\big(M_t,\xi M_t\big)}{\Gamma\big(M_t\big)} = 1-\mathcal{P}_{M_t}\big(\xi M_t\big), \tag{136}$$

where the last equality holds by (6.5.3), (6.5.4), (6.5.13) in [69] and $\mathcal{P}_{M_t}$ is the Poisson distribution function given by (52). Employing (135), integration by parts and similar arguments as in (136) we find that

$$P_{\mathrm{e}}^{\mathrm{OOS}}(\bar{\gamma}) = \frac{1}{\sqrt{4\pi}}\Big(\Gamma\big(\frac{1}{2},\xi\bar{\gamma}\big) - \int_{\xi\bar{\gamma}}^{\infty}\frac{e^{-\gamma}}{\sqrt{\gamma}}\frac{\mathcal{P}_{M_t}\big(M_t\gamma/\bar{\gamma}\big)}{\mathcal{P}_{M_t}\big(\xi M_t\big)}d\gamma\Big). \tag{137}$$

By substituting the expression (52) into (137) and using a suitable change of integration variable we obtain the following expression of $P_{\mathrm{e}}^{\mathrm{OOS}}$ in terms of complementary incomplete gamma function

$$P_{\mathrm{e}}^{\mathrm{OOS}}(\bar{\gamma}) = \frac{1}{\sqrt{4\pi}}\Big(\Gamma\big(\frac{1}{2},\xi\bar{\gamma}\big) - \sqrt{\frac{\bar{\gamma}}{M_t+\bar{\gamma}}}\sum_{m=0}^{M_t-1}\Big(\frac{M_t}{M_t+\bar{\gamma}}\Big)^m\frac{\Gamma\big(m+\frac{1}{2},\xi(M_t+\bar{\gamma})\big)}{\mathcal{P}_{M_t}\big(\xi M_t\big)\Gamma\big(m+1\big)}\Big).$$

In case of large SNR, applying again (6.5.32) in [69] we obtain

$$P_{\mathrm{e}}^{\mathrm{OOS}}(\bar{\gamma}) = \frac{M_t e^{-\xi\bar{\gamma}}}{\sqrt{4\pi\xi\bar{\gamma}^3}}.$$

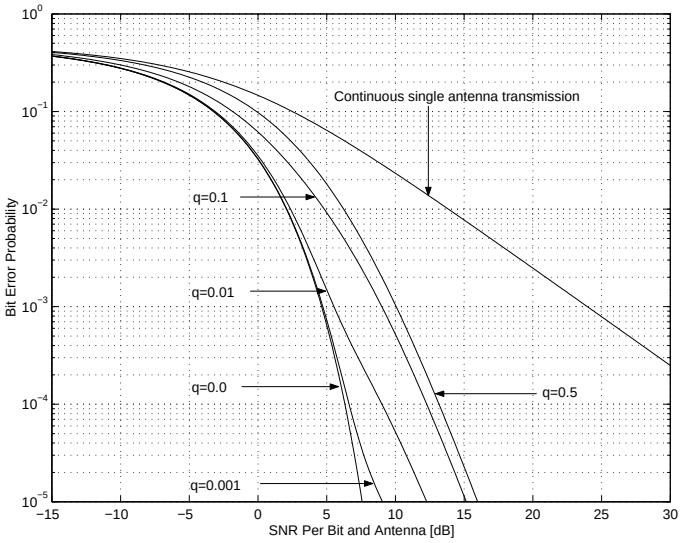

Figure 23: BEP of OOS when STBC is applied, $M_t = 4$, $P_{+,q} = 0.2$ and feedback bit error rate is 0%, 0.1%, 1%, 10% and 50%.

Here ξ does not attain a closed–form expression in terms of $P_{+,q}$. Instead, its value has to be approximated from (136).

The BEP performance of OOS with orthogonal space–time coded transmission when $M_t = 4$ and $P_{+,q} = 0.2$ is given in Figure 23. It is not surprising that the performance of space–time coded transmission is not as good as that of antenna selection. This is due to the fact that space–time coded transmission provides only diversity gain while antenna selection provides also additional SNR gain. However, it might be somewhat surprising that in case of error–free feedback channel the single antenna system outperforms space–time coded transmission. This is because the probability density function corresponding to the space–time coded transmission has the same mean but shorter tails than that of the single antenna transmission. Similar phenomenon has been also observed in case of multi-user diversity [72].

4.7 Effect of Quantization

This far we have applied OOS where feedback signaling is minimized by using one-bit quantization of CQI. Generalization of the one-bit quantization scheme has been studied and corresponding capacity expressions have been derived in [76] assuming that only the users, whose CQI exceeds a given threshold, report their (unquantized) CQIs to the base station. Quantization examples of CQI together with maximum SNR scheduling were also studied in [73] but no clear explanation, how to select the quantization levels, was given. Furthermore, capacity minimizing or block error rate

maximizing quantizations within maximum SNR scheduling were considered in [74] showing that two-bit quantization obtains 90% of the unquantized CQI gain in the example scenarios. The quantization regions were found using numerical optimization.

In this section we study the quantization of CQI in maximum SNR scheduling. We apply the system model of Section 4.1 and show closed-form expressions for BEP assuming suboptimal quantization strategy. Results are based on [19].

General Formulas

Optimal quantization of relative SNR depends on fading statistics as well as the selected performance measure. Below we use the bit error probability as a performance measure,

$$P_{\mathrm{e}}^{Q}(\bar{\gamma}) = \mathrm{E}\{P_{\mathrm{mod}}(\gamma) | \, Q \, \}, \tag{138}$$

where Q refers to the applied quantization. Let us give a general formulation of the studied quantization problem: Assume that $\mathbf{Q}$ is the set of all quantizations and let $Q = \{\xi_l\}_{l=0}^{L+1}$,

$$0 = \xi_0 < \xi_1 < \cdots < \xi_{L+1} = \infty, \quad \xi_l = \gamma_l / \bar{\gamma}, \tag{139}$$

where $\gamma_l = \xi_l \bar{\gamma}$ is boundary point of the true SNR quantization. If BEP is used as a performance measure, then the aim is to find $\hat{Q} \in \mathbf{Q}$ that minimize the BEP for a certain bit rate R, *i.e.*

$$P_{\mathrm{e}}^{\hat{Q}}(\bar{\gamma}) = \min\{P_{\mathrm{e}}^{Q}(\bar{\gamma}) : Q \in \mathbf{Q}, R\}. \tag{140}$$

It turns out that the best quantization $\hat{Q}$ varies with the mean SNR. Hence, the predefined target SNR defines the best quantization.

To this end, we need to compute the object function P_{e}^{Q}. Let q_l be the probability that a shared channel is dedicated to a user, whose received SNR is in the interval (γ_l, γ_{l+1}). Then the PDF f^Q can be expressed in the form

$$f^{Q}(\gamma) = \sum_{l=0}^{L} q_l \cdot \big(u_l(\gamma) f(\gamma) / p_l\big), \tag{141}$$

where f refers to the PDF of the SNR in the reference system and

$$u_l(\gamma) = \begin{cases} 1, \ \gamma \in (\gamma_l, \gamma_{l+1}), \\ 0, \ \text{otherwise}, \end{cases} \qquad p_l = \int_{\gamma_l}^{\gamma_{l+1}} f(\gamma) d\gamma. \tag{142}$$

We note that the function in the brackets in (141) is the PDF of the SNR on the condition that the received reference SNR is in (γ_l, γ_{l+1}). Furthermore, in case of K active users with *i.i.d.* statistics and maximum SNR scheduling

$$q_l = F(\gamma_{l+1})^K - F(\gamma_l)^K, \tag{143}$$

where F is the CDF corresponding to f. Thus, from (138) and (141), the bit error probability becomes

$$P_{\mathrm{e}}^{Q}(\bar{\gamma}) = \sum_{l=0}^{L} q_l/p_l \cdot (I_l - I_{l+1}), \tag{144}$$

where $I_{L+1} = 0$ and

$$\begin{aligned} I_l \doteq \int_{\gamma_l}^{\infty} f(\gamma) P_{\mathrm{mod}}(\gamma) d\gamma &= (1 - F(\gamma_l)) P_{\mathrm{mod}}(\gamma_l) \\ &+ \int_{\gamma_l}^{\infty} (1 - F(\gamma)) \Big(\frac{d}{d\gamma} P_{\mathrm{mod}} \Big)(\gamma) d\gamma, \end{aligned} \tag{145}$$

where we have applied integration by parts. Later it will turn out that this formula simplifies the computations.

If $L \to \infty$, $P_{\mathrm{e}}^{Q} \to P_{\mathrm{e}}^{I}$, where P_{e}^{I} is the receiver BEP after maximum SNR scheduling on the condition that transmitter has perfect CQI. In this case, the PDF of the received SNR is the same as in case of transmit antenna selection over K antennas. Then K defines the slope of the asymptotic BEP that is further related to the degree of diversity. Nevertheless, if CQI is quantized, the asymptotic slope of P_{e}^{Q} is defined by P_{e}, *i.e.* BEP of continuous transmission (round robin scheduling). This is seen from (144), which implies that

$$\min_{0 \le l \le L} \{q_l/p_l\} P_{\mathrm{e}}(\bar{\gamma}) \le P_{\mathrm{e}}^{Q}(\bar{\gamma}) \le \max_{0 \le l \le L} \{q_l/p_l\} P_{\mathrm{e}}(\bar{\gamma}). \tag{146}$$

In other words, instead of transmitting to the user with maximum SNR, the scheduler randomly selects a user among those users whose quantized SNRs belong to the same quantization region. When the number of quantization sets increases, the probability of having more than one user in the same set decreases, and therefore the asymptotic behavior moves toward higher SNR region.

Since the base station transmission power is fixed, the instantaneous received BEP in the mobile may become high during deep channel fades. In order to avoid useless transmission when the reference SNR is low we can suspend the transmission when $\gamma < \gamma_1$ for all active users. This may slightly degrade the capacity in an isolated cell but, on the other hand, it may increase the capacity in a multi-cell network because inter-cell interference is attenuated. In this case we set

$$p_0 = P_{\mathrm{out}}^{1/K}, \quad q_0 = 0, \tag{147}$$

where P_{out} the probability that the SNR of a single user falls below a predefined threshold and transmission to the user is suspended. Thus, in case of K users with i.i.d. statistics, the scheduler suspends the transmission if

the SNRs of all users fall to the lowest quantization region. The probability of the event is P_{out}^K, and the corresponding threshold γ_1 is solved from (142) and (147). This outage probability is a system related parameter that can be defined in advance. Thus, if all users employ a modulation scheme with bit rate R, the system mean rate becomes $(1 - P_{\text{out}}^K)R$.

Example Case

Consider a specific example case assuming flat Rayleigh fading BPSK modulation and SISO scenario. The reference SNR corresponds to that of single antenna transmission. Then by (143) we find that

$$\begin{aligned} p_l &= e^{-\xi_l} - e^{-\xi_{l+1}}, \\ q_l &= (1 - e^{-\xi_{l+1}})^K - (1 - e^{-\xi_l})^K. \end{aligned} \tag{148}$$

Let us first assume that all SNR quantization sets have equal probabilities, i.e., $p_l = 1/(L+1)$. This gives intuitively a natural basis for a fixed quantization. From (148) we find that boundary points ξ_l now attain the form

$$\xi_l = \log\big((L+1)/(L-l+1)\big). \tag{149}$$

These points are used when computing the reference BEP.

For the BEP P_{e}^Q, it remains to compute the integral I_l. By using (145) and (131) we obtain

$$I_l = e^{-\xi_l} P_{\text{mod}}(\xi_l \bar{\gamma}) - \frac{1}{\sqrt{4\pi}} \int_{\gamma_l}^{\infty} \frac{e^{-\gamma(1+1/\bar{\gamma})}}{\sqrt{\gamma}} d\gamma.$$

Here we can apply substitution $t = \gamma(1 + 1/\bar{\gamma})$ and use the definition of complementary incomplete gamma function. Then we find that

$$I_l = \frac{1}{\sqrt{4\pi}} \Big(e^{-\xi_l} \Gamma\big(\frac{1}{2}, \xi_l \bar{\gamma}\big) - \sqrt{\frac{\bar{\gamma}}{1+\bar{\gamma}}} \Gamma\big(\frac{1}{2}, \xi_l(1+\bar{\gamma})\big) \Big). \tag{150}$$

Now the final BEP formula can be deduced by substituting (148) and (150) into (144).

Asymptotic behavior of BEP is illustrated in Figure 24 for $L = 1$ (single-bit feedback word) and $L = 3$ (two-bit feedback word) assuming a fixed quantization, which does not depend on SNR. The number of active users is 2 (symbols 'x') and 8 (symbols 'o'). The fixed quantization is such that probabilities p_l in (142) are equal. It is noticed that the slope of the asymptotic BEP is the same for maximum SNR scheduling with quantized feedback and for round robin scheduling, whereas the slope of the asymptotic BEP of maximum SNR scheduling is proportional to the number of active users when CQI is perfectly known in the transmitter. Moreover, it is found that the quantization loss increases with the number of active users and the SNR

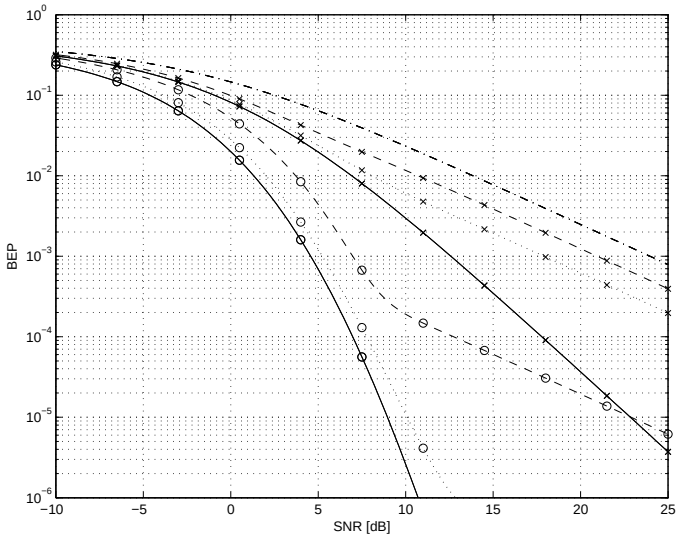

Figure 24: BEP in case of maximum SNR scheduling. Solid curves: CQI is perfectly known. Dashed curves: Fixed quantization with $L = 1$. Dotted curves: Fixed quantization with $L = 3$. Dash-dot curve: round robin scheduling. Number of active users is 2 ('x') and 8 ('o'). Flat Rayleigh fading and SISO are assumed.

region, where the asymptotic behavior of the quantization is visible, depends on quantization sets and the number of users.

Figure 25 depicts the BEP $P_{\mathrm{e}}^{\hat{Q}}$ using optimal quantization when $L = 1$ and $L = 3$. Hence, problem (140) is solved for each value of reference SNR. In practice, it is difficult to adaptively change the quantization. Nevertheless, if the target mean SNR is known in advance, the quantization can be defined such that BEP is minimized when the target is reached. The benefit from using such an optimized quantization instead of fixed quantization according to (149) can be seen by comparing Figures 24 and 25. The results show that noticeable gain can be achieved only if the target mean SNR is large.

Consider next the case where the scheduler suspends the transmission if $\gamma < \gamma_1$ for all K users. Otherwise, the scheduler randomly selects a user among the ones which report $\gamma \geq \gamma_1$. Using (137) we find that BEP in case of ideal CQI, on the condition that transmission is suspended if $\gamma < \gamma_1$, is of the form

$$P_{\mathrm{e}}^{Q}(\bar{\gamma}|\gamma > \gamma_1) = \frac{1}{\sqrt{4\pi}}\Big(\Gamma\big(\frac{1}{2}, \xi_1\bar{\gamma}\big) + \sum_{k=1}^{K}\binom{K}{k}\sqrt{\frac{\bar{\gamma}}{k+\bar{\gamma}}}\frac{(-1)^k\Gamma\big(\frac{1}{2}, \xi_1(k+\bar{\gamma})\big)}{1-P_{\mathrm{out}}}\Big),$$

where P_{out} fixes the probability p_0 according to (147). In the computation of P_{e}^{Q} we apply the quantization where all SNR regions are of equal probability

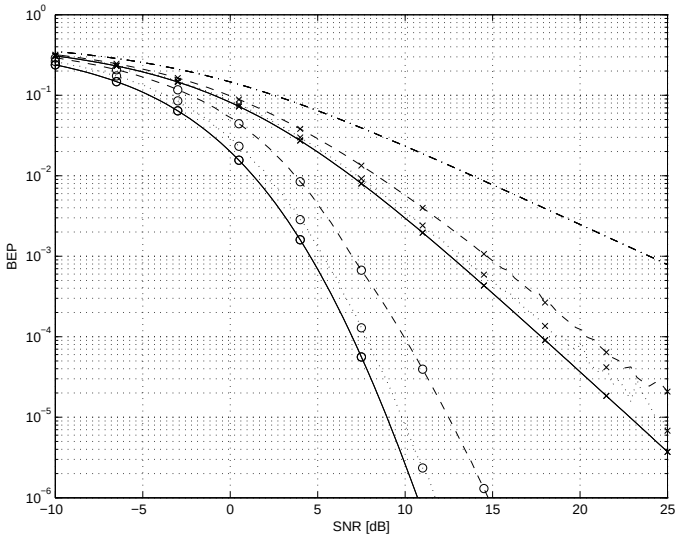

Figure 25: BEP in case of maximum SNR scheduling. Solid curves: CQI is perfectly known. Dashed curves: Optimal quantization according to (140) with $L = 1$. Dotted curves: Optimal quantization according to (140) with $L = 3$. Dash-dot curve: round robin scheduling. Number of active users is 2 ('x') and 8 ('o'). Flat Rayleigh fading and SISO are assumed.

on the condition that $\gamma > \gamma_1$. Thus, $p_l = (1 - p_0)/L$ if $l = 1, 2, \ldots, L$, and the boundary points are given by

$$\xi_l = \log\big(L/(1 - p_0)(L - l + 1)\big). \tag{151}$$

Figure 26 depicts the BEP curves for maximum SNR scheduling when $P_{\text{out}} = 0.01$, $L = 1$ and $L = 3$. Boundary points do not depend on SNR, and the number of active users is 2 (symbols 'x') and 8 (symbols 'o'). Transmission is suspended also in case of perfect CQI, but in case of round robin scheduling transmission is continuous.

It is noticed that the quantization loss is already small in case of two-bit quantization even when the quantization is not optimized according to SNR. Furthermore, it is found that the asymptotic decay of all BEP curves, except the one corresponding to round robin scheduler, are exponential. To confirm this fact we recall (134) from Section 4.6 that shows the asymptotic BEP corresponding to single user SISO system, where the transmission is suspended if $\gamma < \gamma_1$. Now we can apply the bound (146) where maximum and minimum is taken over indices $l = 1, 2, \ldots, L$. Hence, the asymptotic decay of the BEP is exponential also when feedback is quantized.

Transmit power control scheme, which achieves exponentially decaying BEP in MISO flat Rayleigh fading channels has also been reported in [81].

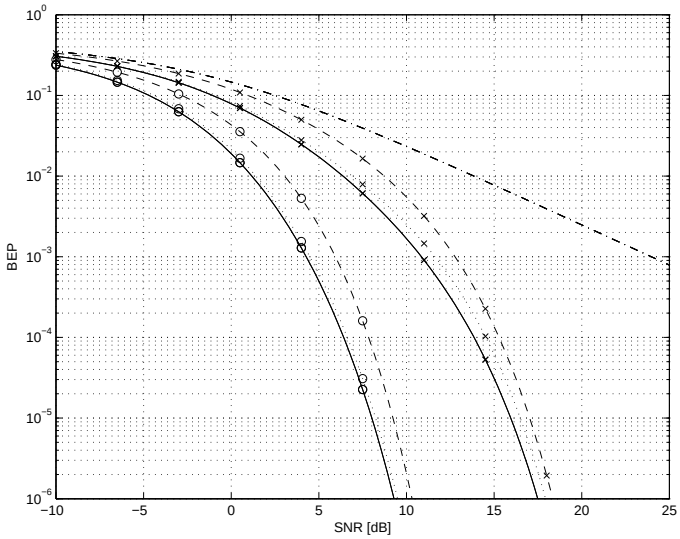

Figure 26: BEP when maximum SNR scheduling is applied with 1% outage probability. Solid curves: CQI is perfectly known. Dashed curves: fixed quantization with $L = 1$. Dotted curves: fixed quantization with $L = 3$. Dash-dot curve: round robin scheduling. Number of active users is 2 ('x') and 8 ('o'). Flat Rayleigh fading and SISO are assumed.

The scheme assumes complete channel state information in the receiver in order to achieve exponentially decaying BEP in every operation point, while the quantized feedback and suspension of transmission in Section 4.6 and in this section provide exponentially decaying BEP asymptotically in high SNR region.

The scheduler that suspends the transmission when SNRs of all users fall below a threshold, provides asymptotically exponentially decaying BEP even with suboptimal quantization. In fact, any reasonable quantization strategy provides this asymptotic performance as long as the system outage is allowed. This makes the system design much easier when compared to the case, where quantization is optimized according to (140).

5 Scheduling for UTRA FDD Uplink

The importance of power control (PC) to the CDMA uplink performance has motivated many studies such as [82], [83]. It is well-known that the mean transmit power in systems with PC depends on the channel fading statistics. The effect of the propagation environment is measured by power rise [84] that defines the ratio of the average transmit power in a fading channel to that in a non-fading channel when the mean receive power is the same in different environments. Antenna diversity reduces channel variations and leads to a lower required transmit power as pointed out in [85], where power rise was analyzed assuming flat fading.

In addition to antenna diversity also channel-aware scheduling will reduce channel variations and thus, it reduces the required transmit power in power controlled systems. Channel-aware scheduling can be beneficially used in uplink provided that base station scheduler can acquire CSI of different users. This is possible in WCDMA uplink where control channel is continuously transmitted. Nevertheless, scheduling can be only applied on the dedicated channel. Scheduling may increase the system efficiency through multi-user diversity if the total number of users in the system is larger than the number of transmitting users. However, since control channels of waiting users are on, the control overhead increases with multi-user diversity. Thus, the increased interference due to control signaling and decreased interference due to scheduling should be considered jointly. This important problem seems to be widely ignored in the literature although there are some research papers concerning uplink scheduling [86], [87], [88].

In this section, we study the effect of OOS to the required transmit power [25]. In OOS we suspend the transmission if the channel power response falls below a predefined threshold. In practice this condition can be explicitly verified from received power if PC is not applied and implicitly from transmitted power if PC is on. In FDD WCDMA downlink, channel state information can be obtained from the common omnidirectional pilot channel that is transmitted with a fixed power. In WCDMA uplink, mobile's transmit power on control channel varies according to channel fluctuations and mobile can monitor its transmit power and suspend transmission on data channel if a predefined power level is exceeded.

5.1 System Model

The basic idea of OOS in uplink is the same as it is in downlink. Hence, let γ_0 denote a cutoff SNR and let γ be the instantaneous SNR. Then we define a relative threshold $\xi = \gamma_0/\bar{\gamma}$ and suspend the transmission if $\gamma/\bar{\gamma} < \xi$. Relative threshold is practical, because only the threshold crossings need to be known in the transmitter and, on the other hand, the selection of TTI is fair if all users with the same service employ equal relative thresholds ξ.

In practical systems, $\bar{\gamma}$ needs to be estimated before OOS can be used. Moreover, receiver and transmitter have to agree on threshold values, but this task can be carried out by employing long-term signaling on higher network layers. We note that in this work we do not fix specific threshold values but show the effect of transmission probability, which is directly connected to the threshold value, to the performance of OOS.

We assume a model where threshold crossings are known to the transmitter. Our generic communication protocol employs control channel (CCH) and data channel (DCH), and fast transmit power control is applied on both channels. A block multi-path Rayleigh fading model is adopted where the channel remains constant during each TTI and channel coefficients between separate TTIs are independent. Receiver has M_r antennas and it employs maximal ratio combining over separate antennas and channel paths. The example radio channel models are ITU Pedestrian A and Pedestrian B profiles [89], where relative mean path powers are 0.0 and -12.7 dB for the former and 0.0, -0.9, -4.9, -8.0, -7.8 and -23.9 dB for the latter model. Pedestrian B provides a realistic and challenging radio channel model for low mobility environments, and it is applied in feasibility studies of uplink of UTRA FDD mode [70].

In the following we define three example systems that are analyzed. We recall that all users connected to to base station need a CCH whether DCH is on or off.

System 1. There are K_{tr} users transmitting on DCH continuously. this case represents a circuit-switched system and possible services are, e.g., audio and video calls.

System 2. DCH transmission is not continuous but transmission times are randomly selected from physical channel state point of view. The number of transmitting users is K_{tr} while the total number of users in the system is K. This case represents a packet-switched system and possible services are, e.g., web browsing and FTP.

System 3. The system is similar to system 2, but now OOS is applied on DCH assuming error-free feedback channel.

System 2 represents a scheduler that does not take into account the state of the physical channel, but transmission time intervals are selected, for example, based on delay requirements or buffer occupancy. The system also provides a good reference, because the use of channel state information is the only difference between systems 2 and 3. Finally, we note that the transmission probability of a user in systems 2 and 3 is defined by the number of active users in the system, *i.e.*, $p_{tr} = K_{tr}/K$. Then cell throughput is the same for all systems.

In Section 5.2 the transmit power gain from OOS is studied assuming

ideal power control, multi-path fading channel and M_r receive antennas. Since these assumptions are well valid in FDD WCDMA uplink we show in Section 5.3 how the OOS gain reflects to the coverage and capacity performance of FDD WCDMA.

The effect of transmission delay is neglected and we assume that data services are able to tolerate unbounded delays. This assumption is, of course, not realistic, but instead of designing a practical scheduling algorithm our aim is to study, how the control signaling overhead may limit the performance of physical layer scheduling. On-off scheduling is compared to two reference systems.

5.2 Analysis of Transmit Power

Due to PC, the target received power in the base station remains approximately the same although the link performance is improved. Furthermore, OOS reduces mobile's mean transmit power, because transmission is suspended during the deep fades. Assuming ideal power control in the sense that the received power remains constant all the time, we have

$$P_{k,d}\gamma = P_{rx,d}, \quad P_c\gamma = P_{rx,c}$$

where $P_{rx,d}$ and $P_{rx,c}$ are the target received powers for data and control channels, respectively, γ is the power response of the physical channel, and $P_{k,d}$ and P_c refer to the instantaneous transmit powers of a user of kth example system on data and control channels respectively. The transmit power of the control channel is assumed to be the same in all systems. This kind of power control essentially inverts the channel and better power control strategies are available [81]. Fast PC in WCDMA approximates the channel inverse, and it has been shown that different MIMO solutions in WCDMA uplink can be analyzed based on the ideal power control assumption [26], [27] and the results closely match to link-level simulations.

In the following the relative link level performance between the three example systems is measured by using the ratio between expected transmit powers. While comparing systems 2 and 3 we use the ratio

$$\rho_{2,3} = \frac{K_{tr}\cdot\bar{P}_{2,d} + K\cdot\bar{P}_c}{K_{tr}\cdot\bar{P}_{3,d} + K\cdot\bar{P}_c} = \frac{p_{tr}\bar{P}_{2,d} + \bar{P}_c}{p_{tr}\bar{P}_{3,d} + \bar{P}_c}, \tag{152}$$

where $\bar{P}_{2,d}, \bar{P}_{3,d}, \bar{P}_c$ refer to the corresponding mean transmit powers. We recall that OOS is applied only on the data channel in System 3. Hence, we can write

$$\bar{P}_{3,d} = E\{P_d|\gamma > \gamma_0\},\ \bar{P}_{2,d} = \bar{P}_{1,d} = E\{P_d\} =: \bar{P}_d.$$

In the following we employ notations

$$\rho_0 = \frac{\bar{P}_d}{\bar{P}_{3,d}}, \quad R = \frac{\bar{P}_c}{\bar{P}_d}\cdot p_{tr}, \tag{153}$$

Data rate on DCH [kbps]	12.2	64	144	384	2048
Power ratio CCH/DCH [dB]	-2.69	-5.46	-9.54	-9.54	-9.54

Table 6: Recommended power ratios between CCH and DCH in FDD WCDMA uplink.

where ρ_0 is the relative power rise that indicates the gain of OOS on the data channel. Moreover, R defines the ratio of mean transmit powers between control and data channels. In general the value of R can be optimized for each service. However, it is easier to apply fixed values that are defined in advance. For FDD WCDMA such values, presented in Table 6, were proposed in [90]. Furthermore, the effect of power offset between enhanced data and control channels was studied in [70].

Mean transmit power of the control channel $\bar{P}_c$ is scaled by the transmission probability to keep the ratio between powers of DCH and CCH the same for all systems although systems 2 and 3 apply discontinuous transmission. After combining (152) and (153) we obtain

$$\rho_{2,3} = \frac{\rho_0(p_{tr}^2 + R)}{p_{tr}^2 + \rho_0 R}. \tag{154}$$

It is worth noticing that $\rho_{2,3} \to 1$ if $p_{tr} \to 0$ or $p_{tr} \to 1$. The former limit follows, because the gain of system 3 against system 2 vanishes when the transmission probability is small and control channel overhead of the users waiting in the queue becomes dominating. On the other hand, the gain also vanishes if $p_{tr} \to 1$, because transmission in systems 2 and 3 becomes continuous. We also note that $\rho_{2,3} = \rho_0$ if control channel does not exist.

While the ratio R is defined by the service, ρ_0 attains a closed-form expression in case of Rayleigh fading environment. Before considering this topic we deduce ratios $\rho_{1,3}$ and $\rho_{1,2}$. We have

$$\rho_{1,3} = \frac{K_{tr}(\bar{P}_d + \bar{P}_c)}{K_{tr} \cdot \bar{P}_{3,d} + K \cdot \bar{P}_c} = \rho_0 \cdot p_{tr} \frac{p_{tr} + R}{p_{tr}^2 + \rho_0 R}. \tag{155}$$

Finally, combining (154) and (155) we obtain

$$\rho_{1,2} = p_{tr} \cdot \frac{p_{tr} + R}{p_{tr}^2 + R}.$$

At this stage we focus on ρ_0. The computation of power rise was previously considered in [85], but the analysis therein covers only continuous transmission ($\gamma_0 = 0$) assuming a single path channel, while our aim is to compute ρ_0 for OOS and PC within multi-path environment. We have

$$\bar{P}_{3,d} = P_{rx,d} \int_{\gamma_0}^{\infty} f(\gamma)/\gamma d\gamma, \tag{156}$$

where $P_{rx,d}$ is the target power for the data channel and f is the PDF of the channel power response. In what follows, we assume a multi-path fading model where impulse responses corresponding to instantaneous channel paths are independent zero mean Gaussian random variables. Assuming that the mean path powers $\bar{\gamma}_l$ are mutually different, the PDF of the channel power response is given by

$$f(\gamma) = \sum_{m=1}^{M_r} \sum_{l=1}^{L} \frac{a_{m,l}}{\Gamma(m)\bar{\gamma}_l} \Big(\frac{\gamma}{\bar{\gamma}_l}\Big)^{m-1} e^{-\gamma/\bar{\gamma}_l}, \tag{157}$$

where Γ is the Gamma function and the coefficients $a_{m,l}$ are defined through the equality

$$a_{m,l} = \frac{G^{(M_r-m)}(-1/j\bar{\gamma}_l)}{(M_r-m)!(j\bar{\gamma}_l)^{M_r-m}},\ G(\xi) = \prod_{k=1,k\neq l}^{L} (1+j\bar{\gamma}_k\xi)^{-M_r}. \tag{158}$$

Formulas (157) and (158) are obtained by a standard procedure: First the characteristic function corresponding to the combined signal is computed using the properties of Fourier transform. Then the product form of the characteristic function is written as a sum with coefficients $a_{m,l}$ and after applying inverse Fourier transform the forms (157) and (158) are achieved. The computation of the coefficients $a_{m,l}$ in case $M_r \leq 4$ is presented in Appendix of [25] in more detail.

By combining (156), (157) and applying the substitution $t = \gamma/\bar{\gamma}_l$ we find that

$$\bar{P}_{3,d} = P_{rx,d} \sum_{m=1}^{M_r} \sum_{l=1}^{L} \frac{a_{m,l}}{\Gamma(m)\bar{\gamma}_l} \int_{\gamma_0/\bar{\gamma}_l}^{\infty} t^{m-2} e^{-t} dt. \tag{159}$$

Furthermore, by (6.5.1), (6.5.15) and (6.5.13) of [69] there holds

$$\int_x^{\infty} t^{m-1} e^{-t} dt = \begin{cases} E_1(x), & m = 0, \\ \Gamma(m)\mathcal{P}_m(x), & m > 0, \end{cases} \tag{160}$$

where E_1 is the exponential integral function, given in (5.1.1) of [69], and $\mathcal{P}_m$ is Poisson distribution, defined by (52). By combining (159) and (160) we find that

$$\frac{\bar{P}_{3,d}}{P_{rx,d}} = \sum_{l=1}^{L} \frac{a_{1,l}}{\bar{\gamma}_l} E_1\Big(\frac{\gamma_0}{\bar{\gamma}_l}\Big) + \sum_{m=1}^{M_r-1} \sum_{l=1}^{L} \frac{a_{m+1,l}}{m\bar{\gamma}_l} \mathcal{P}_m\Big(\frac{\gamma_0}{\bar{\gamma}_l}\Big). \tag{161}$$

For ρ_0 we need also the mean power $\bar{P}_d$ that is obtained by computing the limit for $\bar{P}_{3,d}$ when $\gamma_0 \to 0$. For that purpose we recall from (104) the expansion of exponential integral function. Although E_1 grows without limit when $\gamma_0 \to 0$, there exists a finite limit for $\bar{P}_{3,d}$. To show this, we first note

that $f(0) = 0$ if $M_r \cdot L > 1$. This holds because f is a convolution of $M_r \cdot L$ chi-square distributions. Then we find by (157) that

$$\sum_{l=1}^{L} \frac{a_{1,l}}{\bar{\gamma}_l} = 0. \tag{162}$$

Let us denote $E_1(x) + \log(x) = g(x)$. Then, by employing (162) we can write for any $\gamma_0 > 0$

$$\begin{aligned}\sum_{l=1}^{L} \frac{a_{1,l}}{\bar{\gamma}_l} E_1\Big(\frac{\gamma_0}{\bar{\gamma}_l}\Big) &= \sum_{l=1}^{L} \frac{a_{1,l}}{\bar{\gamma}_l}\Big(E_1\Big(\frac{\gamma_0}{\bar{\gamma}_l}\Big) + \log\Big(\frac{\gamma_0}{\bar{\gamma}}\Big)\Big) \\ &= -\sum_{l=1}^{L} \frac{a_{1,l}}{\bar{\gamma}_l}\Big(\log\Big(\frac{\bar{\gamma}}{\bar{\gamma}_l}\Big) - g\Big(\frac{\gamma_0}{\bar{\gamma}_l}\Big)\Big).\end{aligned}$$

By applying equations $g(0) = -e_0$ and (162) we find that

$$\lim_{\gamma_0 \to 0} \sum_{l=1}^{L} \frac{a_{1,l}}{\bar{\gamma}_l} E_1\Big(\frac{\gamma_0}{\bar{\gamma}_l}\Big) = -\sum_{l=1}^{L} \frac{a_{1,l}}{\bar{\gamma}_l} \log\Big(\frac{1}{\sigma_l^2}\Big), \tag{163}$$

where $\sigma_l^2 = \bar{\gamma}_l/\bar{\gamma}$ refers to the normalized mean path powers. Finally, by using the fact that $\mathcal{P}_m(0) = 1$, and equation (163), we obtain

$$\frac{\bar{P}_d}{P_{rx,d}} = -\sum_{l=1}^{L} \frac{a_{1,l}}{\bar{\gamma}_l} \log\Big(\frac{\bar{\gamma}}{\bar{\gamma}_l}\Big) + \sum_{m=1}^{M_r-1} \sum_{l=1}^{L} \frac{a_{m+1,l}}{m\bar{\gamma}_l}. \tag{164}$$

The expression for ρ_0 is obtained by combining (161) and (164). Applying notation $\xi = \gamma_0/\bar{\gamma}$ we get

$$\rho_0 = \frac{-\sum\limits_{l=1}^{L} \frac{a_{1,l}}{\sigma_l^2} \log\big(\frac{1}{\sigma_l^2}\big) + \sum\limits_{m=1}^{M_r-1} \sum\limits_{l=1}^{L} \frac{a_{m+1,l}}{m\sigma_l^2}}{\sum\limits_{l=1}^{L} \frac{a_{1,l}}{\sigma_l^2} E_1\big(\frac{\xi}{\sigma_l^2}\big) + \sum\limits_{m=1}^{M_r-1} \sum\limits_{l=1}^{L} \frac{a_{m+1,l}}{m\sigma_l^2} \mathcal{P}_m\big(\frac{\xi}{\sigma_l^2}\big)}. \tag{165}$$

The parameter ξ in (165) reflects the effect of the transmission threshold and it can be solved for a given transmission probability p_{tr} from the equation

$$p_{tr} = \int_{\gamma_0}^{\infty} f(\gamma) d\gamma = \sum_{m=1}^{M_r} \sum_{l=1}^{L} a_{m,l} \mathcal{P}_m(\xi) \tag{166}$$

that is obtained by employing the substitution $t = \gamma/\bar{\gamma}_l$ and expression (160). Solution for (166) is found numerically by applying, for example, the bisection method, and the solution is unique because $P(\gamma > \gamma_0)$ is a monotonic

function with respect to γ_0. After solving ξ, the relative power rise ρ_0 is computed by using (165).

Before closing this section we shortly consider two important issues. Firstly, for a fixed ratio R there exists a probability $\hat{p}_{tr}$ such that

$$\hat{\rho}_{2,3} = \max_{0 \le p_{tr} \le 1} (\rho_{2,3}) = \frac{\hat{\rho}_0(\hat{p}_{tr}^2 + R)}{\hat{p}_{tr}^2 + \hat{\rho}_0 R},$$

where $\hat{\rho}_0 = \rho_0(\hat{p}_{tr})$. We will further illustrate this topic in Section 5.4. Secondly, many practical services are delay sensitive and therefore low transmission probabilities are not favorable. A lower bound to the transmission delay is obtained by assuming a memoryless channel such that channel states of consecutive transmission time intervals are independent. Then the probability that the delay exceeds t transmission time intervals is $(1-p_{tr})^t$, which decays rapidly unless p_{tr} is small. However, if a user is moving with a low speed, such that the channel states between consecutive transmission time intervals are highly correlated, the delays can become intolerably long. Our model is rather coarse and a more detailed system model would be needed to carry out a detailed study on delay issues.

5.3 OOS Gain in WCDMA Uplink

Since PC drives the received power to the target value corresponding to the selected service, scheduling gain is seen in the terminal as a decrease in the required transmission power. This gain further effects the system coverage and capacity via the following three mechanisms:

- In isolated cell the decrease in required transmit power in mobile station reflects directly to the cell coverage and service availability.
- If scheduling is applied in the whole network, lower transmit power will also decrease the inter-cell interference. This reflects to increased cell capacity in interference limited cells.
- If system supports adaptive coding and modulation, mobile can increase the link throughput in good channel conditions.

We study in more detail the first two gain mechanisms that can be realized in WCDMA uplink. The third gain mechanism is not applicable in WCDMA uplink because the present specification does not support adaptive modulation and coding in uplink.

Let us consider first the coverage. For that purpose we recall the most widely used Okumura-Hata propagation model model [91, 92] that is valid in macro-cell environments where base station antennas are placed above the rooftop level. The usual operating frequency of WCDMA uplink is 1950 MHz and the corresponding path loss in decibels in Okumura-Hata model is given by

$$L_p = 157.83 - 13.82 \log_{10}(H_{\text{BS}}) - A(H_{\text{MS}}) + \big(B - 6.55 \log_{10}(H_{\text{BS}})\big) \log_{10}(D),$$

Service [kbps]	12.2	64	144	384
Allowed L_p [dB]	140.20	136.86	136.02	132.26
Max. Range [km]	1.12	0.90	0.85	0.67

Table 7: Allowed propagation losses and cell ranges for some service classes in FDD WCDMA uplink.

where D is the distance (km) between base and mobile stations, H_{BS} (m) is the base station antenna height, H_{MS} (m) is the mobile station antenna height, B is a user-defined parameter whose value is commonly set to 44.9, and for large city A is defined by

$$A(H_{\text{MS}}) = 3.2\big(\log_{10}(11.75H_{\text{MS}})\big)^2 - 4.97.$$

We follow [93] where base station and mobile station antenna heights in urban macro-cell are 25 m and 1.5 m, respectively. Then

$$L_p = 138.5 + 35.7\log_{10}(D). \tag{167}$$

Maximum allowed path loss in WCDMA is estimated by radio link budget (RLB) calculation. The RLB contains round 20 parameters and we refer to [93] and [37] for more details. In Table 7 we have recalled from [93], p.121 the allowed propagation loss figures for some services.

The allowed propagation losses in Table 7 are not directly proportional to the data rate because the assumptions, such as coverage probability, are different for different services. The maximum cell ranges for different services can be computed from (167), and the coverage gain of OOS is obtained by comparing the required transmit powers in systems 2 and 3.

Assume that the allowed path loss figures of Table 7 are valid for system 2 with $M_r = 1$. If we replace system 2 by system 3 with OOS, the gain in mobile station transmission power is obtained according to $\rho_{2,3}$ and the corresponding value can be added to the RLB. Then cell ranges D_2 and D_3 for systems 2 and 3 can be calculated from (167) and the corresponding coverage gain is $(D_3^2 - D_2^2)/D_2^2$. If $M_r > 1$, the allowed propagation loss for both systems increases roughly by $\log_{10}(M_r)$.

We would have been able to compute the relative gain from OOS directly from (167). However, by utilizing the link budget examples we are able to compute example ranges showing also an estimate of the absolute gains of OOS. Finally, we note that RLB calculations rely on several variables, some of them being rather uncertain. Therefore, the absolute range figures represent only rough approximations. We will show coverage gain figures in Section 5.4.

Capacity gains are analyzed by using noise rise, denoted by μ, which is defined as a ratio of the total received wideband power to the thermal noise power [37]. Noise rise is a function of system load η,

$$\mu = \frac{1}{1-\eta}. \tag{168}$$

The more loading is allowed in the system, the larger is the required interference margin $\mu_0 = \max\{\mu\}$ and the smaller is the coverage area. Interference margin defines the maximum allowed noise rise and values up to 6 dB are used [37]. The formula for system load is of the form

$$\eta = (1+\nu)\sum_{n=1}^{N_{\text{own}}} \frac{\kappa_n E_{\text{rx},n}}{1+\kappa_n E_{\text{rx},n}}, \tag{169}$$

where $\nu = I_{\text{other}}/I_{\text{own}}$ is the inter-cell to intra-cell interference ratio seen by the base station receiver, N_{own} is the number of own cell users, κ_n is the ratio between the bit rate and chip rate, and $E_{\text{rx},n}$ is the received energy per data bit divided by the noise spectral density (E_b/N_0) of n^{th} user, see Section 6 and [37].

Assume that the number of receive antennas is fixed. OOS reduces the mobile's transmit power but it does not reduce the received E_b/N_0, because power control maintains the received power at the target level defined by the required QoS. Therefore, OOS does not improve capacity in isolated cell where $\nu = 0$ and inter-cell interference does not exist. However, OOS decreases the inter-cell interference in interference limited cases where $\nu > 0$. Let us consider the effect in more detail: According to (168), the theoretical capacity limit is reached when load approaches the 100% level and the corresponding maximum number of users is obtained from (169). Assuming that all users employ the same service we may denote $\kappa_n =: \kappa$, $E_{\text{rx},n} =: E_{\text{rx}}$ and the computation of the cell throughput is straightforward. Suppose that the number of receive antennas and the number of users are fixed in systems 2 and 3. By (169) we obtain

$$\frac{\eta_3}{\eta_2} = \frac{E_{\text{rx},3}(1+\kappa\cdot E_{\text{rx},2})}{E_{\text{rx},2}(1+\kappa\cdot E_{\text{rx},3})}\cdot\frac{1+\nu_3}{1+\nu_2} = \frac{1+\nu_3}{1+\nu_2}, \tag{170}$$

where numbers 2 and 3 refer to different systems and the latter equality follows because the target E_b/N_0 remains constant. Inter-cell interference ratio ν_3 can be written as

$$\nu_3 = \frac{\nu_3}{\nu_2}\cdot\nu_2 = \frac{I_{\text{other},3}}{I_{\text{other},2}}\cdot\nu_2. \tag{171}$$

Hence, it remains to study the inter-cell interference. There holds

$$I_{\text{other},k} = \sum_{n=1}^{N_{\text{other}}} E\{Q_{n,k}\gamma_n\} = \sum_{n=1}^{N_{\text{other}}} \bar{Q}_{n,k}\bar{\gamma}_n, \tag{172}$$

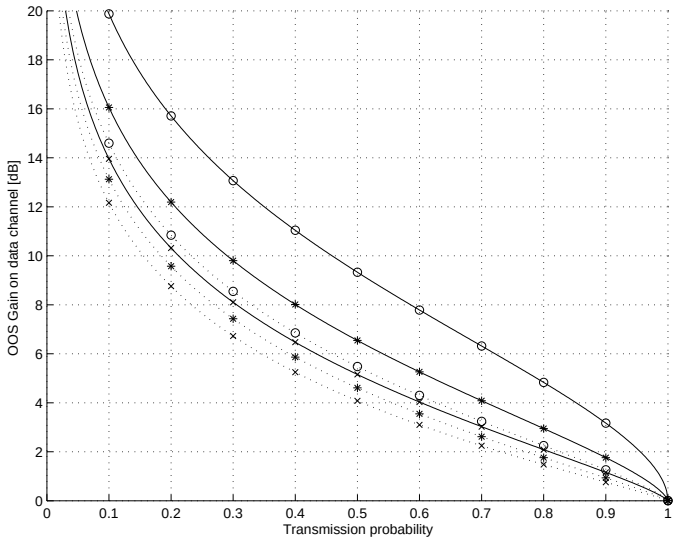

Figure 27: OOS gain ρ_0 on the data channel as a function of transmission probability when $M_r = 1$ (-o-), $M_r = 2$ (-*-) and $M_r = 4$ (-x-). Pedestrian A (solid curves) and Pedestrian B (dotted curves) channels are assumed.

where transmit power $Q_{n,k}$ of user n in the interfering cell does not depend on the channel attenuation γ_n in the own cell. Here we can write $\bar{Q}_{n,k} = c_n \bar{P}_k$ where $\bar{P}_k$ is the mobile station's mean transmit power in system k and c_n reflects the variation in the transmitted power due to the path loss between the base station and nth interfering user. By combining (170), (171) and (172) we obtain

$$\eta_3 = \frac{1 + \nu_2/\rho_{2,3}}{1 + \nu_2} \cdot \eta_2, \tag{173}$$

where $\rho_{2,3}$ is defined by (154). Now, the OOS gain in terms of load and noise rise can be computed from (173) and (168) provided that initial load η_2 and initial inter-cell interference ratio ν_2 are known.

5.4 Performance Results and Conclusions

Figure 27 displays the relative power rise ρ_0 as a function of transmission probability in Pedestrian A (solid curves) and Pedestrian B (dotted curves) channels when the number M_r of receive antennas is 1, 2 and 4. It is found that large gains can be achieved already when the transmission probability p_{tr} is between 0.5 and 1 while the gains are extremely high when the transmission probability is less than 0.5. Moreover, it is seen that ρ_0 is largest in Pedestrian A channel with $M_r = 1$, and additional diversity, whether it is antenna or multi-path diversity, reduces the value of ρ_0. The results,

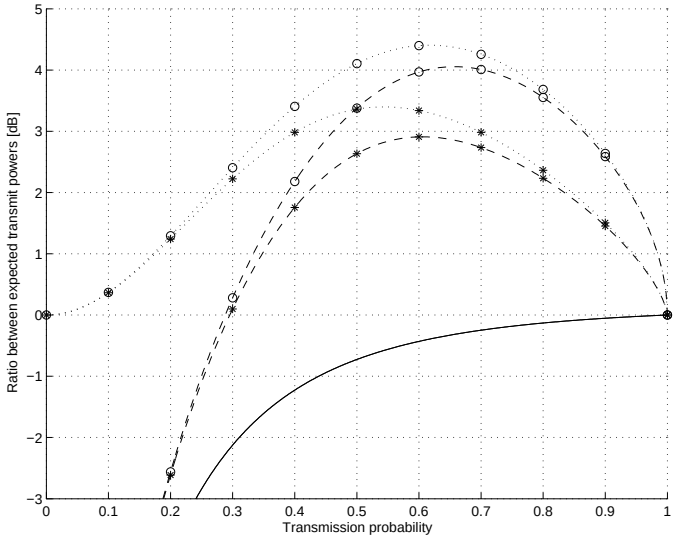

Figure 28: Ratio ρ_{13} (dashed curves) and ρ_{23} (dotted curves) as a function of transmission probability when $M_r = 1$ (-o-), $M_r = 2$ (-*-) and $R = -9.54$ dB. Pedestrian A channel is assumed. Ratio ρ_{12} between systems 1 and 2 is depicted by a solid curve.

however, do not directly define the performance of system 3 against systems 1 and 2 because the effect of control channel overhead is not taken into account.

Figures 28 and 29 show the relative transmit powers ρ_{12}, ρ_{13} and ρ_{23} in Pedestrian A and B channels as a function of transmit probability when the number of receive antennas is 1 and 2, and the power ratio between control and data channels is -9.54 dB (adopted from Table 6). Since OOS is not applied on the control channel, the gain of system 3 against systems 1 and 2 vanishes when the transmission probability is small and control channel overhead of the waiting users becomes dominating. On the other hand, the gain also vanishes if $p_{tr} \to 1$, because transmission in systems 2 and 3 becomes continuous. As noticed before, there exists a transmission probability that maximizes the relative gain of system 3 against systems 1 and 2. The probability giving the maximum gain depends on the channel profile, M_r and the ratio R while the magnitude of the maximum gain mainly depends on R. Before further studying this subject we note that according to Figures 28 and 29, the performance of system 2 is inferior to system 1 as one can expect, because control channel overhead is smaller in system 1.

Figure 30 depicts the maximum gain of system 3 against system 2 as a function of R. As expected, the OOS gain is large when R is small showing that the best OOS gains are obtained when transmit power on data channel

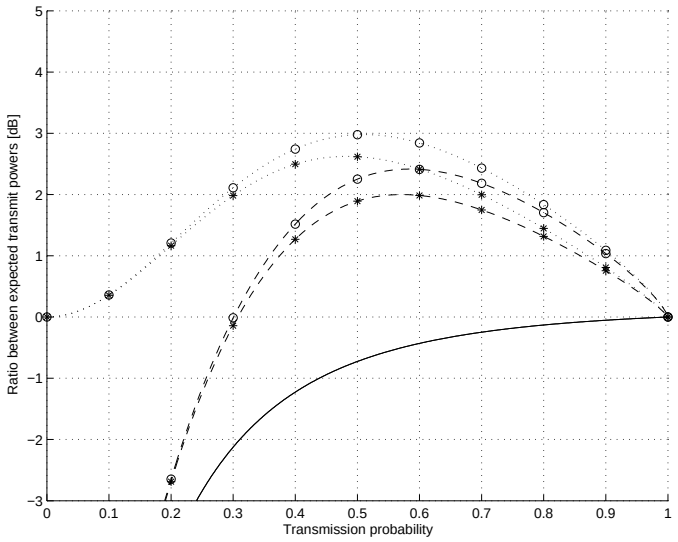

Figure 29: Ratio ρ_{13} (dashed curves) and ρ_{23} (dotted curves) as a function of transmission probability when $M_r = 1$ (-o-) and $M_r = 2$ (-*-) and $R = -9.54$ dB. Pedestrian B channel is assumed. Ratio ρ_{12} between systems 1 and 2 is depicted by a solid curve.

is large when compared to control channel power. This is usually the case for high data rates.

Figure 31 displays the transmission probabilities corresponding to the largest gains $\hat{\rho}_{2,3}$ as a function of R. It is found that the transmission probability $\hat{p}_{tr}$ giving the best performance is increasing with R. However, in practice users' data rates and the number of users cannot be very large simultaneously, because the cell capacity is limited. Therefore, small transmission probabilities are usually not feasible in practice.

Let us now recall the RLB example of Table 7. Table 8 lists maximum cell ranges for 384 kbps service in systems 2 and 3 assuming Pedestrian A and Pedestrian B channels and one and two receive antennas. Ranges are computed using (167) and the allowed path loss according to Table 7. System 2 with $M_r = 1$ serves as the reference and maximum OOS gain $\hat{\rho}_{2,3}$ is applied.

It is found that relative coverage gains are large. However, when services have different ratios R the gains would be smaller, because there is no optimal transmission probability for all services. Moreover, the analysis does not take into account practical unidealities like threshold estimation and feedback errors. Yet, it can be expected that OOS remarkably improves the availability of medium and high data rate services.

Finally, Figure 32 illustrates the decrease in system load when applying

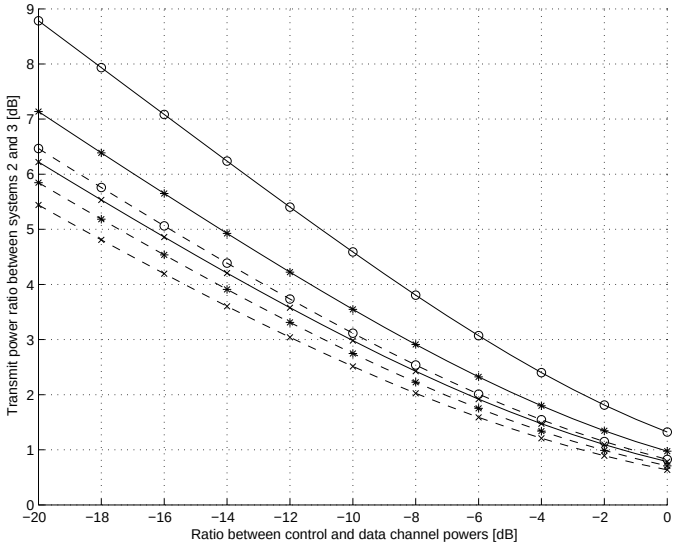

Figure 30: Ratio $\hat{\rho}_{23}$ as a function of R when $M_r = 1$ (-o-), $M_r = 2$ (-*-) and $M_r = 4$ (-x-). Pedestrian A (solid curves) and Pedestrian B (dashed curves) channels are assumed.

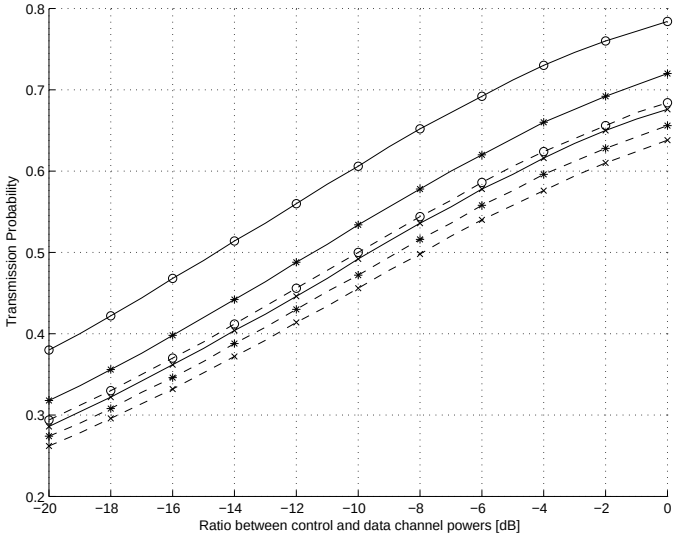

Figure 31: Transmission probability $\hat{p}_{tr}$ as a function of R when $M_r = 1$ (-o-), $M_r = 2$ (-*-) and $M_r = 4$ (-x-). Pedestrian A (solid curves) and Pedestrian B (dashed curves) channels are assumed.

Channel Setup	D, system 2 [km]	D, system 3 [km]	Coverage gain
Ped. A, $M_r = 1$	0.67	0.89	76%
Ped. A, $M_r = 2$	0.81	1.01	55%
Ped. B, $M_r = 1$	0.67	0.81	46%
Ped. B, $M_r = 2$	0.81	0.96	40%

Table 8: Cell ranges for 384 kbps service when Pedestrian A and B are assumed and $M_r = 1, 2$.

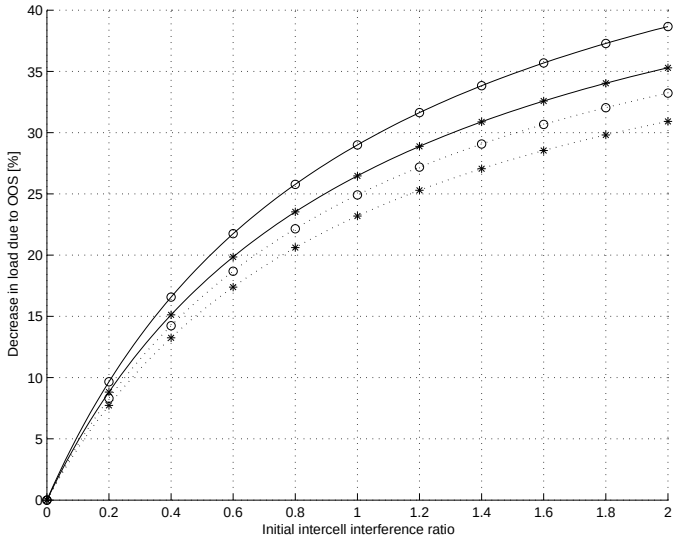

Figure 32: Decrease in FDD WCDMA uplink load due to OOS as a function of inter-cell interference ratio ν_2 when $R = -9.54$ dB and $\eta_2 = 0.75$. Channels are Pedestrian A (solid curves) and Pedestrian B (dotted curves), and number of receive antennas are $M_r = 1$ (-o-) and $M_r = 2$ (-*-).

OOS. The curves are deduced from equation (173) by assuming $\eta_2 = 0.75$ and employing ratio (154) with $R = -9.54$ dB. It is seen that the load of system 3 is remarkably smaller than that of system 2. Nevertheless, the gain strongly depends on the initial inter-cell interference ratio ν_2. For example, for omnidirectional base station antennas $\nu_2 = 0.55$ [37]. Moreover, OOS gains are smaller when initial load η_2 is small.

6 MIMO in UTRA FDD Uplink

The introduction of MIMO [94], [95], [96] has fueled several research papers, see [97]. Most of the studies assume broadcast channel and are applicable in cellular downlink but there are also some works that consider MIMO in CDMA uplink [98], [99] that is our focus in this section.

Similarly with the main stream research, in 3GPP the MIMO discussion has focused on downlink [100]. Nevertheless, the introduction of new services such as videophones will make it extremely important to reach high spectral efficiency also in the uplink direction. Besides this service based demand, there are also two evident reasons why MIMO in UTRA FDD uplink is attractive and thus, worth of a closer study. Firstly, base stations will have two or more antennas in the near future, and at the same time two-antenna mobiles, which are at least capable of interference cancellation, will become more common. Secondly, in contrast with UTRA FDD downlink, only minor changes to the UTRA FDD specifications are needed to enable simple uplink MIMO approaches. The content of this section is based on [26], [27] and [28].

6.1 MIMO Algorithms

We divide MIMO techniques into two main classes, namely to diversity and information MIMO. UTRA FDD uplink provides good means to implement diversity and information MIMO techniques, because uplink users are separated by different scrambling codes and therefore the whole channelization code space is available for any one user.

Diversity MIMO

In diversity MIMO, M_t replicas of the same data stream are transmitted by using different orthogonal channelization codes but the same scrambling code. This is depicted in Figure 33 which shows the system model of diversity MIMO for two transmit antennas. The received signal in kth base station antenna becomes

$$\begin{aligned} y_k(t) &= \sum_{i=-\infty}^{\infty} \sum_{m=1}^{M_t} h_{m,k}(t) * \frac{\sqrt{P_{\text{tx}}}}{M_t} \big\{ S_{d,m}(t) + j \cdot S_{c,m}(t) \big\}, \\ S_{x,m}(t) &= b_x[i] \cdot \beta_x \cdot c_{x,m}(t - iT_x - \delta) \otimes s_{\text{dpch}}(t - iT_s - \delta), \end{aligned} \tag{174}$$

where $x \in \{d, c\}$, $*$ refers to convolution with multi-path channel $h_{m,k}$, and $\otimes$ refers to chip-by-chip multiplication of user's scrambling code s_{dpch} and channelization codes $c_{d,m}$ and $c_{c,m}$ of dedicated physical data channel (DPDCH) and dedicated physical control channel (DPCCH), respectively. Total transmit power is given by P_{tx} and power ratio between DPDCH and DPCCH is adjusted by scaling factors β_d and β_c, and user's transmitted

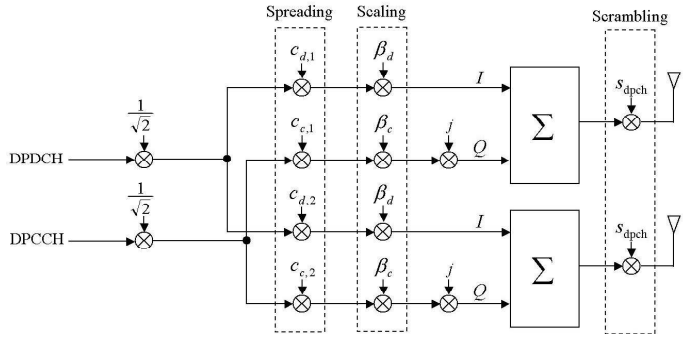

Figure 33: System model for diversity MIMO.

bits in DPDCH and DPCCH are denoted by b_d and b_c. Users are not synchronized in uplink, and the delay is denoted by δ. Finally T_d, T_c, and T_s refer to the lengths of the two channelization codes and the scrambling code.

Each transmit antenna uses different channelization codes $c_{d,m}$ and $c_{c,m}$ so that the base stations can separate the signals from different antennas and later combine them using maximal ratio combining. Thus, the scheme doubles the usage of uplink channelization codes when compared to single antenna transmission. The achievable bit rate with diversity MIMO is at maximum 2 Mbps/M_t. This reduction of maximum bit rate could be partly avoided by puncturing the applied error correcting codes, but information MIMO provides a more attractive choice because the reduced code rate quite rapidly destroys system performance. However, for low and medium bit rate services this does not present a problem.

We note that in case of flat fading and perfect CSI in the receiver, the link performance of the proposed two-antenna diversity MIMO algorithm is the same as with STTD, because the diversity order of both schemes is two. However, the system utilizing orthogonal channelization codes is more robust, because orthogonality of the received signals does not depend on the channel estimation as in the case of space-time coding.

Information MIMO

In case of information MIMO of Figure 34, a composite data stream is multiplexed into two or more independent substreams that are transmitted from separate antennas by employing different scrambling codes. All streams contain DPDCH and DPCCH so that in base station they can be interpreted as signals from different independent users. The received wideband signal

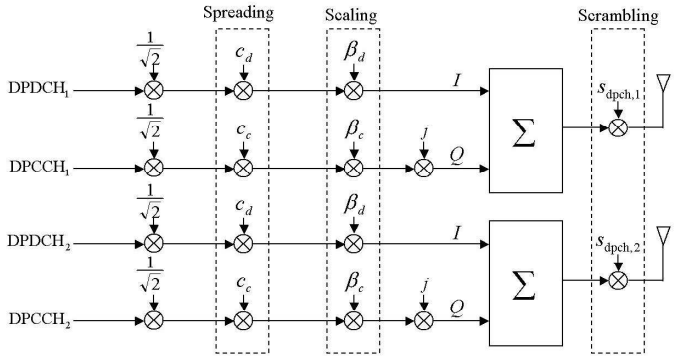

Figure 34: System model for information MIMO.

in kth antenna is given by

$$\begin{aligned} y_k(t) &= \sum_{i=-\infty}^{\infty} \sum_{m=1}^{M_t} h_{m,k}(t) * \frac{\sqrt{P_{\text{tx}}}}{M_t} \{S_{d,m}(t) + j \cdot S_{c,m}(t)\}, \\ S_{x,m}(t) &= b_{x,m}[i] \cdot \beta_x \cdot c_x(t - iT_x - \delta) \otimes s_{\text{dpch},m}(t - iT_s - \delta), \end{aligned} \tag{175}$$

where again $x \in \{d, c\}$. We note that now information bits as well as scrambling code chips vary between antennas. Nevertheless, the channelization code can be the same in all antenna branches.

The present UTRA FDD specification allows the mobile to use only a single scrambling code as well as a single DPCCH and DPDCH. For the proposed information MIMO, the specification should be changed such that the use of multiple scrambling codes is allowed in the mobile end. Then, it would be possible to independently apply DPCCH and DPDCH to each scrambling code. This does not represent a big change to radio interface, because it only requires that a single user can set up M_t different links. For the effective use of several simultaneous links, some new code puncturing sets would also be needed.

Advanced Receiver Techniques

As mentioned before, UTRA FDD uplink is interference limited. The interference limited nature of CDMA systems results from the receiver design: the reception is typically based on a matched filter that does not take into account multiple access interference (MAI). However, MAI arises in multipath channels or with asynchronous communications when spreading codes do not usually stay completely orthogonal any more. This limitation can be relaxed by employing advanced multi-user receiver algorithms which aim to

reduce MAI. Information MIMO increases MAI in base station, and therefore advanced receivers become important to the system performance when implementing information MIMO techniques.

In order to avoid the overwhelming complexity of multi-user detection various sub-optimal multi-user receivers have been developed to cope with MAI. The multi-user receivers can be categorized in several ways. One possibility is to classify the receivers to linear (decorrelating detector, minimum mean square error (MMSE) detector) and non-linear receivers. Subtractive interference cancellation (IC) is one example of the latter category which first estimates the MAI component and then subtracts it from the received signal to improve the reliability of the symbol decisions.

Cancellation of MAI can be carried out in parallel to all users, *i.e.* with parallel interference cancellation (PIC) receivers, or in a serial fashion, i.e. using serial interference cancellation (SIC) receivers. In un-decoded (conventional) PIC receivers, IC is based on tentative symbol decisions. The quality of the tentative decisions is essential, because incorrect decisions increase interference instead of decreasing it. In practice, the error rate of un-decoded bits varies between 5% and 20% in UTRA FDD uplink. The error rate depends mainly on the effective coding rate (i.e., rate of the channel encoder taking into account possible repetition and puncturing), the radio environment and the quality of service requirements.

Unreliable tentative bit decisions compromise the performance of un-decoded PIC. One possibility to improve the reliability of the decisions is to first decode the received symbols, re-encode the decoded symbols again, and finally subtract the contribution of the re-encoded symbols from the received signal. For more details we refer to [101] where this kind of decoded PIC is applied to the convolutionally coded CDMA system. In [102], this idea is extended to Turbo coded CDMA system.

6.2 Uplink Load Equations

Load equations provide a useful tool in both initial planning and performance analysis of the network. Here we represent the load equations [37], [93] that will serve as a basis for further studies.

Basic Load Equations

In the following N_{own} and N_{other} refer to the number of own cell and other cell users, respectively. The received wideband signal in baseband at time instant t can be expressed in the form

$$r(t) = \sum_{n=1}^{N_{\text{own}}} y_n(t) + \sum_{n=1}^{N_{\text{other}}} z_n(t) + n(t), \tag{176}$$

where $n(t)$ is complex zero-mean Gaussian, $y_n(t)$ is the interference from nth own cell user and $z_n(t)$ is the interference from nth other cell user. The system load can be estimated from the sum of received wideband powers of different users. Signals from different users are mutually independent and from (176) the received wideband power is given by

$$\mathrm{E}\{|r(t)|^2\} = I_{\mathrm{total}} = I_{\mathrm{own}} + I_{\mathrm{other}} + P_{\mathrm{N}},$$

where P_{N} is the noise power and

$$I_{\mathrm{own}} = \sum_{n=1}^{N_{\mathrm{own}}} \mathrm{E}\{|y_n(t)|^2\}, \quad I_{\mathrm{other}} = \sum_{n=1}^{N_{\mathrm{other}}} \mathrm{E}\{|z_n(t)|^2\}.$$

Received energy per data bit divided by the noise spectral density is an important variable in the analysis of UTRA FDD uplink. For user n it is given by

$$E_{\mathrm{rx},n} = \frac{1}{\kappa_n} \cdot \frac{P_{\mathrm{rx},n}}{I_{\mathrm{total}} - P_{\mathrm{rx},n}}, \tag{177}$$

where $P_{\mathrm{rx},n}$ refers to the received power, and κ_n is the ratio between bit rate and chip rate of user n. In UTRA FDD uplink, fast power control tries to keep $E_{\mathrm{rx},n}$ at a target level. Therefore, changes in the interference do not reflect to $E_{\mathrm{rx},n}$ as long as power control is able to compensate the increased interference through $P_{\mathrm{rx},n}$. From (177) we easily find that

$$P_{\mathrm{rx},n} = \frac{\kappa_n E_{\mathrm{rx},n}}{1 + \kappa_n E_{\mathrm{rx},n}} \cdot I_{\mathrm{total}} =: \eta_n \cdot I_{\mathrm{total}},$$

where η_n is the load from nth user. For the received wideband power in the own cell there holds

$$I_{\mathrm{own}} = \sum_{n=1}^{N_{\mathrm{own}}} P_{\mathrm{rx},n} = \sum_{n=1}^{N_{\mathrm{own}}} \eta_n \cdot I_{\mathrm{total}}. \tag{178}$$

Furthermore, the total wideband power can be written in the form

$$I_{\mathrm{total}} = I_{\mathrm{own}} + I_{\mathrm{other}} + P_{\mathrm{N}} = \big(1 + \nu\big) I_{\mathrm{own}} + P_{\mathrm{N}}, \tag{179}$$

where $\nu = I_{\mathrm{other}}/I_{\mathrm{own}}$ is the inter-cell to intra-cell interference ratio seen by the base station receiver. After combining (178) and (179) and solving I_{total} from the resulting formula we obtain the following expression for the noise rise

$$\mu = \frac{I_{\mathrm{total}}}{P_{\mathrm{N}}} = \Big(1 - (1 + \nu) \sum_{n=1}^{N_{\mathrm{own}}} \eta_n\Big)^{-1},$$

where the sum term defines the own cell load η. In UTRA FDD uplink, load control drives noise rise to a target level. The more loading is allowed

in the system, the larger is the required interference margin $\max\{\mu\}$ and the smaller is the coverage area. Interference margin defines the maximum allowed noise rise and typically values $1.0 - 3.0$ dB are used for coverage-limited cases with 20-50% load, and in capacity limited case, higher interference margins up to 6 dB can be used [37].

Load Equations for MIMO

In diversity MIMO with Rake receiver, the load from the nth user is of the form

$$\eta_n^{\mathrm{D}} = \frac{\kappa_n E_{\mathrm{rx},n}^{\mathrm{D}}}{1 + \kappa_n E_{\mathrm{rx},n}^{\mathrm{D}}},$$

where the superscript D refers to the diversity MIMO. Diversity MIMO reduces the required energy per data bit and there holds

$$E_{\mathrm{rx},n}^{\mathrm{D}} = \delta_{M_t,M_r} E_{\mathrm{rx},n}/M_r, \tag{180}$$

where the received energy per data bit $E_{\mathrm{rx},n}$ in single antenna system is divided by the number of receiver antennas, because Rake collects energy from M_r independent antenna branches. Factor δ_{M_t,M_r} depends on the channel diversity and system related issues such as the accuracy of channel estimation. Only in simple channels such as single path and ITU Pedestrian A channels the effect of δ_{M_t,M_r} may be noticeable, while in more realistic channels such as ITU Vehicular A and ITU Pedestrian B δ_{M_t,M_r} is round 0 dB. The ITU channel profiles [89, 70] are listed in Table 9.

In information MIMO with Rake the uplink load of a single user is of the form

$$\eta_n^{\mathrm{I}} = \sum_{m=1}^{M_t} \frac{\kappa_{n,m} E_{n,m}^{\mathrm{I}}}{1 + \kappa_{n,m} E_{n,m}^{\mathrm{I}}}, \tag{181}$$

where $\kappa_{n,m}$ is the ratio between bit rate and chip rate of mth data stream and $E_{n,m}^{\mathrm{I}}$ is the received energy per data bit divided by the noise spectral density for the mth data stream. We note that with M_r receive antennas and Rake receiver there holds

$$E_{\mathrm{rx},n}^{\mathrm{I}} = \delta_{M_r} E_{\mathrm{rx},n}/M_r, \tag{182}$$

where δ_{M_r} depends on the diversity gain and is round 0 dB in case of multi-path diversity. In contrast to diversity MIMO, δ_{M_r} depends only on the number of receive antennas because each transmit antenna applies a different scrambling code. Without CSI in the transmitter data rates in different transmit antenna branches are kept equal and (181) becomes

$$\eta_n^{\mathrm{I}} = M_t \cdot \frac{\kappa_n E_{\mathrm{rx},n}^{\mathrm{I}}}{1 + \kappa_n E_{\mathrm{rx},n}^{\mathrm{I}}}. \tag{183}$$

Equation (183) indicates that base station receiver sees the usage of information MIMO as an increased number of SISO users. This additional load can be effectively reduced by applying PIC, which removes part of the own cell interference in the detection process. Let us denote the PIC efficiency by β, $0 \leq \beta \leq 1$. Then the average load of a single user can be written as

$$\eta_n = (1-\beta)\frac{\kappa_n E_{\mathrm{rx},n}}{1+\kappa_n E_{\mathrm{rx},n}}.$$

Since PIC is not able to remove the inter-cell interference the total wideband power seen by base station receiver is of the form

$$I_{\mathrm{total}} = (1-\beta)I_{\mathrm{own}} + I_{\mathrm{other}} + P_{\mathrm{N}} = (1-\beta+\nu)I_{\mathrm{own}} + P_{\mathrm{N}}$$

and the corresponding cell load is given by

$$\eta = (1-\beta+\nu)\sum_{n=1}^{N_{\mathrm{own}}} \eta_n. \tag{184}$$

In case of PIC diversity MIMO operates in a similar manner as in case of SISO. For a single user load we have

$$\eta_n^{\mathrm{D}} = (1-\beta)\frac{\kappa_n E_{\mathrm{rx},n}^{\mathrm{D}}}{1+\kappa_n E_{\mathrm{rx},n}^{\mathrm{D}}}. \tag{185}$$

Furthermore, for information MIMO the single user load is given by

$$\eta_n^{\mathrm{I}} = (1-\beta)\sum_{m=1}^{M_t} \frac{\kappa_{n,m} E_{\mathrm{rx},n,m}^{\mathrm{I}}}{1+\kappa_{n,m} E_{\mathrm{rx},n,m}^{\mathrm{I}}}. \tag{186}$$

6.3 Performance Comparisons

In the following we show performance results for UTRA FDD uplink and discuss the connection between the results and the load equations. Simulations use full 3GPP link level modeling with inner and outer loop power control and realistic channel and interference estimation algorithms. The radio channel is modeled according to ITU models in Table 9. Our system model follows accurately the present UTRA FDD specifications and simulations are done following strictly the recommendations given in [89].

Let us consider two systems where the number of users is the same and all users employ the same service. Assume that the number of receive antennas is the same in both systems but the first system applies the diversity MIMO while the second one employs single-input multiple-output (SIMO). In both systems, base station applies Rake receiver. Then, according to (180) the ratio between cell loads is given by

$$\frac{\eta_{\mathrm{sys}_2}}{\eta_{\mathrm{sys}_1}} = \frac{\delta_{1,M_r} E_{\mathrm{rx}}/M_r(1+\kappa\cdot\delta_{M_t,M_r}E_{\mathrm{rx}}/M_r)}{\delta_{M_t,M_r}E_{\mathrm{rx}}/M_r(1+\kappa\cdot\delta_{1,M_r}E_{\mathrm{rx}}/M_r)}\cdot\frac{1+\nu_2}{1+\nu_1},$$

Model	delay profile [ns]	power profile [dB]
Ped. A	0, 110, 190, 410,	0, −9.7, −19.2, −22.8
Ped. B	0, 200, 800, 1200, 2300, 3700	0, −0.9, −4.9, −8.0, −7.8, −23.9
Veh. A	0, 310, 710, 1090, 1730, 2510	0, −1, −9, −10, −15, −20

Table 9: ITU multipath channel profiles.

where E_{rx} refers to the received energy per bit in SISO system and ν_1 and ν_2 denote inter-cell interference ratios in systems 1 and 2. Since δ_{M_t,M_r} and δ_{1,M_r} are round 0 dB we can approximate

$$\eta_{\mathrm{sys}_2} \approx \frac{1+\nu_2}{1+\nu_1} \cdot \eta_{\mathrm{sys}_1}$$

as in (170). Thus, there is no noticeable capacity gain from additional transmit antennas in isolated cell where $\nu_1 = \nu_2 = 0$. Assume that we know the inter-cell to intra-cell interference ratio ν_1 and the original load η_{sys_1}. Then we can compute the capacity gain provided that the ratio ν_2/ν_1 can be deduced. We have

$$\frac{\nu_2}{\nu_1} = \frac{I_{\mathrm{own},1}}{I_{\mathrm{own},2}} \cdot \frac{I_{\mathrm{other},2}}{I_{\mathrm{other},1}} = \frac{I_{\mathrm{other},2}}{I_{\mathrm{other},1}},$$

where the latter equality holds because the number of own cell users is the same in both systems and power control drives SIR to the same target value. Hence, ν_2/ν_1 depends only on the ratio between other cell interferences that are proportional to the average mobile transmission power. After computing the mean transmit powers in diversity MIMO and SIMO systems it is found that [26, 84, 85]

$$\nu_2 = \frac{M_t(M_r-1)}{M_tM_r-1} \cdot \nu_1, \quad M_r > 1. \tag{187}$$

This equality holds in flat fading. Table 10 shows the relative reduction $(\eta_{\mathrm{sys}_1} - \eta_{\mathrm{sys}_2})/\eta_{\mathrm{sys}_1}$ of the cell load for diversity MIMO when the reference system applies SIMO. The results show that the gain from diversity MIMO can be noticeable especially when the initial inter-cell interference ratio ν_1 is large.

While the gain of diversity MIMO strongly depends on the inter-cell interference level, the gain from additional receive antennas is remarkable also in isolated cell. Due to (180), the required energy per data bit and noise spectral density is approximately inversely proportional to the number of receive antennas M_r. Another measure for the cell coverage is the power per data bit that is required to compensate the path loss and multi-user interference. Assume that all users apply the same service. Then by (177), (178)

$\eta = 0.75$	$M_r = 2$	$M_r = 4$
$\nu_1 = 0.5$, $M_t = 2$	11.1%	4.8%
$\nu_1 = 0.5$, $M_t = 4$	14.3%	6.7%
$\nu_1 = 2.0$, $M_t = 2$	22.2%	9.5%
$\nu_1 = 2.0$, $M_t = 4$	28.6%	13.3%

Table 10: Gain of diversity MIMO relative to SIMO in terms of reduced cell load.

Carrier Frequency	1940 MHz
Chip rate	3.840 Mchips
Sampling rate	1 sample/chip
Power control	ON, both inner and outer loops
BLER target (QoS)	10%
Rake finger allocation	Known delays
Max. number of allocated Rake fingers	five per receive antenna
Channel estimation	Estimated (DPCCH)
Signal-to-interference estimation	Estimated (DPCCH)

Table 11: Simulation parameters.

and (182) we have in isolated cell

$$\frac{P_{\text{rx}}}{P_{\text{N}}} = \frac{\delta_{M_r} \cdot \kappa \cdot E_{\text{rx}}}{M_r - (N_{\text{own}} - 1) \cdot \delta_{M_r} \cdot \kappa \cdot E_{\text{rx}}}, \tag{188}$$

where E_{rx} is the energy per data bit and noise spectral density for SISO. We note that although the Equation (182) is given for MIMO system, it is applicable also in case of SIMO. Equation (188) shows that required transmit power, which is directly proportional to the received power, does not depend only on the number of receive antennas but it also depends on the number of users. It is found that the range gain from additional receive antennas increases with the load while the absolute cell radius is decreasing when load is growing.

In the following we study the system performance also by simulations. The main simulation parameters and assumptions are shown in Table 11. Full 3GPP link level modelling was used with inner and outer loop power control and realistic channel and interference estimation algorithms. For more details, see [90].

Figure 35 depicts the received power per bit and antenna for SIMO in terms of the number of 0.96 Mbps users assuming isolated cell and Pedestrian B channel with 3 km/h mobile speed. The results in Figure 35 were obtained through multi-user simulations but they are well in line with equation (188).

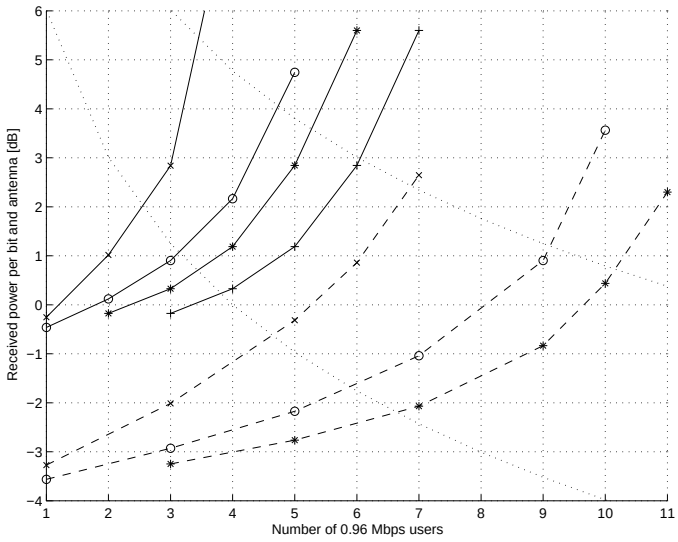

Figure 35: Received power per bit and antenna as a function of 0.96 Mbps users assuming 2 (solid curves) and 4 (dashed curves) receive antennas in Pedestrian B channel with 3 km/h mobile speed. Receivers are Rake (x), conventional PIC (o), coded turbo PIC with 1 iteration (*) and coded turbo PIC with 3 iterations (+). Dotted curves show the 3 dB and 6 dB noise rise levels.

It is found that the range gain from additional receive antenna is of the order of 3 dB in the single user case, but the gain grows rapidly with additional users. If, however, noise rise is fixed, the range gain from additional antennas is proportional to M_r. This is seen by studying the intersection points between power and noise rise curves.

Cell capacity can be also estimated from the results in Figure 35. We recall that the load control of the network drives the noise rise to a predefined target value that is usually between 3 dB and 6 dB depending on the network configuration. From Figure 35 we find that with Rake receiver cell throughput can reach up to round 3.4 Mbps and 6.8 Mbps with 2 and 4 receive antennas, respectively. In addition to Rake curves, Figure 35 shows performance results for conventional PIC and coded turbo PIC. Although the largest gains are obtained by increasing the number of receive antennas, PIC provides an efficient way to improve cell coverage and capacity when the number of receive antennas is fixed. In two-antenna case coded turbo PIC with 3 iterations results in cell throughput up to 6 Mbps and the range gain against Rake is round 2.5 dB for 6 dB noise rise. Assuming four receive antennas and coded PIC with single iteration allows round 10 Mbps throughputs for 6 dB noise rise.

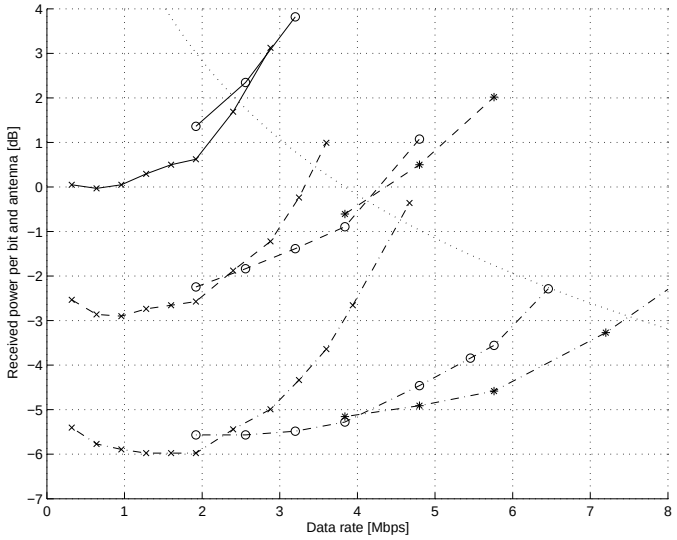

Figure 36: Received power per bit and antenna as a function of data rate assuming Rake with 2 (solid curves), 4 (dashed curves) and 8 (dashed and dotted curves) receive antennas in Vehicular A channel with 30 km/h mobile speed. Numbers of transmit antennas are 1 (x), 2 (o) and 3 (*). Dotted curve shows the 3 dB noise rise level.

We recall from (185) and (186) that the effect of PIC can be modeled through the efficiency β. This parameter is not constant but depends on cell conditions such as the number of users and channel model. According to simulations the efficiency for uncoded PIC is round 0.4 at maximum while coded PIC with turbo receiver can provide maximum efficiency of round 0.7.

Figure 35 shows the performance for SIMO configuration. However, the performance for information MIMO can be deduced from the same figure by setting the data rate to $M_t \times 0.96$ Mbps and scaling the number of users accordingly. In the analysis this equivalence is seen in equation (183). Thus, there is no throughput gain at the cell level from information MIMO for low user data rates. Instead, the performance may suffer, because user's pilot power is divided between multiple transmit antennas which deteriorates channel estimation in the receiver.

The benefits of information MIMO become visible with high user data rates. The main reason for the superiority of information MIMO to SIMO and diversity MIMO is that in information MIMO high data rates can be obtained without heavy code puncturing because independent data streams are transmitted from separate antennas. Both SIMO and diversity MIMO face serious performance degradation when effective code rate increases due to puncturing. We note that adaptive modulation and coding in uplink is

not supported in UTRA FDD specification, and therefore code puncturing cannot be avoided when SIMO and diversity MIMO are used on high data rates.

Figure 36 shows the received power per bit and antenna in Vehicular A channel with 30 km/h mobile speed assuming information MIMO and Rake receiver. Six multi-codes of spreading factor 4 were applied for data rates higher than 2 Mbps. Data rates higher than $M_t \times 2$ Mbps were generated by using the code puncturing. It is found that additional transmit antennas provide a remarkable performance gain when base station has 4 or 8 receive antennas. Especially in case of 8 receive antennas the gain from the second and the third data stream is large and data rates up to 7.5 Mbps are obtained with 3 dB noise rise. On the other hand, with two receive antennas channel estimation errors slightly degrade the system performance when the second data stream is added. For low data rates this phenomenon is also visible when $M_r > 2$. Besides the channel estimation errors the poor orthogonality properties of different scrambling codes also have a negative impact to the system performance. Figure 36 also shows the detrimental effect of code puncturing. Especially in SIMO curves, rapid degradation in performance is clearly noticeable when data rate exceeds 2 Mbps.

7 Conclusions

It has been known for quite some time that in order to communicate efficiently over the wireless channel, one should exploit multi-path diversity by benefiting from independent fading propagation paths. This led to the development of efficient open-loop (OL) and closed-loop (CL) transmit diversity solutions with the idea of enhancing capacity by means of taking advantage of the spatial diversity available in the channel. In Section 3 we analyzed CL extended mode 1 (e-mode 1) and extended mode 2 (e-mode 2) that were designed based on universal terrestrial radio access (UTRA) frequency division duplex (FDD) CL mode 1 and 2. Although being suboptimal these algorithms are efficient and at the same time they admit analysis in terms of signal to noise ratio (SNR) gain, link capacity and bit error probability (BEP).

Results of the analysis in Section 3 show that both e-mode 1 and e-mode 2 clearly outperform transmitter selection combining (TSC) that is used as a reference. Furthermore, by e-mode 2 it is possible to achieve almost the same performance as with perfect channel state information (CSI). Results indicate that in the presence of flat fading the SNR gain of both e-mode 1 and 2 grow linearly with additional antennas while the SNR gain of TSC admits only logarithmic growth. In case of two transmit antennas it is shown that link capacity of CL transmit diversity (TD) methods can be accurately approximated using SNR gain and link capacity formula of maximal ratio combining. Also the analysis of approximation error is provided. Through BEP formulas it is further shown that the studied CL TD methods provide full diversity gain if feedback is error-free. On the contrary, if feedback is corrupted the slope of the BEP curve in asymptotic SNR region is the same for multi-antenna CL TD methods and single antenna transmission. Nevertheless, the CL processing provides a constant BEP gain in high SNR region.

In on-off scheduling (OOS) the selection between positive acknowledgment (ACK) and negative acknowledgment (NACK) is based on a SNR threshold that is known in both transmitter and receiver. In Section 4 OOS was studied in downlink framework assuming a similar shared channel as in UTRA FDD high-speed downlink packet access (HSDPA). Contrary to HSDPA, in our model only a single user can transmit during each transport time interval (TTI). Three different physical layer scheduling algorithms were considered. In system 1, served user is selected irrespective of the CSI. In system 2 all users apply OOS and send ACK or NACK message after each TTI based on received relative SNR. Served user is selected among those with positive ACK and if no ACK is received in BS, the served user is selected randomly. Finally, in system 3, transmission is assigned to the user with the best relative channel conditions. Thus, the amount of transmitter CSI is one bit per user in system 2 while system 3 applies unquantized

feedback. Furthermore, TSC is applied on top of each system.

Results in Section 4 indicate that in case of system 2 with OOS there exists an ACK probability and the corresponding relative SNR threshold that maximize the capacity on the shared channel. With optimal ACK probability system 2 is able to achieve more than 75% of the capacity gain of full SNR feedback, provided that OOS feedback is error-free. It is further shown that the effect of feedback errors may be crucial to OOS. It turns out that when ACK probability is small, system 2 is sensitive to feedback errors. When feedback error rate is less than 5% performance losses remain at acceptable level in most cases.

Uplink framework presented in Section 5 assumes fast transmit power control (PC) and the OOS threshold corresponds to the relative transmit power, measured by mobile terminal. Contrary to downlink framework in Section 4, in uplink all users have their control channels on, which enables continuous transmit power measurements in terminals. This creates control channel overhead that limits the gain of channel-aware scheduling.

The required mean transmit power of OOS was compared to two reference systems that do not exploit CSI. We assumed a model where OOS is applied only on the data channel while the control channel is on all the time, and fast transmit power control is used on both channels. This model is compatible with proposed UTRA FDD HSUPA. It was found out that OOS can remarkably reduce the mean transmit power provided that the power ratio between control and data channels remains small. On the other hand, it was shown that the control channel overhead might limit the performance of OOS although users could tolerate unbounded delays. Furthermore, antenna and multi-path diversity reduce the relative gain of OOS. Obtained OOS gains were also translated into gains in FDD WCDMA coverage and capacity. We showed how OOS is able to improve service availability by using a radio link budget example. The achievable capacity gain from OOS strongly depends on the load and interference conditions in the network, the gain being largest in a heavily loaded system with high inter-cell interference level.

In Section 6 it was shown that the uplink coverage and capacity of UTRA FDD mode can be greatly improved by single-input multiple-output (SIMO) and multiple-input multiple-output (MIMO) transceivers. We studied two approaches referred to as diversity MIMO and information MIMO. In the former case, a single data stream is transmitted and multiple antennas are used to decrease the variance of the received signal and thereby improve the quality of the radio link. In the latter case, multiple transceiver antennas are used for parallel multiplexing, *i.e.* to transmit several data streams simultaneously to a user to increase peak data rates.

While the gain from diversity MIMO is noticeable only in the presence of heavy inter-cell interference, the gain from additional receive antennas is remarkable also in isolated cell. The information MIMO shows its power

when high user data rates are needed. This is mostly due to the fact that heavy code puncturing can be avoided by using the information MIMO. UTRA FDD uplink is not code limited and therefore diversity and information MIMO can be implemented by allocating additional channelization or scrambling codes to different transmit antennas. Thus, the receiver in base station can separate the signals from different antennas in code domain and it is not necessary to rely on spatial signatures and space-time code design. This makes the system more robust and receivers can utilize well-known multi-user and interference cancellation receivers developed for CDMA systems. Furthermore, these MIMO schemes can be implemented with only minor changes to the present specification.

References

[1] J. Hämäläinen, R. Wichman, "Closed–loop transmit diversity for FDD WCDMA systems," 34^{th} *Asilomar Conference on Signals, Systems and Computers*, October 2000.

[2] J. Hämäläinen, R. Wichman, "Multiple antenna transmission utilizing side information for WCDMA systems," *The* 5^{th} *CDMA International Conference and Exhibition*, Seoul, Korea, November 2000.

[3] J. Hämäläinen, R. Wichman, "Feedback schemes for FDD WCDMA systems in multipath environments," *IEEE Vehicular Technology Conference*, Rhodes, Greece, May 2001.

[4] J. Hämäläinen, R. Wichman, "Performance analysis of closed–loop transmit diversity in the presence of feedback errors," *IEEE International Symposium on Personal, Indoor and Mobile Radio Communications*, September 2002.

[5] J. Hämäläinen, R. Wichman, "Asymptotic bit error probabilities of some closed–loop transmit diversity schemes," *IEEE Global Telecommunications Conference*, November 2002.

[6] J. Hämäläinen, R. Wichman, "Capacity of generalized UTRA FDD closed–loop transmit diversity modes," in preparation.

[7] R. Wichman, J. Hämäläinen, "Transmit diversity weight generation for wireless FDD systems with feedback," *IEEE and EURASIP Workshop on Nonlinear Signal and Image Processing*, Baltimore, Maryland, USA, June 2001.

[8] J. Hämäläinen, R. Wichman, "The effect of feedback delay to the closed-loop transmit diversity in FDD WCDMA," *IEEE International Symposium on Personal, Indoor and Mobile Radio Communications*, San Diego, California, September 30–October 3, 2001.

[9] J. Hämäläinen, R. Wichman, "Closed–loop transmit diversity for FDD WCDMA in fading channels," *Second Finnish Wireless Communications Workshop*, Tampere, Finland, October 2001.

[10] J. Hämäläinen, O. Piirainen, R. Wichman, "On the SNR gain of polarization matching," *Finnish Wireless Communications Workshop*, May 2002.

[11] J. Hämäläinen, R. Wichman, "On optimality of closed–loop transmit diversity," *Finnish Wireless Communications Workshop*, May 2002.

[12] J. Hämäläinen, R. Wichman, "On the performance of FDD WCDMA closed–loop transmit diversity modes in Nakagami and Ricean fading channels," *IEEE International Symposium of Spread Spectrum Techniques and Applications*, Prague, Czech Republic, September 2002.

[13] J. Hämäläinen, R. Wichman, T. Kähkönen, J. Hulkkonen, T. Korpi, M. Säily, "On the performance of GERAN transmit diversity schemes when employing dual–polarized antennas," *IEEE Vehicular Technology Conference*, Korea, April 2003.

[14] J. Hulkkonen, T. Kähkönen, J. Hämäläinen, T. Korpi, M. Säily, "Capacity gain from transmit diversity methods in limited bandwidth GERAN networks," *IEEE Vehicular Technology Conference*, Korea, April 2003.

[15] J. Hämäläinen, R. Wichman, "On the site selection diversity transmission," *IEEE International Symposium on Personal, Indoor and Mobile Radio Communications*, September 2003.

[16] J. Hämäläinen, R. Wichman, T. Korhonen: Chapter "Multi-channel adaptive beam-forming" in book *"Adaptive Antenna Arrays"*, ed. by S. Chandran, Springer Verlag, 2004.

[17] J. Hämäläinen, R. Wichman, "Capacities of physical layer scheduling strategies on a shared link," *Wireless Personal Communications*, vol. 39 no. 1, pp. 115-134, October 2006.

[18] J. Hämäläinen, R. Wichman, "Bit error probabilities in a two–rate communication system," *IEEE International Conference on Communications*, May 2003.

[19] J. Hämäläinen, R. Wichman, "Quantization of channel quality indicator in maximum SNR scheduling," *Nordic Radio Symposium*, August 2004.

[20] J. Hämäläinen, R. Wichman, "Combining multiuser diversity and WCDMA transmit diversity modes," *IEEE Nordic Signal Processing Symposium*, October 2002.

[21] J. Hämäläinen, R. Wichman, "Performance of transmit time selection diversity in multipath fading channels," *The 6th International Symposium on Wireless Personal Multimedia Communications*, October 2003.

[22] J. Hämäläinen, R. Wichman, "Performance of multiuser diversity in the presence of feedback errors," *IEEE International Symposium on Personal, Indoor and Mobile Radio Communications*, September 2004.

[23] G. Corral-Briones, A. A. Dowhuszko, J. Hämäläinen, R. Wichman, "Achievable data rates for multiple transmit antenna broadcast channels with closed–loop transmit diversity modes," *IEEE International Conference on Communications*, May 2005.

[24] G. Corral-Briones, A. A. Dowhuszko, J. Hämäläinen, R. Wichman, "Downlink multiuser scheduling algorithm with FDD WCDMA closed–loop feedback information," *IEEE Vehicular Technology Conference*, May 2005.

[25] J. Hämäläinen, R. Wichman, "The effect of control channel overhead upon physical layer scheduling," *Wireless Personal Communications*, vol. 35, no. 4, pp. 337-352, December 2005.

[26] J. Hämäläinen, K. Pajukoski, E. Tiirola, R. Wichman, J. Ylitalo, "On the performance of multiuser MIMO in UTRA FDD uplink," *EURASIP Journal on Wireless Communications and Networking, Special Issue on Multiuser MIMO Networks*, Vol. 2, pp. 297–308, 2004.

[27] J. Hämäläinen, K. Pajukoski, E. Tiirola, R. Wichman, J. Ylitalo, "MIMO performance in UTRA FDD uplink," *IEEE International Symposium of Spread Spectrum Techniques and Applications*, September 2004.

[28] J. Hämäläinen, R. Wichman, M. Kuusela, E. Tiirola, K. Pajukoski: Chapter "Multiuser MIMO for UTRA FDD" in book *"MIMO antenna technology for wireless communications"*, ed. by G. Tsoulos, CRC Press, 2006.

[29] E. Tiirola, J. Hämäläinen, K. Pajukoski, J. Ylitalo, "Performance analysis for some practical high data rate extensions of UTRA FDD uplink," *IEEE Vehicular Technology Conference*, September 2004.

[30] J. Hämäläinen, R. Wichman, "On the correlations between dual–polarized base station antennas," *IEEE Global Telecommunications Conference*, November 2003.

[31] J. Ylitalo, J. P. Nuutinen, J. Hämäläinen, T. Jämsä, M. Hämäläinen, "Multi–dimensional wideband radio channel characterization for 2-6 GHz band," *Wireless World Research Forum*, WWRF11 Meeting in Oslo, June 2004.

[32] J. Hämäläinen, S. Savolainen, R. Wichman, K. Ruotsalainen, J. Ylitalo, "Integral equation formulation for scatter density problem," *Electronics Letters*, vol. 41, no. 2, pp. 82-83, January 2005.

[33] J. Hämäläinen, J. P. Nuutinen, R. Wichman, J. Ylitalo, T. Jämsä, "Analysis and measurements for indoor polarization MIMO in 5.25 GHz band," *IEEE Vehicular Technology Conference*, May 2005.

[34] J. Hämäläinen, S. Savolainen, R. Wichman, K. Ruotsalainen, J. Ylitalo, "On solution of scatter density in geometry–based channel models," accepted to *IEEE Trans. Wireless Commun.*, June 2005.

[35] 3GPP Technical specification 25.201, "UTRA physical layer general description," ver. 6.2.0, June 2005.

[36] 3GPP Technical specification 25.213, "Spreading and modulation," ver. 6.4.0, September 2005.

[37] Holma, H. and A. Toskala (eds.), *WCDMA for UMTS*, Wiley, third edition, 2004.

[38] 3GPP Technical specification 25.211, "Physical channels and mapping of transport channels onto physical channels (fdd)," ver. 6.6.0, September 2005.

[39] 3GPP Technical report 25.848, "Physical layer aspects of UTRA high speed downlink Packet Access," ver. 4.0.0, April 2001

[40] 3GPP Technical report 25.899, "HSDPA enhancements," ver. 6.1.0, September 2005.

[41] R. Knopp, P. Humblet, "Information capacity and power control in single cell multiuser communications," *International Conference on Communications*, June 1995.

[42] R. Knopp, *Coding and multiple–access over fading channels*, Ph.D. dissertation, Ecole Polytehnique Fédérale de Lausanne, 1997.

[43] K. Pedersen, P. Mogensen, and J. Ramiro-Moreno, "Application and performance of downlink beamforming techniques in UMTS," *IEEE Commun. Mag.*, vol. 41, no. 10, pp. 134–143, 2003.

[44] E. Tiirola and J. Ylitalo, "Comparison of beam–forming and diversity techniques in terms of UTRA FDD uplink capacity," in *Nordic Radio Symposium*, August 2004.

[45] S. Alamouti, "A simple transmitter diversity technique for wireless communications," *IEEE J. Select. Areas Commun.*, vol. 16, no. 8, pp. 1451–1458, October 1998.

[46] 3GPP Technical specification 25.214, "Physical layer procedures (FDD)," ver. 4.6.0, April 2003.

[47] 3GPP Technical report 25.869, "Transmitter diversity solutions for multiple antennas (withdrawn from rel. 6)," ver. 1.2.0, September 2003.

[48] V. Tarokh, N. Seshadri, A. R. Calderbank, "Space–time codes for high data rate wireless communications", *IEEE Trans. Inform. Theory*, vol. 44, no. 2, pp. 744-765, March 1998.

[49] V. Tarokh, H. Jafarkhani, A. R. Calderbank, "Space–time block codes from orthogonal designs", *IEEE Trans. Inform. Theory*, vol. 45, no. 5, pp. 1456-1467, July 1999.

[50] A. Narula, M. J. Lopez, M. D. Trott, G. W. Wornell, "Efficient use of side information in multiple–antenna data transmission over fading channels," *IEEE J. Select. Areas Commun.*, vol. 17, no. 8, pp. 1423-1436, October 1998.

[51] M. Sandell, "Analytical analysis of transmit diversity in WCDMA on fading multipath channels", *IEEE International Symposium on Personal, Indoor and Mobile Radio Communications*, 1999.

[52] W. C. Y. Lee, "Estimate of channel capacity in Rayleigh fading environment," *IEEE Trans. Veh. Technol.*, vol. 39, pp. 187–190, August 1990.

[53] A. Goldsmith, P. Varaiya, "Capacity of fading channels with channel side information," *IEEE Trans. Inform. Theory*, vol. 43, pp. 1896–1992, November 1997.

[54] M-S. Alouini, A. J. Goldsmith, "Capacity of Rayleigh fading channels under different adaptive transmission and diversity–combining techniques," *IEEE Trans. Veh. Technol.*, vol. 48, no. 4, pp. 1165–1181, July 1999.

[55] R. W. Health, A. Paulraj, "A simple scheme for transmit diversity using partial channel feedback," 32^{th} *Asilomar Conference on Signals, Systems and Computers*, pp. 1073–1078, 1998.

[56] E. Onggosanusi, A. Gatherer, A. Dabak, S. Hosur, "Performance analysis of closed–loop transmit diversity in the presence of feedback delay," *IEEE Trans. Commun.*, vol. 49, no. 9, pp. 1618–1630, September 2001.

[57] J. Choi, "Performance analysis for transmit antenna diversity with/without channel information," *IEEE Trans. Veh. Technol.*, vol. 51, no. 1, pp. 101–113, January 2002.

[58] E. Visotsky, U. Madhow, "Space–time transmit precoding with imperfect feedback," *IEEE Trans. Inform. Theory*, vol. 4, no. 6, pp. 2632–2639, September 2001.

[59] S. Miller, J. Shapira, "Transmission considerations for polarization–smart antennas," in *IEEE Vehicular Technology Conference*, May 2001.

[60] S. Miller, J. Shapira, "A novel polarization smart antennas," in *IEEE Vehicular Technology Conference*, May 2001.

[61] B. Raghothaman, G. Mandyam, R. T. Derryberry, "Performance of closed loop transmit diversity with feedback delay, 34^{th} *Asilomar Conference on Signals, Systems and Computers*, pp. 102–105, October 2000.

[62] C. W. Sung, S. C. Ip, K. K. Leung, "A simple algorithm for closed-loop transmit diversity with a low-data-rate feedback channel," *IEEE Pacific Rim Conference on Communications, Computers and Signal Processing*, pp. 384-387, 2005.

[63] K. Kiran Mukkavilli, A. Sabharwal, E. Erkip, B. Aazhang, "On beamforming with finite rate feedback in multiple-antenna systems," *IEEE Trans. Inform. Theory*, vol. 49, no. 10, pp. 2562-2579, 2003.

[64] D. J. Love, R. W. Heath, T. Strohmer, "Grassmannian beamforming for multiple-input multiple-output wireless systems," *IEEE Trans. Inform. Theory*, vol. 49, no. 10, pp. 2735-2747, 2003.

[65] W. C. Jakes (ed), *Microwave mobile communications*, IEEE Press, 1974.

[66] J. Lieblein, "On moments of order statistics from the Weibull distribution," *Ann. Math. Stat.* 26, pp. 330–333, 1955.

[67] M. Nakagami, "Statistical characters of short–wave fading," *J. IEICE Jap.*, vol. 27, no. 2, pp. 145-150, February 1943.

[68] M. Nakagami, "The m-distribution-A general formula of intensity distri- bution of rapid fading," in *Statistical Methods of Radio Wave Propagation*, W. C. Hoffman Ed. New York: Pergamon Press, pp. 3–36, 1960.

[69] M. Abramowitz and I. Stegun, Eds., *Handbook of mathematical functions.* Washington DC: National Bureau of Standards, 1972.

[70] 3GPP Technical report 25.896, "Feasibility Study for Enhanced Uplink for UTRA FDD," ver. 6.0.0, March 2004.

[71] J. Proakis, *Digital Communications.* McGraw-Hill, 1995.

[72] P. Viswanath, D.N.C. Tse, and R. Laroia, "Opportunistic beamforming using dumb antennas," *IEEE Trans. Inform. Theory*, vol. 48, no. 6, pp. 1277–1294, June 2002.

[73] M. Johansson, "Benefits of multiuser diversity with limited feedback," *IEEE International Workshop on Signal Processing Advances in Wireless Communications*, 2003.

[74] F. Florén, O. Edfors, and B.-A. Molin, "The effect of feedback quantization on the throughput of a multiuser diversity scheme," *Global Telecommunications Conference*, vol. 1, pages 497–501, 2003.

[75] S. Zhou, Z. Wang, G. B. Giannakis, "Quantifying the power loss when transmit beamforming relies on finite-rate feedback," *Trans. Wireless Commun.*, vol. 4, no. 4, pp. 1948-1957, 2005.

[76] D. Gesbert and S. Alouini, "How much feedback is multi–user diversity really worth?," *IEEE International Conference on Communications*, Paris, France, 2004.

[77] L. T. Berger, T. E. Kolding, J. Ramiro-Moreno, P. Ameigeiras, L. Schumacher, P. E. Mogensen, "Interaction of transmit diversity and proportional fair scheduling," *IEEE Vehicular Technology Conference*, April 2003.

[78] J. Ramiro-Moreno, K. I. Pedersen, P. E. Mogensen, "Network performance of transmit and receive antenna diversity in HSDPA under different packet scheduling strategies," *IEEE Vehicular Technology Conference*, April 2003.

[79] R. Gonzali, R. M. Buehrer, B. D. Woerner, "The impact of multiuser diversity on space–time block coding," *IEEE Commun. Letters*, vol. 7, no. 5, May 2003.

[80] J. Torrance, L. Hanzo, "Upper bound performance of adaptive modulation in a slow Rayleigh fading channel," *Electronics Letters*, vol. 32, no. 8, pp. 718-719, April 1996.

[81] A. Rangarajan and V. Sharma, "Achieving exponential diversity order in Rayleigh fading channels," *National Communication Conference (NCC) 2004*, Bangalore, India, 2004.

[82] A. M. Viterbi, A. J. Viterbi, "Erlang capacity of power controlled CDMA system," *IEEE J. Select. Areas Commun.* vol. 11, no. 6, pp. 892–900, August 1993.

[83] A. J. Viterbi, A. M. Viterbi, E. Zehavi, "Other–cell interference in cellular power-controlled CDMA," *IEEE Trans. Commun.* vol. 42, Issue 234, Part 3, pp. 1501–1504, February/March/April 1994.

[84] A. Viterbi, *CDMA: Principles of spread spectrum communication*, Addison-Wesley, Reading, Mass, USA, 1995.

[85] Ariyavisitakul, S. and L. Chang, "Signal and interference statistics of a CDMA system with feedback power control," *IEEE Trans. Commun.* vol. 41 no. 11, pp. 1626–1634, 1993.

[86] D. Raja, A. Sabharwal, B. Aazhang, "Impact of multiple access on uplink scheduling," *IEEE Information Theory Workshop*, September 2001.

[87] K. Lau, "Analytical framework for multiuser uplink MIMO space–time scheduling design with convex utility functions," *IEEE Trans. Wireless Commun.*, vol. 3, no. 5, pp. 1832–1843, September 2004.

[88] J. Meilong, V. K. Lau, "Performance analysis of proportional fair uplink scheduling with channel estimation error in multiple access system," *IEEE International Symposium on Personal, Indoor and Mobile Radio Communications*, September 2004.

[89] ITU, "Guidelines for evaluation of radio transmission technologies for IMT–2000," Recommendation ITU-R.M.1225, 1997.

[90] 3GPP Technical specification 25.104, "BS Radio Transmission and Reception (FDD)," ver. 7.0.0, June 2005.

[91] Hata, M., "Empirical formula for propagation loss in land mobile radio services," *IEEE Trans. Veh. Technol.* VT-29, no. 3, 1980.

[92] Okumura, Y., E. Ohmori, T. Kawano, and K. Fukuda, "Field strength and its variability in the VHF and UHF land mobile service," *Review Electronic Communication Lab.* vol. 16 no. 9-10, pp. 825–873, 1968.

[93] Laiho, J., A. Wacker, and T. Novosad, *Radio network planning and optimization for UMTS*, Wiley, 2002.

[94] G. J. Foschini, "Layered space–time architecture for wireless communication in a fading environment when using multi-element antennas," *Bell Labs. Tech. J.*, pp. 41–59, 1996.

[95] G. J. Foschini, M. J. Gans, "On limits of wireless communications in a fading environment when using multiple antennas," *Wireless Personal Communications*, vol. 6, pp. 311–335, March 1998.

[96] E. Telatar, "Capacity of multi-antenna Gaussian channels," *European Trans. Telecomm.*, vol. 10, no. 6, pp. 585–595, Nov/Dec 1999, based on AT& T Bell Laboratories, Internal Tech. Memo, June 1995.

[97] D. Gesbert, M. Shafi, D-S. Shiu, P. J. Smith, A. Naguib, "From theory to practise: An overview of MIMO space-time coded wireless systems," *IEEE J. Select. Areas Commun.*, vol. 21, no. 3, pp. 281-302, April 2003.

[98] F. Horlin, L. Vandendorpe, "MU-MIMO channel adapted precoding for MAI/ISI-free uplink burst transmission," *IEEE Trans. Commun.*, vol. 52, no. 1, pp. 100–109, January 2004.

[99] H. Boche, M. Wiczanowski, "Optimal transmit covariance matrices for MIMO high speed uplink packet access," *IEEE Wireless Communications and Networking Conference*, March 2004.

[100] 3GPP Technical report 25.867, "Multiple-input multiple-output in UTRA (withdrawn from release 6)," ver. 1.7.1, October 2005.

[101] Y. Sanada and Q. Wang, "A co-channel interference cancellation technique using orthogonal convolutional codes," *IEEE Trans. Commun.*, vol. 44, no. 5, 1996.

[102] H. C. Kwon, K. J. Kim, B. H. Park, and K. C. Whang, "Turbo coded CDMA system with an interference cancellation technique," *IEICE Trans. Commun.*, vol. E81-B, no. 12, 1998.

[103] S.G. Wilson, "Magnitude/phase quantization of independent Gaussian variates", *IEEE Trans. Commun.*, vol. 28, November 1980, pp. 1924-1929.